Optical systems for next wireless standard (5G) generation delivery

Hamza Hallak Elwan

Communauté
UNIVERSITÉ Grenoble Alpes

THÈSE

Pour obtenir le grade de

DOCTEUR DE LA COMMUNAUTÉ UNIVERSITÉ GRENOBLE ALPES

Spécialité : OPTIQUE ET RADIOFREQUENCES

Arrêté ministériel : 25 mai 2016

Présentée par

Hamza HALLAK ELWAN

Thèse dirigée par **Béatrice CABON** , Professeur, , et codirigée par **Julien POETTE**

préparée au sein du **Laboratoire Institut de Microélectronique, Electromagnétisme et Photonique - Laboratoire d'hyperfréquences et de caractérisation**
dans **l'École Doctorale Electronique, Electrotechnique, Automatique, Traitement du Signal (EEATS)**

Systèmes optiques dédiés à la 5° génération de réseaux sans fils (5G)

Optical Systems for next Wireless Standard (5G) Generation Delivery

Thèse soutenue publiquement le **7 septembre 2017**, devant le jury composé de :

Monsieur Liam BARRY
Professeur, Dublin City University, Examinateur
Monsieur Andreas STOHR
Professeur, Universität Duisburg-Essen , Rapporteur
Madame Anne-Laure BILLABERT
Maître de Conférences, Conservatoire National des Arts et Métiers, Rapporteur
Monsieur Jean-Emmanuel BROQUIN
Professeur, Institut polytechnique de Grenoble, Président
Madame Béatrice CABON
Professeure, Institut polytechnique de Grenoble, Directeur de thèse

Acknowledgements

First of all, I would like to thank Allah Almighty for being the foundation of my life and for His unlimited blessings upon me. Without His help and support I would never have been able to reach this far.

I would like to thank from all my heart and soul who has loved me, shared with me the happy and sad moments in my whole life, and given me the best, Mom, Dad, Sister, Brothers, and Brother-in-Law.

I would like to express my deepest and sincerest gratitude to Prof. Béatrice CABON and Dr. Julien POËTTE for their important advices, tenacious supports, continual encouragement, and his faith in my abilities throughout my research work. Indeed I have learnt from them various things in the research field, and their ideas have inspired me to walk along new roads in my professional work.

My warmest thanks to the engineers Nicolas CORRAO, Xavier MESCOT, and Gregory GROSA for their strong support during the experiments.

A special thanks goes to my relatives, my friends, and to all I have not mentioned, who appeared in my life and shared my light with me, thank you.

Abstract

This thesis is for the development of future devices, systems and networks supporting the 5th Generation (5G) high-speed wireless internet. The demand for very high bit rate requires a sufficient large bandwidth, and therefore Millimeter-Wave (mm-wave) frequency band has a lot of interest. Several number of technologies will need to converge, co-exist and interoperate, and most importantly, cooperate, if this vision is to be efficiently and cost-effectively realized. The main concept within this next 5G is the integration of optical fiber networks and radio networks through Radio-over-Fiber (RoF) technology at mm-wave frequencies, to provide high-bandwidth front/backhaul services and enable scalable and manageable networks without a highly complex interface structure and multiple overlaid protocols.

In this thesis, the mm-wave RoF communication systems are theoretically studied and experimentally demonstrated to investigate the system impairments. The work presented in this thesis is focused on optical noise represented by phase and intensity noise induced by optical source and chromatic dispersion introduced by optical fiber. The optical noise is analyzed and measured for different optical generation techniques. Two different down-conversion stages, mixer and envelope detector, are applied for signal processing and to decorrelate phase and intensity noise. We would like to highlight that this study and the model can be applicable to any kind of optical heterodyne generation system and any frequency range. The correlation among optical modes in optical frequency comb is examined to show the impact of chromatic dispersion. This thesis also exhibits the mm-wave power distribution over fiber span and how the chromatic dispersion effect on the RoF network is modified by varying dispersion parameters. Then, this thesis demonstrates how the optical phase decorrelation induced by chromatic dispersion results in mode partition noise at mm-wave RoF communication networks.

When transmitting some types of data over the system, the results demonstrate the impact of optical noise and chromatic dispersion on the signal quality. The simulation results are presented and are in very good agreement with experimental results. The error vector magnitude through online process shows the impact of the system impairments on the system performance. The data rate and system evolution are compliance with communication standards at mm-wave.

Résumé

Cette thèse concerne le développement de futurs appareils, systèmes et réseaux prenant en charge l'internet haute vitesse, sans fil 5éme génération (5G). La demande de débit très élevé nécessite une bande passante suffisante, et ainsi la bande de fréquence millimetrique (mm-wave) a beaucoup d'intérêt. Un certain nombre de technologies devront converger, coexister et interagir, et surtout, coopérer, si cette vision doit être efficace et rentable. Le concept principal de cette de 5G est l'intégration de réseaux de fibre optique et Les réeseaux radio grâce à la technologie Radio-sur-Fibre (RoF) aux fréquences d'onde millimetriques, pour fournir des services à large bande passante et permettre des rèseaux évolutifs et gérables sans structure d'interface très complexe et multiples protocoles superposés.

Dans cette thèse, les systèmes de communication RoF à ondes millimetriques sont theoriquement étudiés et démontrés expérimentalement pour étudier les altérations du système. Le travail présenté dans cette thèse est axé sur le bruit optique représenté par le bruit de phase et d'intensité induit par la source optique et la dispersion chromatique introduite par la fibre optique. Le bruit optique est analysé et mesuré pour différentes techniques de génération optique. Deux dispositifs différents de conversion, un mélangeur et un détecteur d'enveloppe sont, appliqués pour le traitement du signal et pour décorréler la phase et le bruit d'intensité. Nous souhaitons souligner que cette étude et le modèle peuvent s'appliquer à tout type de systéme de génération optique hétérodyne et à toute gamme de fréquences. La corrélation entre les modes optiques en peigne à fréquence optique est examinée pour montrer l'impact de la dispersion chromatique. Cette thèse présente la distribution d'énergie des ondes millimetriques et son influence sur la portée des fibres et la façon dont l'effet de dispersion chromatique sur le réseau RoF depend des paramètres de dispersion. Ensuite, cette thèse démontre comment la décorrélation de la phase optique induite par la dispersion chromatique entraîne un bruit de partition de modes dans les réseaux de communication RoF à ondes millimétriques.

Lors de la transmission de certains types de données sur le système, les résultats démontrent l'impact du bruit optique et de la dispersion chromatique sur le qualité du signal. Les résultats de simulation sont présentés et sont en très bon accord avec les résultats expérimentaux. La grandeur du vecteur d'erreur evaluée par en processus en ligne montre l'impact des altèrations du système sur les performances du système. Le débit de données et l'évolution du système présentée sont en conformité avec les normes de communication comme à ondes millimétriques.

List of Acronyms

1G	First Generation
2G	Second Generation
3G	Third Generation
4G	Fourth Generation
5G	Fifth Generation
ASE	Amplified Spontaneous Emission
AWG	Arbitrary Waveform Generator
AWG	Arrayed Waveguide Grating
BB	Base Band
BS	Base Station
BBOF	BaseBand-over-Fiber
BER	Bit Error Rate
BL	Bit Rate-Distance Product
BPSK	Binary Phase Shift Keying
CEPT	Conference of Postal ans Telecommunications Administrations
CMOS	Complementary Metal Oxide Semiconductor
CP	Cyclic Prefix
CS	Central Station
DAS	Distributed Antennas System
DC	Direct Current
DDMZM	Dual-Drive Mach-Zehnder Modulator
DFB	Distributed FeedBack
DSB	Double Side Band
DSO	Digital Storage Oscilloscope
ECMA	European Computer Manufacture Association
ED	Envelope Detector
EDFA	Erbium-Doped Fibre Amplifier
EOM	External Optical Modulator
ESA	Electrical Spectrum Analyzer
ETSI	European Telecommunications Standards Institute
EVM	Error Vector Magnitude
FCC	Federal Communication Commission
FDM	Frequency Division Multiplexing
FDMA	Frequency Division Multiplexing Access

FFT	Fast Fourier Transform
FSR	Free Spectral Range
FT	Fourier Transform
FTTB	Fibre to the Block
FTTC	Fibre to the Cabinet
FTTH	Fibre to the Home
FTTN	Fibre to the Node
FTTx	Fibre to the x
GPRS	General Packet Radio Service
GSL	Gain Switched Laser
GSM	Global Standard for Mobile
HDTV	High Definition Television
HFC	Hybrid Fiber-Coaxial
IF	Intermediate Frequency
IFFT	Inverse Fast Fourier Transform
IFoF	IF over Fiber
IR	InfraRed
ISI	Inter Symbol Interference
ITU	International Telecommunication Union
LMPN	Laser Mode Partition Noise
LNA	Low Noise Amplifier
LO	Local Oscillator
LTE	Long Term Evolution
MAC	Medium Access Control
MCM	Multiple-Carrier Modulation
MIMO	Multiple Input Multiple Output
MLLD	Mode Locked Laser Diode
MMF	Multi-Mode Fiber
mm-wave	Millimeter-Wave
MS	Mobile Station
MPHPT	Ministry of Public Management, Home Affairs, Post and Telecommunication
MUX/DEMUX	Multiplexer and Multiplexer
MZM	Mach-Zehnder Modulator
OFDM	Orthogonal Frequency Division Multiplexing
O/E	Optic-Electric Convert
OIL	Optical Injection Locking

OLT	Optical Line Terminal
ONU	Optical Network Unit
OPL	Optical Phase Locking
OPLL	Optical Phase Locked Loop
PAL	Protocol Adaption Layer
PC	Polarization Controller
PHY	PHysical Layer
PLL	Phase Locked-Loop
PMLLD	Passively Mode Locked Laser Diode
PSD	Power Spectral Density
QCL	Quantum Cascade Laser
QoS	Quality of Signal
QPSK	Quadrature Phase Shift Keying
RAU	Remote Antenna Unit
RF	Radio Frequency
RIN	Relative Intensity Noise
RN	Remote Node
RNU	Remote System Unite
RoF	Radio-over-Fiber
S	Scattering Parameters
SMF	Single-Mode Fiber
SNR	Signal to Noise Ratio
SSB	Single Side Band
SSMF	Standard Single-Mode Fiber
TDMA	Time Division Multiplexing Access
THz	TeraHertz
UMTS	Universal Mobile Telecommunication System
UTC	Uni-Traveling Carrier
VCO	Voltage-Controlled Oscillator
VNA	Vector Network Analyzer
VOA	Variable Optical Attenuator
VSA	Vector Signal Analyzer
WCDMA	Wide Code Division Multiplexing Access
WiMAX	Worldwide Interoperability for Microwave Access
WLAN	Wireless Local Access Network
WRC	World Radiocommunication Conference
WSS	Wavelength Selective Switch

Contents

List of Figures

List of Tables

Chapter 1

Millimeter-Wave Radio-over-Fiber Access Networks

1.1 Introduction

Wireless communications are an important topic of study to facilitate the transmission of the signals among different users and systems. Several research activities have been demonstrated to increase data rates and transmission distance with a high performance of wireless communication systems. The ever-increasing challenge and complexity in wireless networks demand the trend to higher frequency carriers and microwave photonics [1]. The convergence between radio and optical infrastructures has been proposed to provide a plethora of optical wireless research community [2], where the microwave photonic components emerge a lot of current and future applications and services with ultimate capacity and flexibility of communication networks [3].

For wireless cellular standards, the first generation (1G) was deployed as an analog signal for simple voice services while the second generation (2G) was employed a digital signal for voice and data transmission [4]. Afterwards, broadband systems were implemented for third and fourth generation (3G/4G) to support greater data rate and more mobility in various applications where different technologies were arising since the hindrances of bandwidth and wireless channel [5]. In the previous standards higher data rate, increasing reliability and reducing complexity are significantly required to realize imperative services in the daily life. As the current operating frequency is in a crowed radio spectrum, the means to augment such kind of services are difficult, and therefore the interests in higher frequencies are strongly needed which possesses a greater available bandwidth [6].

Millimeter-wave (mm-wave) and TeraHertz (THz) frequency band has been proposed for next wireless standards, termed as fifth generation (5G) [6],[7]. High-speed wireless systems are ubiquitous, and new communication technologies are developed for highly system performance. The radio components destined for the generation of mm-wave signals are low cost-efficient and high complexity, and the signal transmission in these frequency bands is suffered from enormous attenuation at 60 GHz due to atmospheric oxygen [8]. However, new wireless technologies are required to derive solutions to mitigate the impairments of existing radio systems. Lasers possess unique properties to generate mm-wave carriers through optical het-

erodyning between optical lines, and optical fiber can be employed as the transmission medium to distribute mm-wave signals in the access network with low losses and unlimited available bandwidth [1]. Therefore, microwave photonics have be intended for a seamless integration between wireless and optical access networks to satisfy the needs of both bandwidth availability and wireless dispersive media. Radio-over-fiber (RoF) is a promising technology to achieve multi Gbps wireless communications where the data is distributed from the core network to end users through optical fiber [9]. Furthermore, two important components in mm-wave RoF communication systems are the optical source and the electro-optic conversion whereby the data are carried onto the mm-wave carrier by an optical mechanism.

The signal quality is degraded by noise effects and channel distortions. In mm-wave RoF communication systems, the optical sources deployed result in optical phase and intensity noise while the optical fiber destined for propagation induces distortion effects, which make a significant drop in the system performance and transmission distance [10],[11]. These impairments in mm-wave RoF communication systems had been studied and demonstrated for improving system performances. The complexity and cost associated with implementing systems must be considered for optimum purposes. The system performance should be investigated to meet the communication standards for sustainable developments.

1.2 Wireless and Optical Networks

The evolution of wireless systems has been focused on increasing the reliability to satisfying high-speed applications. In wireless channels, the transmitted signal is propagated over multipath channel with different attenuations and delays due to phenomena such as reflection, diffraction, scattering and shadowing. These channel disturbances cause constructive or destructive interferences which alter the behavior of the transmitted signal at receivers. Therefore, some significant parameters: coherence time, coherence bandwidth, Doppler spread and delay spread are key statistical parameters to characterize the constituent parts of communication systems in time-varying channel and frequency-selective channel which induce Inter Symbol Interference (ISI) and deep fading effects [12].

1.2.1 Wireless Transmission Systems

Modern wireless communication systems utilize multiple access technologies designed to share a common communication channel among multiple users, or a base station is simultaneously transmitting signals over a same channel to several users. Multiple access schemes invest the orthogonality concept to avoid multi-user interference in the communication systems [12]. In 1G cellular mobile services, Frequency Division for Multiple Access (FDMA) was specified for simple voice calls. The data of multiple users are allocated different frequency bands and transmitted over the same time on the channel [4]. Time Division for Multiple Access (TDMA) was used for 2G cellular standards such as Global Standard for Mobile (GSM) and General Packet Radio Service (GPRS) where the information of different users are assigned different time slots over entire bandwidth of the channel resource [4]. The demands for increasing capacity and data rates in many applications push towards 3G and 4G wireless standards which

substantially employed Code Division for Multiple Access (CDMA), Multiple Input Multiple Output (MIMO) and Orthogonal Frequency Division Multiplexing (OFDM) to dominate on ramifications of constituent system components [14].

Code division for multiple access (CDMA) is the most popular technology for use in 3G wireless standards such as Wide band CDMA (WCDMA) and Universal Mobile Telecommunications System (UMTS). In CDMA the data of a multiple users are allocated different codes and transmitted simultaneously over the entire bandwidth of the channel while each user has a certain code to extract identical symbol at the receiver. The basic principle of the CDMA transmitter is that the symbols of each user are multiplied by respective codes and combining the outcomes to transmit the sum signal over frequency-selective channel. The received sum signal correlates with respective codes of each user to recover corresponding symbols. Furthermore, the bandwidth of original signal is spread over the channel after the modulation between the symbols and codes [12]. RoF communication systems are exploited CDMA technique to provide high data-rates which utilized the entire bandwidth through the CDMA concept [13].

Multiple input multiple output (MIMO) is a promising technology used for 3G/4G wireless standards such as Worldwide Interperability for Microwave Access (WiMax). Diversity is a key idea in MIMO communication systems which represents through a multiple antennas in MIMO transceiver to realize the advancements on the performance of wireless link. The major aspects in MIMO system are transmit beamforming to provide power gain and cause channel variations to control on the fading effects. When same data streams are simultaneously transmitted on a multiple antennas known as spatial diversity, the reliability of the link is increasing because the diversity gain is increasing in MIMO channel. While a multiple data streams are transmitted in parallel known as spatial multiplexing, higher data rate is obtained since a degree of freedom is increase [12]. MIMO can also be applied on mm-wave RoF communication systems for increasing the data rates and diversity [14],[15].

Orthogonal frequency division multiplexing (OFDM) is a prevalent technology deployed in 4G cellular standard which provides data rates up to a few hundreds of Mbps. OFDM has been adopted by various applications: several Wi-Fi and Wireless Local Access Network (WLAN) such as IEEE 802.11a, g, n, WiMax and Long Term Evolution (LTE). The main principle of OFDM is based on a Multi-Carrier Modulation (MCM) technique where high-data rate symbols are split into a multiple lower data rate symbols and are transmitted in parallel [16]. In broadband wireless systems, the transmission of a single-carrier over frequency-selective channel induces ISI because the symbol time is less than delay spread of wireless channel. An important concept when implementing a MCM technique is the increase of the symbol time where the signal-carrier is spread out on sub-carriers and in turn, a signal bandwidth to sub-bands. The sub-carriers spectra in OFDM overlap and are orthogonal to increase the number of sub-carriers and to improve the spectral efficiency. This is an important differentiator from Frequency Division Multiplexing (FDM) which also utilizes MCM technique. In the OFDM transmitter, since a much number of sub-carriers is used, a numerous number of modulators or oscillators is required with having a precise sub-carriers spacing. The design such that physical system is extremely complicated, and consequently Inverse Fast Fourier Transform (IFFT) is implemented to generate sub-carriers which are harmonically related. Then, the use of Cyclic Prefix (CP) is also an efficient step to overcome ISI whereas a portion from the end of sub-

carrier is appended to the beginning of the sub-carrier [17]. The length of CP must be greater than maximum delay spread of wireless channel to combat ISI. After the symbols are transmitted, the inverse processes are naturally applied in the OFDM receiver to extract the transmit symbols. OFDM is a convenient technology in mm-wave RoF communication systems to eliminate fiber impairments. The symbols transmitted over the optical fiber are suffered from time delay induced by the chromatic dispersion effect of the fiber, and thus the addition of a CP can overcome the effect of disperitive channel. RoF can use OFDM to increase power efficiency and to improve the performance of systems and increasing the distance [18],[19].

1.2.2 Optical Systems

Microwave communication systems are deployed to both wired and wireless applications while the data rates are a several tens of MHz, and the number of repeater spacing required is high to compensate the transmission losses. Optical systems with advent the laser and optical fiber have been attracted a lot of concerns for optical communications, which support unlimited bandwidth and very low losses for long distance. The first common semiconductor laser was demonstrated in 1969 and was developed to be used as an optical source for transmission systems [20]. The optical fiber was pioneered in the 1970s and was suffering from losses more than electrical cables [21]. Afterwards, during 1980s and beyond, steady progress in the optical transmission systems was initially achieved a high advanced performance of laser and optical fiber.

Optical systems are significantly permeated in communication networks after much developments on optical components. The Bit rate-Distance (BL) has increased to meet the requirements of high-speed communication networks, where B is the bit rate and L is the repeater spacing. The first generation of lightwave systems employed lasers operating near 0.8 microns and used a multi-mode fibers for a bit rate of 45 Mbps, with repeater spacings of up to 10 km. Then, lasers working at wavelength of 1.3 microns were used in the second generation of optical networks, and the data rates transmitted through single-mode fiber were up to 1.7 Gbps for 50 Km of a repeater spacing. Afterwards, developments were obtained a single longitudinal mode laser and very low losses of optical fiber. The third generation commercially operated at 1.55 microns with single longitudinal modes where the bit rates achieved up to 10 Gbps, and the distance between electronic repeaters was limited to 60-70 km [1].

Then, optical fiber amplifiers were invented in 1989 for high expanded transmission distance while operating over the C-band, with low cost and very low noise. Electronic repeaters were replaced by optical amplifiers, allowing to be the signal in the optical domain. The fourth generation of lightwave systems using optical amplifiers can meet the requirements of the transmission distance problem [1]. With all these developments on optical source, fiber, and amplifier, different technologies are implemented to increase data rates for RoF transmission purposes.

Wavelength Division Multiplexing (WDM) is a widespread technology deployed for the internet to reduce traffic induced by increasing number of applications. Along advent a WDM in 1992, the data rates increased for network throughput, and bit rate of 10 Tbps was achieved in 2001. WDM exploits a multiplexing technique similar to FDM in the radio communications in order to increase the network capacity. It uses Multiplxer and Demultiplxer (MUX/DEMUX) to switch the information in the optical domain. This technology divides the optical spectrum into

several channels, and the data is independently applied with direct or external optical modulator on the optical carriers. Then, the MUX using Arrayed Waveguide Grating (AWG), as an example, with precise phase shift is used to add different wavelength and transmitting by a single optical fiber. The receiver part used DEMUX for spread the data corresponded wavelengths. Optical amplifiers such as Erbium Doped Fiber Amplifier (EDFA) are the main component for long-haul transmission with higher data rates in WDM technology. In this case, all WDM channels must operate EDFA operating range. It is important to mention that the data rate on each WDM channel have a lot of concerns because it influences on the available operational wavelengths. Then, the crosstalk problem can be occurred when the grid spacing is lower than data bandwidth as compared to a high-data rate [22].

Passive Optical Network (PON) is proposed for the next generation of optical communications networks. In the PON configuration, a core network or Central Station (CS) is connected to a Remote Node (RN) by a single optical fiber [23-25]. Optical Line Terminal (OLT) in the core network is employed to carry signals from different users which can be multiplexed in time, wavelength or OFDM. When each user has been assigned corresponding data in different time slot which is applied TDMA technology, the topology is termed as TDMA PON networks [26]. The data of users can be allocated using different wavelengths, the architecture is called as WDM PON networks [27-29]. When the OFDM signals are separated by sub-carries to a specific user, the technique is known as OFDM PON networks [30]. However, passive and active optical components are used to manage the network connectivity in the RN. The received signals are then split using passive multiplexers which control optical signals to the dedicated Optical Network Unit (ONU). Then, the active optical-electric conversion is used to convert the data from optical domain to electrical domain for transmitting the data to end-user. ONU can send data from RN to OLT as upstream data in radio standards.

Fiber To The Home (FTTH) the greater data rates for large transmission distance are achieved in core networks and metropolitan area networks from WDM and PON. However, investigations are now concentrated on how can all optical access networks be implemented to perfectly exploit inherent advantages of the optical fiber for future broadband services. Access networks are basically indicated to the 'first/last' mile of optical networks, which connect end-users to the nearest node on the metro network. Electrical cables such as coaxial cable are used in current access networks due to cost-effective, but these cables prevent using the unlimited bandwidth and worthwhile distribution. Therefore, a promising solution is to open the "last-mile bottleneck" for higher data rate and distance through the use of optical fiber. This is known as FTTH which is future-proof for next generations of all optical access networks 10 years ago [31]. The cost for replacing a copper transmission medium in fiber-based optical systems is very high, and the developments are in process to attain all optical access networks. Further categories of FTTH are implemented: Fiber To The Node (FTTN) is utilized for 150 km of fiber length to transmit data, Fiber To The Cabinet (FTTC) with 150 m of the end-user and Fiber To The Block (FTTB) for commercial nodes, but FTTH is directly used optical fiber from household to the end-users. They can be referred as Fiber To The X (FTTx) for various acronyms architectures where the data rate is expected up to 100 Mbps downstream per user [32]. Current solution is to keep the coaxial cable in the access network with implementing advanced modulation formats to increase in spectral efficiency for exploiting a huge data rates

from core or metro networks involved optical fiber. The architecture of networks utilizing optical fiber and coaxial cable can be termed as Hybrid Fiber-Coaxial (HFC) network [7]. For data transmission, a coaxial cable used between each subscriber and an RN carries lower data rate while the electric-optical conversion process is carried out to transmit higher data rate from RN to the core network for uplink and from the core network to RN for downlink.

1.3 Millimeter-wave in Communication Systems

Technological and cultural evolution would substantially depend on wireless communication systems. Through past years, wireless communications are ubiquitous, and they are deployed in many different applications, from communications to sensing. Ultra high-data rates and improving performances of wireless networks are important subjects of concern to satisfy future customer requirements. Inherently, a system requiring a high-data rate is directly translated to a demand of high available bandwidth [7]. Since a majority of current wireless communication systems utilizes highly crowded frequency bands, various wireless technologies such as CDMA, MIMO and OFDM exploited the limited bandwidth for increasing data rates of exacting and future communication systems [12]. However, this increasing is insufficient, and those technologies increase complexity, cost and power consumption [6]. Therefore, the use of much higher carrier frequencies was proposed as a key solution for larger available bandwidth [2],[7]. The sizes of RF components at higher frequencies is much smaller and can be integrated with other circuits to reduce the challenges of the design [7].

Millimeter-wave (mm-wave) frequency band and beyond has been driven a lot of research to overcome the saturation of spectral resources [7]. The mm-wave corresponds to frequency from 30 GHz to 300 GHz, associated to wavelength from 10 mm to 1 mm, respectively. Considerable numbers of commercial applications are present such as high-speed wireless networks, online video streaming and conferencing, high-speed file exchange, high-definition TV (HDTV) and tera-bit medical video data transfer. The premise behind mm-waves is to offer a high available bandwidth and a high transmitted power. Wireless communications at 60 GHz has been attracted much attention where the unlicensed continuous frequency band of 5 GHz around 60 GHz in many countries is allocated for wireless transmission while maximum power around 10 dBm is necessary to avoid a high path loss [6]. Consequently, 60 GHz systems do not require complex modulation formation that reduces cost efficient and complexity.

Due to different propagation characteristics in mm-wave and THz, new architectures are strongly needed to constitute mm-wave communication systems. Phase Locked-Loop (PLL) frequency synthesizer and Voltage-Controlled Oscillator (VCO) can generate mm-wave carriers which lower phase noise, low power consumption, sufficient output power, large frequency tuning range and small chip area are strictly required as important specifications of communication systems. Since early experiments, III-V semiconductors were used for 60 GHz transceiver components while in the past few years, Complementary Metal Oxide Semiconductor (CMOS) and BiCMOS technology were employed for designing and fabrication of active and passive components such as filters, modulators, amplifiers and antennas in 2006 [33],[34]. Some challenges were emerged because the solid-state materials are much demanded for designing and fabrication of electric components in most mm-wave applications [35],[36]. In 60 GHz region,

wireless transmission is suffered from a huge attenuation due to the free-space path loss, governed by Friis transmission equation, which increases with square of frequency. The enormous atmospheric attenuation due to oxygen resonance at 60 GHz makes wireless communications in this frequency range adapted for short distance or indoor systems as can be shown in Fig. 1.1 [8]. The atmospheric attenuation varies significantly with frequency as presented in Fig. 1.1. Peaks absorption values at 60, 119, 183, and 325 GHz correspond to a high molecular absorption. From this figure, these peaks can divide the spectrum into four windows: 35, 90, 140, 220 GHz which can overcome the limitation of radio waves. The specifications of these windows by the lower attenuation value and wide bandwidth can be suited these windows to wireless communications with high-data rate [37]. Few bandwidths at these frequencies are used for other communication applications.

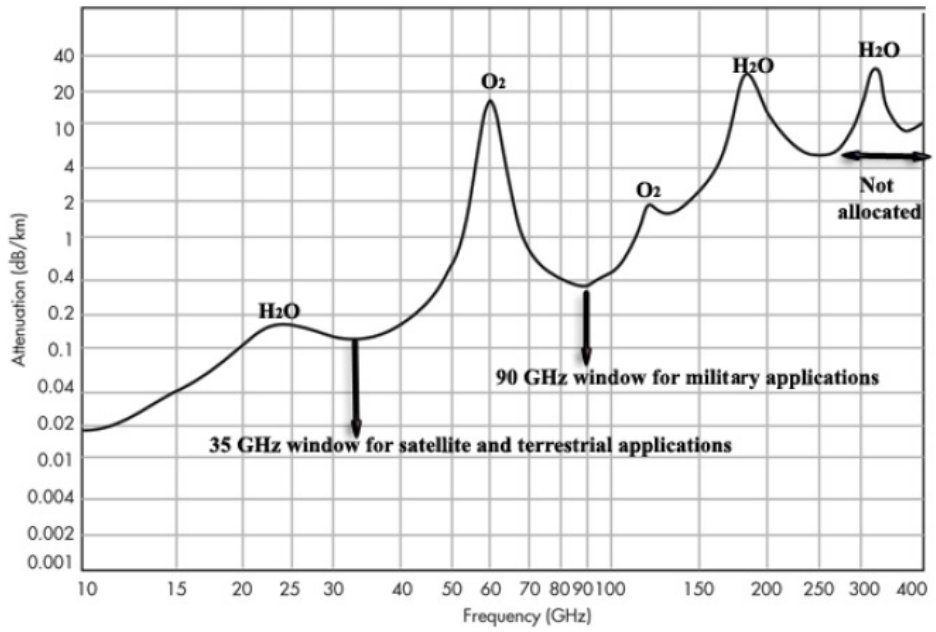

Figure 1.1: Attenuation through different frequencies [8].

With arising interesting in 60 GHz technology, regulators proposed unlicensed frequency allocation and all parameters used for communication systems in many countries. The European Telecommunications Standards Institute (ETSI) and the European Conference of Postal and Telecommunications Administrations (CEPT) in Europe established a frequency allocation the 57-66 GHz for unlicensed operations [38]. In the United States, the Federal Communication Commission (FCC) legislated the unlicensed band at 59-64 GHz [39]. In Japan, the Ministry of Public Management, Home Affairs, Post and Telecommunication (MPHPT) standardized the 59-66 GHz unlicensed frequency allocation [40]. After the number of commercial applications utilizing 60 GHz communications was rapidly growing, the radio regulatory organizations legislated different international standards. The European Computer Manufacturers Association (ECMA) ratified the first edition of standard ECMA 387 in December 2008 for high-rate 60 GHz wireless networks in short range communications to standardize PHysical Layer (PHY), distributed Medium Access Control (MAC) and a HDMI Protocol Adaption Layer (PAL). The second version was issued in December 2010 [41]. IEEE 802.15.3c was published to develop

alternative PHY for IEEE 802.15.3 WPAN, and the amendments would be carried out for other IEEE edits [42]. All of the standards utilize different formats of digital modulation and single carrier or multi-carriers.

On the other hand, TeraHertz (THz) frequency band offers another solution for higher frequency carriers where the unprecedented growth in wireless communication systems [7]. Future applications demand higher than the available bandwidth of 5 GHz around 60 GHz to achieve higher data-rates and to reduce the network traffic where THz frequency range refers to the band between 300 GHz and 3 THz. The use of THz are applied for imaging, spectroscopic applications, and high-resolution multimedia services [43]. In THz frequency range, there are unoccupied bandwidth of gigahertz windows while the attenuation from water vapour adds losses with the free space path loss [8]. The IEEE802.15 Terahertz Interest Group was established in 2007 to provide the feasibility and conditions of the THz band. The World Radiocommunication Conference (WRC) have started to legislate a standard for THz specifications for wireless transmission systems [44].

In particular, THz communication links require THz generation, and therefore, it can be carried out different approaches. As mm-wave, THz can be generated by oscillators or synthesized taking into account the specifications of the THz signals. Due to extremely limited spectral frequency in microwaves, the up-conversion of microwaves to THz can be realized using mixer, but mixer behavior can limit the efficiency of this method. While the InfraRed (IR) frequency band can be a solution with big problems because there are some hindrances such as incoherent receivers, eye-safety and light noise, the down-conversion of the infrared waves can be generated THz radiation [7].

After improvements of THz components, the applications are now focused on how can be exploited the huge available bandwidth. THz technology is based on solid-state materials for developing the THz sources. The linewidth of the THz carriers are the main topic of concern to increase the signal quality. Mm-wave and THz carriers can provide broadband applications while increasing the system performance, but the limitation of the path loss limits these applications.

1.4 Radio-over-Fiber Communication Systems

The broadband communication systems completely employ a large available bandwidth at frequency of 60 GHz, but the free space losses at that frequency is a huge hurdle in an RF wireless transmission. For this, the tendency is to find other techniques for transmitting ultra high-data raters through very long distance. With the developing laser and optical fiber, optical communications have been carried out for transmission purposes [1]. The integration between radio and optical components is accomplished for the provision of a prevalent technology known Radio-over-Fiber (RoF). Microwave photonics have intensely been expanded to implement compact mm-wave RoF communication systems which can use the unlicensed spectral bandwidth of 5 GHz in most countries and high performance of the transmission link [45]. The RoF technology is a pioneer architecture and has been attracted much interest for future wireless applications. The advanced priorities of laser can generate mm-wave carrier through optical hetero-

dyning on a high-speed photodiode (PD) with cost-efficient, higher power, and large tunable frequency range based on generation technique. The generous available bandwidth and very low loss of optical fiber can enlarge data rates and transmission coverage [2].

The mm-wave RoF communication system is proposed in Fig. 1.2. Generally, optical generation is implemented in the Central Station (CS) while the optical signals carrying data are transmitted from the CS to the Base Station (BS) by an optical fiber, where baseband or Intermediate Frequency (IF) signals can be transmitted to BS for other applications used, known as BaseBand-over-Fiber (BBOF) or Intermediate Frequency-over-Fiber (IFOF). Optical modes are mixed on a high-speed PD at the BS to generate electrical mm-wave signal which is then transmitted to a Remote Antenna Unit (RAU) or Remote System Unite (RSU). Then, the generated signal in BS is distributed to Mobile Station (MS). In this architecture, the complexity of generation and modulator is suited in the CS to reduce the amount of components in the BS where filer and amplifier can be added in the BS to improve the performance link. For the uplink, the data from users is transmitted to BS at mm-wave frequencies, and then the mm-wave signals are down-converted to a lower frequency band to avoid a high frequency modulation in each BS and broadband optical receiver in CS. The down-converted uplink signal can modulated the optical carrier from laser using External Optical Modulator (EOM). At the CS, the low cost optical receiver can recover the data which is in a low frequency band. Multi-Mode Fiber (MMF) can carry the data for downlink as well as uplink directions along the same fiber. WDM can also be employed for two directions at different wavelengths with the same optical fiber.

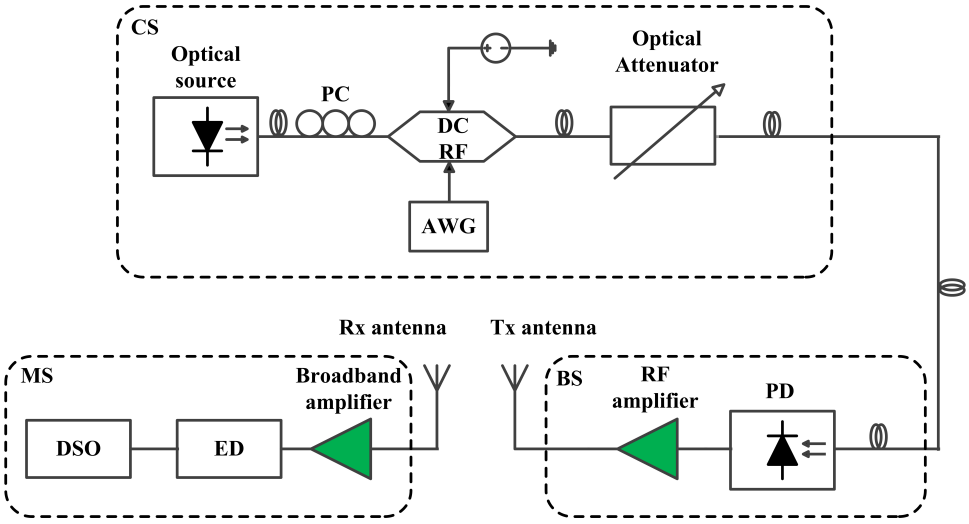

Figure 1.2: A simplified RoF configuration.

Distributed Antennas System (DAS) can be used in RoF systems for increasing the capacity in some locations such as building, hotel, airport, and hospital [46]. The signals are transmitted from CS to a large number of remote sites known as pico cells through optical fiber. Then, DAS transmit the electrical mm-wave signals through antennas to the end-users [47].

In the CS optical generation is needed where at least two coherent optical lines can be mixed on a high-speed PD at the BS to generate mm-wave signal. An advantage of heterodyning advantage is that mode beating avoids any external electrical oscillator [48], for example by

beating two independent running lasers [9]. In this approach, the resultant signal exhibits a large phase noise induced by laser linewidth, wavelength fluctuations and mode correlation [49]. Then, monolithic dual Distributed FeedBack (DFB) lasers are developed for obtaining a narrow linewidth beat note with reduced phase noise [50]. Another approach uses quantum dash mode-locked laser (QD-MLL) to demonstrate mm-wave beat note linewidth around 100 KHz [48]. The applied advanced modulation on the 60 GHz RoF communication systems is carried out for very high data rates [9]. In the THz frequency domain, the transmission of 350 carriers in the indoor environment has been studied in [51]. Photonic components are a popular technology to generate THz carriers transmitting over fiber [51]. Uni-Traveling Carrier (UTC) photodiode can be utilized for heterodyning process at THz frequency band [52]. Two free coherent lasers or a Quantum Cascade Laser (QCL) can be used to provide a linedwidth of THz carrier of tens of kHz [53],[54].

1.5 Optical Generation

The principle of generating mm-wave signals through optical heterodyning requires a beating of at least two optical lines on a high-speed photodiode (PD). The frequency difference between optical lines equals to the desired mm-wave frequency. The optical fields of two lasers are represented as:

$$E_1(t) = E_{01} \exp\Big[j\big(2\pi f_1 t + \phi_1(t)\big)\Big] \tag{1.1}$$

$$E_2(t) = E_{02} \exp\Big[j\big(2\pi f_2 t + \phi_2(t)\big)\Big] \tag{1.2}$$

where E_{01} and E_{02} are the amplitude, f_1 and f_2 are the frequency and ϕ_1 and ϕ_2 are the phase of individual optical waves. The photodetected current at the output of a PD is proportional to the square of the combined two signals which is expressed as:

$$\begin{aligned} I_{PD}(t) &= RP_{opt} \\ &\propto R\Big(E_1(t) + E_2(t)\Big)\Big(E_1(t) + E_2(t)\Big)^* = R\Big|E_1(t) + E_2(t)\Big|^2 \\ &= R\Big(E_{01}^2 + E_{02}^2\Big) + 2RE_{01}E_{02}\cos\Big(2\pi(f_2 - f_1)t + \big(\phi_2(t) - \phi_1(t)\big)\Big) \end{aligned} \tag{1.3}$$

where R and P_{opt} represent the responsivity of the PD and the received optical power, respectively. The first term of Eq. (1.3) demonstrate DC components of the two optical waves while the second term denotes the beating signal created during the simultaneous detection of the two optical fields. The optical heterodying exhibits a phase noise $(\phi_2(t) - \phi_1(t))$ and the frequency stability of the electrical mm-wave signal which varies due to the correlation between these optical signals. Therefore, several optical techniques for generating have been implemented on how the two optical waves are beating to reduce the phase noise.

1.5.1 Two Incoherent Single-Mode Lasers

The simplest and cheapest method to generate mm-wave signals is a beating of two independent single-mode lasers on a high-speed PD which is known as optical heterodning. Two lasers, such

as DFB lasers can be employed, and they are adjusted and controlled by the temperature and the bias current to tune in frequency range and optical power. The schematic diagram of two independent lasers is shown in Fig. 1.3. In this approach, the generation of higher frequencies and THz frequencies can be carried out while the limitation of the PD bandwidth can constrain the carrier frequency.

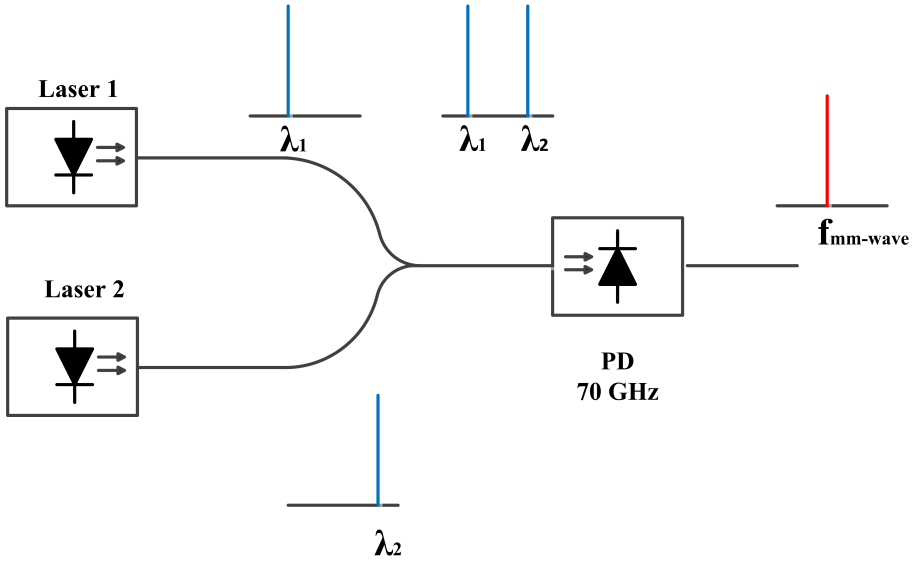

Figure 1.3: Two free running lasers generating mm-wave.

Without any locking scheme, the resultant signal exhibits a large phase noise which is induced by laser linewidth, wavelength fluctuations and mode correlation [55]. The important concept when generating mm-wave carrier is the purity of the mm-wave signal. The last term of Eq. (1.3) presents the phase noise on the mm-wave signal, and therefore the frequency stability of the system is very low. In this configuration, two phase correlated or locked optical lines are required because the phase noise can be mitigated for better system quality.

1.5.2 Optical Phase Lock Loop (OPLL)

According to the independence of two laser sources, optical phase lock loop method is implemented to increase a generated signal quality. Two incoherent lasers are used to generate beating signal, but the mm-wave signal is then split into two paths. The resulting mm-wave signal in one branch is amplified and mixed with a reference signal by an RF mixer. The resulting phase error between the mm-wave signal and the LO signal is injected into one of the lasers, slave laser, to track the master laser with a frequency separation equal to the desired mm-wave frequency [56-58]. The other path is connected to the RAU for transporting mm-wave signals to mobile stations. The cost and complexity are high because of the required pure signal from LO, and the setup is presented in Fig. 1.4.

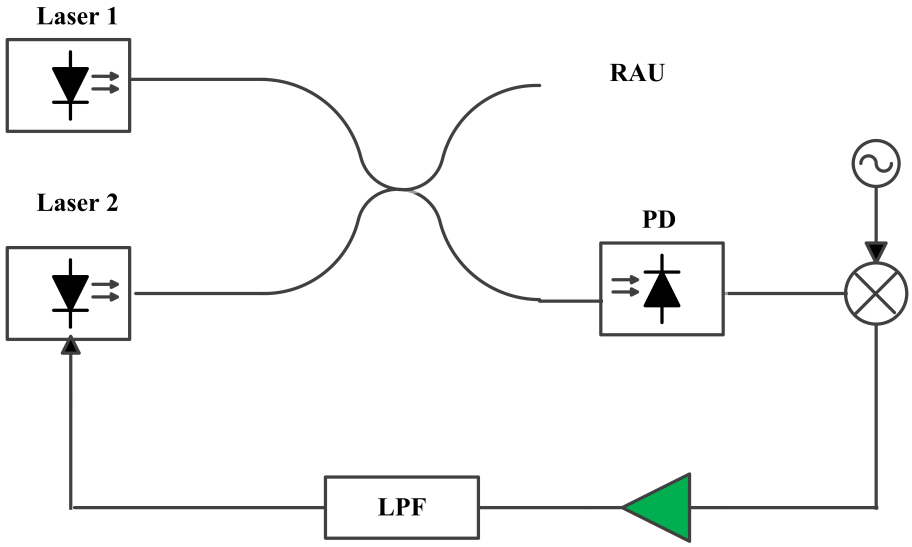

Figure 1.4: Generation of mm-wave using OPLL.

1.5.3 Optical Injection Locking (OIL)

In particular, optical injection technique reduces the phase noise of the mm-wave carrier through phase correlated or locked among optical signals. A direct modulation is applied on the master laser, and thus several sideband components around the central wavelength of the optical signal are generated where the frequency separation equal to the LO frequency. Then, the output of master laser is injected into two slave lasers which their wavelengths are tuned close to the nth sideband components in order to achieve injection locking process [59],[60]. As can be seen in Fig. 1.5, the implementation of this technique is shown. In this approach, the generated mm-wave possesses very low phase noise, and the low frequency of LO is used because the slave laser is locked with one of the several sideband components. On the contrary, due to injection process the system implementation for this technique is suffered from a high complexity.

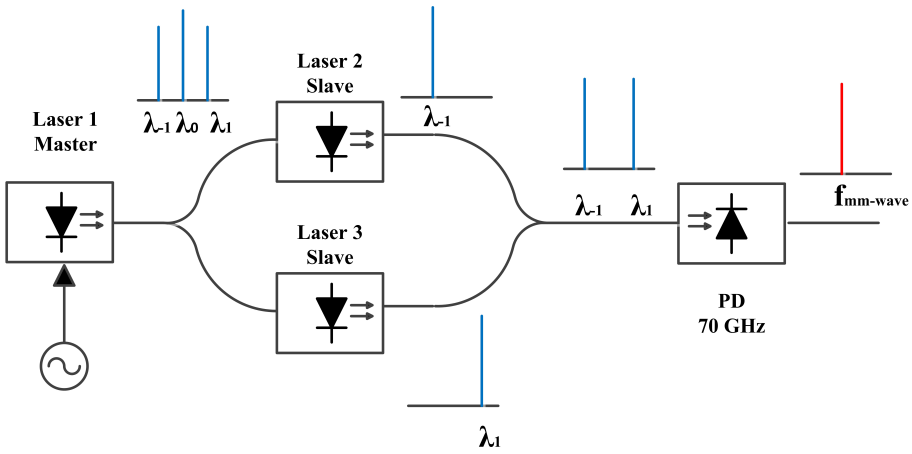

Figure 1.5: Generation of mm-wave using OIL.

1.5.4 Optical Injection Phase Locking (OIPL)

This method combines OPLL and OIL concepts where the master laser is directly modulated by an RF source. Therefore, the resulting optical wave with its sidebands is split into two paths: one is injected into the slave laser as in OIL method, and the second is combined with the output of the slave laser to beat on a PD. The generated mm-wave signal is mixed by an RF mixer to compare with the reference signal and then it is injected on the slave to lock the phase error [61]. Fig. 1.6 shows the implementation of the approach.

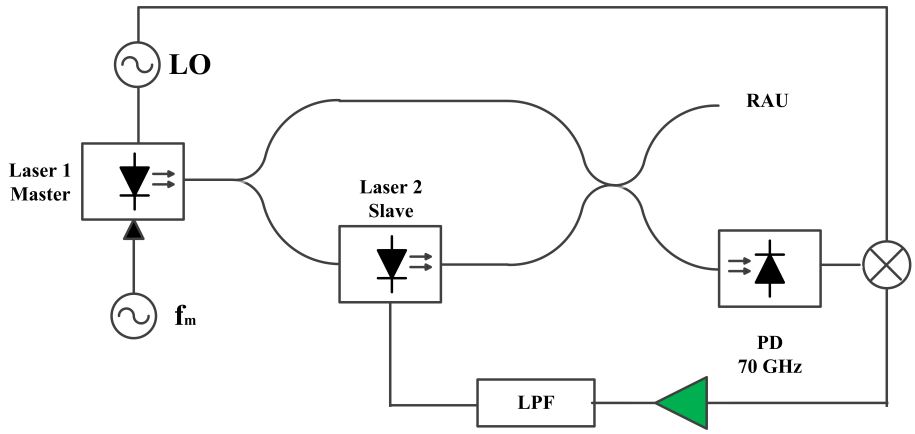

Figure 1.6: Generation of mm-wave using OPLL and OIL.

1.5.5 Optical Modulation

A single-mode laser and intensity modulation can be employed to generate a desired mm-wave and to minimize phase noise, as well. In this approach, the coherent optical signals are generated from directly or externally optical modulation of the laser intensity using an RF signal. Therefore, the Double Side Bands (DSB) around the optical frequency are exhibited at a desired frequency. The phase noise on electrical generated signals is induced from the quality of the RF signal applied for modulation. The first scheme in Fig. 1.7 (a) presents direct modulation by simply modulating the bias current of the laser by an RF source. The configuration of this technique is very simple, but the modulation bandwidth is limited to 10 GHz. This technique is exploited on the base band optical transmission, but this also induces chirp.

According to the limited bandwidth of the direct modulation, an external modulation through Electro-Optic Modulator (EOM) such as Mach-Zehnder Modulator (MZM) is applied on the optical field from a laser as shown in Fig. 1.8 (b). The optical spectrum at output of the EOM contains the optical carrier and DSB separated with the desired mm-wave frequency, which results in the chromatic dispersion of the mm-wave power. This technique also suffers from a high insertion loss [62]. Other techniques are implemented to increase the quality of a mm-wave signal. Single Side Band (SSB) can be realized by optical filtering or one of side band [63]. Dual-Drive Mach-Zehnder Modulator (DDMZM) can generate SSB with the optical carrier. When biasing an EOM at the minimum transmission point, the optical carrier is omitted at the output of EOM [62]. In this case, half of the frequency for the LO is required to separate

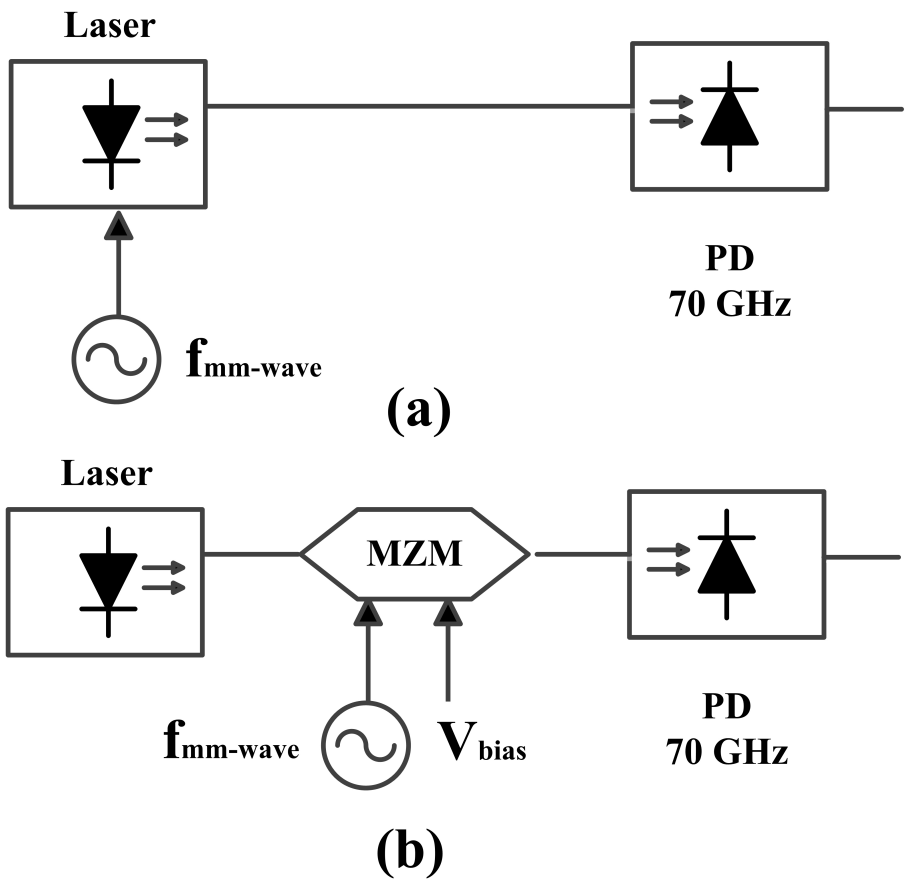

Figure 1.7: Generation of mm-wave using (a) Direct (b) External modulation.

the desired mm-wave frequency between two side bands, but a large RF drive power is required on external modulator.

1.5.6 Optical Multiple Optical Waves

An optical frequency comb can be a good approach to generate mm-wave carrier with low complexity. RF signal oscillator and optical modulation can be avoided by using optical frequency comb. In comb source, multiple optical lines are emitted simultaneously whereas the frequency separation between two optical modes is equal to the desired mm-wave carrier known as Free Spectral Range (FSR). This FSR can be adjusted during laser fabrication by changing in the laser cavity.

The schematic diagram is shown in Fig. 1.8. In this method, a mode locked is important to produce a strong correlation between the optical modes in order to reduce the phase noise on the mm-wave. since the phase of optical modes differ by a constant phase shift, the time would be a constant. Thus, more frequency stability is induced as well as low phase noise. For this approach, the chromatic dispersion is a big disadvantage, so optical filter can be used to choose two optical modes.

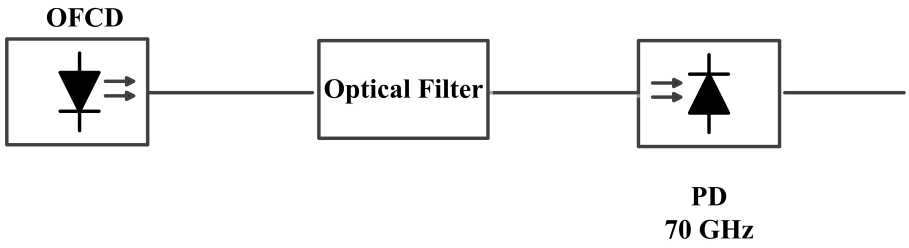

Figure 1.8: Generation of mm-wave using MLLD.

MLLD can be fabricated by two different techniques: active mode locked laser and passively mode locked laser. In active way, a periodic modulation of the cavity is required where a very fast shutter is placed in the laser cavity to make light plus which makes a round trip inside it. This can be achieved by a semiconductor electro-absorption modulator or an acousto-optic modulation [64]. Passive way, for ultra-short optical pulses a non-linear medium is placed into laser cavity such as saturable absorber. Using non-linear optics where the light intensity modifies the refractive index can generate the short optical pulse [65].

A Gain Switched Laser (GSL) is another method to generate optical comb through the gain switching technique. It works by switching the optical gain through direct modulation on the laser. The vast priority of GSL is an easy control on the frequency repetition through changing the RF source frequency. A Direct Current (DC) bias and an RF signal generator are applied on a semiconductor laser such as DFB. In the beginning, when the bias current is increasing, the photon density in increasing. After the biased current is above the threshold current, the lasing process occurs and the carrier density reaches a maximum. Then, the carrier density is reduced to start with the second peak when the RF source continues his process [66],[67].

Fabry Perot laser is another approach for multi modes laser using ALGAINAS-InP. It is exhibits phase locking which induce a narrow linewidth of the beat note. This kind of lasers is well studied in [68].

1.6 Transmission over radio over fiber

When a data is transmitted over a transmission system to a receiver, it is essential to determine the effects of system imperfections on the data. Important metrics are defined for measuring and expressing a system performance, i.e.; Error Vector Magnitude (EVM), Signal-to-Noise Ratio (SNR), and Bit Error Rate (BER). The optical source and the optical fiber are two major aspects which can influence on the mm-wave RoF communication systems.

1.6.1 Metrics

Error vector magnitude: After a complex digital modulation format is applied on an ideal transmission system, the symbols of transmitted or received signals should be in the ideal locations on the constellation diagram. EVM is a main metric to characterize by how much the received symbol has deviated from the ideal symbol. Thus, the EVM values represent the effect

of various imperfections on the actual transmission system due to fluctuations in the amplitude and phase of symbols [69]. The EVM is a common parameter quoted specification for system performance in ECMA 387 and IEEE 802.15.3c. The definition of EVM is the ratio between average power of the error $P_{error}$and the power of the reference signal P_{signal} as expressed:

$$\text{EVM(dB)} = 10 \times \log\left(\frac{P_{error}}{P_{signal}}\right) \tag{1.4}$$

The Root-Mean-Square (RMS) of EVM can be calculated as [70]:

$$\text{EVM}_{\text{rms}} = \sqrt{\frac{\frac{1}{N}\sum_{i=1}^{N}|R_i - S_i|^2}{\frac{1}{N}\sum_{i=1}^{N}|S_i|^2}} \tag{1.5}$$

where R_i and S_i denote the reference and measured symbol of i point, respectively. N is the number of the transmitted symbols. The expression of EVM which demonstrates the impact of the amplitude and phase noise can be shown as:

$$\text{EVM} = \sqrt{\frac{1}{\text{PAPR}}\left(\frac{1}{\text{SNR}} + 2 - 2\exp(\frac{-\sigma^2}{2})\right)} \tag{1.6}$$

where SNR is the signal-to-noise ratio, σ is rms value of the phase noise, and $PAPR$ is the peak-to-average power ratio for a given modulation determined from the ideal constellation.

Signal-to-noise ratio: The noise of transmission system can influence on the signal quality [12], SNR measures this effect on the system which represented as:

$$\text{SNR} = \frac{P_{signal}}{P_{noise}} \tag{1.7}$$

where P_{signal} and P_{noise} are the signal and noise power, respectively. SNR can be related to the EVM which can further be defined as:

$$\text{SNR} \approx \frac{1}{\text{EVM}_{\text{rms}}^2} \tag{1.8}$$

Bit error rate: is a widespread metric for any type of communication system based on a digital information [12]. In the contrary, BER can detect the fluctuations on the amplitude and the phase signals when the large variations are occurred.

1.6.2 Optical Impairments

The phase noise degrades the signal quality where the ideal signal is pure signal and the stabilization is very high, but in the actual system the impact of phase noise is exhibited and the system has low stability.

The optical sources employed in mm-wave RoF communication systems generate optical noise which degrades the system performance. The purity of mm-wave signals is very important when generating mm-wave frequency. Optical source produces optical noise represented in phase and intensity noise. Coherent optical source is a conventional method for generating

correlated phase optical lines which reduces the impact of phase noise on the beat note carriers. Mode-Locked Laser Diode (MLLD) as a coherent comb source generates a wide optical spectrum with precise frequency space. Utilizing coherent optical comb in CS and transmitting optical modes through kilometers of optical fiber, chromatic dispersion inevitably results in Group Velocity Dispersion (GVD) on a PD in BS. In case a high optical power is deployed, a non-linearity effect can be emerged as well. Chromatic dispersion can decorrelate the phase among optical lines, and thus the beating signal at MS has lowering Quality of Service (QoS) in the system [11],[72].

1.7 References

[1] G. P. Agrawal, "Fiber-Optic Communication Systems", 4th Edition. Wiley, 2010.

[2] A. J. Seeds, and Keith J. Williams. "Microwave photonics", Journal of Lightwave Technology 24.12 (2006): 4628-4641.

[3] R. Gaudino, et al., "Perspective in next-generation home networks: Toward optical solution?", Communications Magazine, IEEE, vol. 48, no. 2, pp. 39-47, 2010.

[4] M. J. Halonen, T. and J. R. Garcia,"GSM, GPRS and EDGE Performance Evolution Towards 3G/UMTS", Halsted Press, New York, NY, USA, 2002.

[5] B. G. Lee and S. Choi, "Broadband Wireless Access and Local Networks: Mobile WiMax and WiFi", Artech House, London/ Boston, 2008.

[6] N. Guo et al, "60 GHz millimeter-wave radio: principle, technology and new results", Eurasip J. Wireless Communication Networks, P. 8, 2007.

[7] T. Kleine-Ostmann and T. Nagatsuma, "A Review on Terahertz Communications Research", J. InfraredMilli TerahzWaves, Vol. 32, pp. 143-171, Feb. 2011.

[8] P. Smulders, "Exploiting the 60 GHz band for local wireless multimedia access: prospects and future directions", Communications Magazine, IEEE, vol. 40, no. 1, pp. 140-147, 2002.

[9] A. Stohr et al., "60 GHz radio-over-fiber technologies for broadband wireless services" OSA J. Optical Networking, vol. 8, no. 5, pp. 471-487, May 2009.

[10] R. Khayatzadeh, J. Poette, and B. Cabon, "Impact of phase noise in 60 GHz radio-over-fiber communication system based on passively mode locked laser," IEEE J. Lightw. Technol., vol. 32, no. 20, pp. 3529-3535, May 2014.

[11] F. Brendel, J. Poette, B. Cabon, T. Zwick, F. van Dijk, F. Lelarge, and A. Accard, "Chromatic dispersion in 60 GHz radio-over-fiber networks based on mode-locked lasers," IEEE J,

Lightw. Technol., vol. 29, no. 24, pp 3810-3816, Dec. 2011.

[12] U. Madhow, "Fundamentals of digital communication", Cambridge University Press, 2008.

[13] H.B. Kim, et al., "A radio over fiber network architecture for road vehicle communication systems." In 2005 IEEE 61st Vehicular Technology Conference (Vol. 5, pp. 2920-2924). IEEE.

[14] Kanno, Atsushi, et al. "Optical and millimeter-wave radio seamless MIMO transmission based on a radio over fiber technology." Optics Express 20.28 (2012): 29395-29403.

[15] Lin, Chun-Ting, et al., "MIMO radio-over-fiber system at 60 GHz employing frequency domain equalization." Optics express 20.1 (2012): 562-567.

[16] J. Armstrong, "OFDM for Optical Communications," Journal of Lightwave Technology, vol. 27, no. 3, pp. 189-204, 2009.

[17] W. Sheih and I. Djordjevic, "OFDM for Optical Communications", Academic Press, USA, 2010.

[18] C. Browning, K. Shi, S. Latkowski, P.M. Anandarajah, F. Smyth, B. Cardiff, R. Phelan, and L.P. Barry, "Performance Improvement of 10Gb/s Direct Modulation OFDM by Optical Injection using Monolithically Integrated Discrete Mode Lasers," Optics Express, vol. 19, B289-B294, 2011.

[19] E. Martin, T. Shao, P. Anandarajah, C. Browning, V. Vujicic, R. Llorente and L. Barry, "25 Gb/s OFDM 60 GHz Radio over Fibre System Based on a Gain Switched Laser", (Invited Paper), Journal of Lightwave Technology, Vol. 33, Iss. 6, Jan. 2015.

[20] Agrawal, Govind P., and Niloy K. Dutta. "Long wavelength semiconductor lasers", (1986).

[21] K. C. Kao and G. A. Hockham, "Dielectric fiber surface waveguides for optical frequencies", Proceedings IEEE, 1966.

[22] C. Murthy and M. Gurusam, "WDM Optical Networks: Concepts, Design, and Algorithms", Prentice Hall, NJ, USA, 2002.

[23] L. Spiekman, "Active Devices in Passive Optical Networks", Lightwave Technology, Journal of, vol. 31, no. 4, pp. 488-497, 2013.

[24] J.-i. Kani, F. Bourgart, A. Cui, A. Rafel, M. Campbell, R. Davey, and S. Rodrigues, "Next-generation PON-part i: Technology roadmap and general requirements", Communications Magazine, IEEE, vol. 47, no. 11, pp. 43-49, November 2009.

[25] R. Davey, J. Kani, F. Bourgart, and K. McCammon, "Options for future optical access

networks", IEEE Communications Magazine, vol. 44, no. 10, pp. 50-56, Oct. 2006.

[26] L. Chang-Hee, W. Sorin, and K. Byoung-Yoon, "Fiber to the Home Using a PON Infrastructure", Lightwave Technology, Journal of, vol. 24, no. 12, pp. 4568-4583, 2006.

[27] Hsueh, Yu-Ting, et al. "A novel bidirectional 60-GHz radio-over-fiber scheme with multiband signal generation using a single intensity modulator", IEEE photonics technology letters 21.18 (2009): 1338-1340.

[28] Pham, Tien-Thang, et al. "A WDM-PON-compatible system for simultaneous distribution of gigabit baseband and wireless ultrawideband services with flexible bandwidth allocation", IEEE photonics journal 3.1 (2011): 13-19.

[29] Chung, Yun C. "Recent advancement in WDM PON technology", European Conference and Exposition on Optical Communications, Optical Society of America, 2011.

[30] K. Kanonakis, E. Giacoumidis, and I. Tomkos, "Physical-Layer-Aware MAC Schemes for Dynamic Subcarrier Assignment in OFDMA-PON Networks", Lightwave Technology, Journal of, vol. 30, no. 12, pp. 1915-1923, June 2012.

[31] J. Park, G. Y. Kim, H. Park, and J. Kim, "FTTH deployment status and strategy in korea", in Globecom 2008, 2008.

[32] S. Gupta, "Residential broadband technologies for high-speed internet access", in IET International Conference on Wireless, Mobile and Multimedia Networks, Jan. 2008, pp. 279-282.

[33] S. K. Moore, "Cheap chips for next wireless frontier", IEEE Spectrum, vol. 43, pp. 12-13, 2006.

[34] B. Gaucher, "Completely integrated 60 GHz ISM band front end chip set and test results", IEEE 802.15 TG3c document: 15-06-0003-00-003c, January 2006.

[35] A. El Oualkadi, "Trends and Challenges in CMOS Design for Emerging 60 GHz WPAN Applications", Advanced Trends inWireless Communications, In Tech, Feb. 2011.

[36] C. Mann, "Practical challenges for the commercialization of terahertz electronics", in-Proc. IEEE MTT-S Int.Microwave Symp., Honolulu, pp. 1705-1708, June 2007.

[37] Attenuation by Atmospheric Gases, ITU-R Standard P.676-6, 2005.

[38] European Telecommunications Standards Institute. ETSI TR 102 555: Electromagnetic compatibility and radio spectrum matters (ERM): System reference document: Technical characteristics of multiple gigabit wireless systems in the 60 GHz range.

[39] Code of Federal Regulation, Telecommunication, title 47, chapter 1, part 15.255, Fed-

eral Communication Commission Std., 2004.

[40] Regulations for enforcement of the radio law 6-4-2 specified low power radio station (11) 59-66 GHz band,Ministry of PublicManagement, Home Affairs, Posts and Telecommunication, Japan Std., 2000.

[41] http://www.ecma-international.org/

[42] https://standards.ieee.org/findstds/standard/802.15.3c-2009.html

[43] B. J. Drouin, F. W. Maiwald, and J. C. Pearson, "Application of cascaded frequency multiplication to molecular spectroscopy", Review of scientific instruments 76.9 (2005): 093113.

[44] B(08)058 annex 3draft cept brief on wrc-11 agenda item 1.6 (bands above 275 Ghz), www.ero.dk.

[45] Su-Khiong Yong, P. Xia, and A. Valdes-Garcia, "60 GHz technology for Gbps WLAN and WPAN: from theory to practice", John Wiley and Sons, 2011.

[46] D. Novak, R. Waterhouse, N. Ampalavanapillai, C. Lim, B. Masuduzzaman, and P. Gamage, "Microwave Photonics", 1st ed. USA: CRC Press, 2007, ch. Hybrid Fiber Radio Concepts and Prospects.

[47] A. Ngoma and M. Sauer, "Radio-over-fiber technologies for high data rate wireless applications", in Sarnoff Symposium, 2009. SARNOFF 2009. IEEE, March 2009, pp. 1-6.

[48] F. Brendel et al., "Low-cost analog fiber optic links for in-house distribution of millimeter-wave signals", International Journal of Microwave and Wireless Technologies, pp. 231-236, Apr. 2011.

[49] L. A. Johansson, and A. J. Seeds, "Generation and transmission of millimeter-wave data modulated optical signals using an optical injection phase-lock loop", J. Lightw. Technol., 21 (2), pp. 511-520, Feb. 2003.

[50] F. Van Dijk et al, "Monolithic dual wavelength DFB lasers for narrow linewidth heterodyne beat-note generation", IEEE International Topical Meeting on Microwave Photonics 2011, pp. 73-76, 18-21, Oct. 2011.

[51] A. J. Seeds, et al., "TeraHertz photonics for wireless communications", Journal of Lightwave Technology 33.3 (2015): 579-587.

[52] C. C. Renaud, D. Moodie, M. Robertson, and a. J. Seeds, "High output power at 110 Ghz with a waveguide uni-travelling carrier photodiode", in Proc. IEEE Lasers Electro-Optics Soc. Annu. Meet. Conf., Oct. 2007, pp. 782-783.

[53] E. Martin, R. Watts, L. Bramerie, and L. Barry, "THz-Bandwidth Coherence Measurements of a Quantum Dash Laser in Passive and Active Mode-Locking Operation", in Optics Letters Vol. 37, Iss. 23, pp. 4967-4969, 2012.

[54] T. Shao et al., "Phase Noise Investigation of Multicarrier Sub-THz Wireless Transmission System Based on an Injection-Locked Gain-Switched Laser", Terahertz Science and Technology, IEEE Transactions, vol. 5, no. 4, pp. 590-597, 2015.

[55] A. Hirata, M. Harada, K. Sato, and T. Nagatsuma, "Low-cost millimeter-wave photonic techniques for Gigabit/s wireless link", IEICE Trans. Electron., vol. E86-C, no. 8, pp. 1296-1300, Aug. 1997.

[56] Z. C. F. Fan and M. Dagenais, "Optical generation of a megahertz-linewidth microwave signal using semiconductor lasers and a discriminator-aided phase-locked loop", IEEE Trans.Microw. Theory Techn., vol. 45, pp. 1296-1300, Aug 1997.

[57] K. J.Williams, et al., "6-34 GHz offset phase-locking of Nd:YAG 1319 nm nonplanar ring lasers", Electron. Lett., vol. 25, pp. 1242-1243, 1989.

[58] L. N. Langley, et al., "Optical phase locked loop (OPLL) module for use as a 9 GHz source in phased array communications antennas", International TopicalMeeting onMicrowave Photonics, 1998, pp. 141-142.

[59] J. Genest, et al., "Microwave signals generated by optical heterodyne between injection locked semiconductor lasers", Quantum Electron., IEEE Journal of, vol. 33, pp. 989-998, 1997.

[60] L. Goldberg, et al., "Microwave signal generation with injection-locked laser diodes", Electron. Lett., vol. 19, pp. 491-493, 1983.

[61] C. Walton, A. C. Bordonalli, and A. Seeds, "High-performance heterodyne optical injection phase-lock loop using wide linewidth semiconductor lasers", Photonics Technology Letters, IEEE, vol. 10, no. 3, pp. 427-429, March 1998.

[62] G. Smith, D. Novak, and Z. Ahmed, "Overcoming chromatic-dispersion effects in fiber-wireless systems incorporating external modulators", Microwave Theory and Techniques, IEEE Transactions on, vol. 45, no. 8, pp. 1410-1415, 1997.

[63] J. Capmany, B. Ortega, A. Martinez, D. Pastor, M. Popov, and P.-Y. Fonjallaz, "Multiwavelength single sideband modulation for wdm radio-over-fiber systems using a fiber grating array tandem device", Photonics Technology Letters, IEEE, vol. 17, no. 2, pp. 471-473, 2005.

[64] L. Hargrove, R. Fork, and M. Pollack, "Locking of he:ne laser modes induced by synchronous intracavity modulation", Applied Physics Letters, vol. 5, no. 1, pp. 4-5, Jul 1964.

[65] J. Javaloyes, S. Balle, E.A. Avrutin, G. Tandoi, P. Stolarz, M. Sorel, C.N. Ironside, J.Marsh,

"Dynamics of semiconductor passively mode-locked lasers: Experiment and theory", In 15th International Conference on Transparent Optical Networks (ICTON), Cartagena, June 2013.

[66] D. Pataca, P. Gunning, M. Rocha, J. Lucek, R. Kashyap, K. Smith, D. Moodie, R. Davey, R. Souza, and A. Siddiqui, "Gain-Switched DFB Lasers", Journal of Microwaves and Optoelectronics, vol. 1, no. 1, May 1997.

[67] H. Shams, P. Anandarajah, P. Perry, and L. Barry, "Optical generation of modulated millimeter waves based on a gain-switched laser", Microwave Theory and Techniques, IEEE Transactions on, vol. 58, no. 11, pp. 3372-3380, 2010.

[68] A. D. Simard, et al., "Multiwavelength super-structured Bragg grating laser for tunable repetition rate mode-locked operation", Optics express 22.14 (2014): 17050-17062.

[69] S. Forestier, P. Bouysse, R. Quere, A. Mallet, J.-M. Nebus, and L. Lapierre, "Joint optimization of the power-added efficiency and the error-vector measurement of 20Ghz pHEMT amplifier through a new dynamic bias-control method", IEEE Transactions on Microwave Theory and Techniques, vol. 52, no. 4, pp. 1132-1141, Apr. 2004.

[70] A. Georgiadis, "Gain, phase imbalance, and phase noise effects on error vector magnitude", IEEE Trans. Veh. Technol., vol. 53, no. 2, pp. 443-449,March 2004.

[71] T. Shao, E. Martin, P. M. Anandarajah, C. Browning, V. Vujicic, R. Llorente, and L. P. Barry, "Chromatic Dispersion-Induced Optical Phase Decorrelation in a 60 GHz OFDM-RoF System", Photon. Technol. Lettrs., vol. 26, no. 20, pp. 2016-2019, Oct., 2014.

Chapter 2

Impact of Relative Intensity Noise on Millimeter-Wave Radio-over-Fiber Communication Systems

This chapter investigates the impact of laser intensity noise on Millimeter-Wave (mm-wave) Radio-over-Fiber (RoF) communication systems employing two different techniques to generate mm-wave signals. The Relative Intensity Noise (RIN) transferred during optical heterodyning of mm-wave signal is theoretically studied and experimentally investigated. Laser RIN induces noise at the resultant electrical mm-wave signal and is directly generated from an initial RIN at low frequency. Therefore, RIN impairs the performance of the mm-wave RoF system. The model of RIN is also presented and is in very close agreement with the experiment results. Furthermore, wireless transmission experiments to demonstrate the intensity noise effect are carried out and are compliant with the communication standards at mm-wave. Wireless transmission up to 3 m can be achieved using a transmit power of +4.5 dBm.

2.1 Introduction

Future wireless applications demand a large sufficient bandwidth to satisfy greater data rates. In the chapter 1, mm-wave frequency band and beyond has been proposed as a solution to overcome the saturation of spectral resources, and RoF has been utilized using optical sources to distribute mm-wave signals. The optical sources employed in mm-wave RoF communication systems generate optical noise which degrades the system performance. The optical noise predominantly originates from laser dynamics and spontaneous emission that induce fluctuations in both amplitude and phase of the optical source field. Phase noise of mm-wave signal generated by optical heterodyning is analyzed and measured in [1].

Laser intensity noise characterized by RIN of laser is an indicator of the laser intensity stability and is usually measured from DC to some GHz in [2] for different RIN levels. In this chapter, the study of RIN in mm-wave RoF communication systems would be explored, and the impact of RIN on close to the mm-wave carrier would be observed on the electrical spectrum. The novelty and originality of the idea are the demonstration of RIN effect on mm-

wave frequency band using two techniques for optical heterodyne generation techniques. The first technique uses two independent Disturbed FeedBack (DFB) lasers without any locking scheme which is the simplest and cheapest way. In this case, phase noise is larger than in other solutions due to high decorrelation between optical lines. The second technique is based on a Passively Mode-Locked Laser Diode (PMLLD) at 60.64 GHz to generate mm-wave signal with advantage of lower phase noise due to the correlation among optical modes of the PMLLD. At the receiver-end, a coherent receiver using a mixer is used for electrical down-conversion. Both theoretical and experimental studies confirm that the RIN phenomenon in mm-wave frequency band is generated from the initial RIN at low frequency. It is worth mentioning that the results of the presented study are applicable to any kind of optical frequency generation technique. Depending on the heterodyne process and the optical power of optical lines, it is shown that RIN at mm-wave signal can be larger than the initial RIN at low frequency and causes spectral degradation in optical heterodyne signals.

The results presented in this chapter examine the impact of intensity noise on EVM for 60 GHz RoF wireless system using 60 GHz antennas and envelope detector (ED) as incoherent receiver. Data rates of 397 Mbps and 794 Mbps with binary phase shifting keying (BPSK) modulation format are applied as well as a data rate of 1588 Mbps with quadrature phase shifting keying (QPSK) modulation format to comply with communication standards at 60 GHz [3],[4].

2.2 Theoretical Principles of RIN

Generating mm-wave signals by optical heterodyning requires at least two optical signals. The optical field of these two signals $E_i(t)$ can be expressed as:

$$E_i(t) = A_i\big(1 + \delta_i(t)\big) \exp\Big[j\big(2\pi f_i t + \phi_i(t)\big)\Big] \tag{2.1}$$

where A_i, δ_i, f_i, and ϕ_i are the amplitude, amplitude noise, frequency, and phase noise of the optical field of mode (*i*), respectively. Different components in an RoF system result in an intensity noise which can be sorted out by optical and electrical noise such thermal noise, shot noise, and RIN.

Thermal noise is caused through electric agitation of electrons when applying a voltage on a conductor. The value of thermal noise depends on the temperature and resistance value of the conductor. The mean squared thermal noise current of load resistance can be described as:

$$\sigma^2_{\textbf{thermal}} = \frac{4kTF\Delta f}{R_L} \tag{2.2}$$

where $k, T, F, \Delta f$, and R_L are Boltzmann constant, temperature, amplifier noise figure, received signal bandwidth, and load resistance, respectively.

Shot noise is generated by optic-electric (O/E) convert component because in any time the statistical value of photons detected by a photo-diode (PD) is intrinsically random. The shot noise varies with the average power at a fixed temperature of the system. The mean squared noise current when a PD in the receiver can expressed as:

$$\sigma^2_{\textbf{shot}} = 2qI|H(f)| = 2qRP_{opt}|H(f)| \tag{2.3}$$

where q is the electron charge ($1.6e^{-19}$ Coulomb), I is the photodetected current of the PD, R is the responsivity of the PD, and P_{opt} is the optical power while $|H(f)|$ represents the transfer function of the system.

Relative intensity noise is originated by a laser source because the output power of the laser fluctuates around the average optical power. When RIN value exceeds the thermal noise and shot noise level of mm-wave RoF communications systems, RIN degrades the system performance. For a standard laser, RIN for each contribution is defined as:

$$\text{RIN}_i(\omega) = \frac{\langle|\delta_{opt}(\omega)|^2\rangle}{\langle P_{opt}\rangle^2} = \frac{\text{PSD}(\omega)}{P_{elec}} = 4\delta_i^2(\omega) \tag{2.4}$$

where $\delta_{opt}(\omega)$ is the optical power variation spectrum, P_{opt} is the optical power, PSD is the power spectral density of the intensity noise, P_{elec} is DC electrical power, and $\delta_i(\omega)$ is the Fourier transform of $\delta_i(t)$, ($\delta_i(\omega) = \text{FT}(\delta_i(t))$). The mean squared current of RIN can be expressed as:

$$\sigma^2_{\text{RIN}} = 10^{\frac{RIN_{dB}}{10}} I^2|H(f)| = 10^{\frac{RIN_{dB}}{10}} R^2 P^2_{opt}|H(f)| \tag{2.5}$$

For each laser, RIN expression from the rate equation was described in [5] as:

$$\text{RIN}(\omega) = \frac{B + C\omega^2}{\left[\omega^2 - \left(\omega_r^2 + \Gamma^2\right)\right]^2 + 4\omega^2\Gamma^2} \tag{2.6}$$

where ω is the considered angular frequency, ω_r and Γ_r are the relaxation angular frequency and damping factor, respectively. B and C are coefficients linked to physical steady state properties of the laser such as gain, spontaneous emission, photon and charge densities.

The total noise detected from all receivers is thermal noise, shot noise and laser intensity noise. Since RIN would solely be determined in the system, the thermal noise and shot noise must be removed from the total noise of the system. All these types of noise at the receiver can be assumed as independent Gaussian noise, and thus, the total system noise is the linear summation of noise effects as:

$$\text{PSD}_{total} = \text{PSD}_{thermal} + \text{PSD}_{shot} + \text{PSD}_{RIN} \tag{2.7}$$

When a laser is turned off, the thermal noise of the system can be measured and extracted from the total noise. Therefore, the shot noise and intensity noise are remained on the total noise.

The statistical determination of the RIN value can be calculated through different methods [2]. The first method depends on measuring a transfer function of the system by a Vector Network Analyzer (VNA) through Scattering (S) parameters. Then, the shot noise can be calculated using Eq. (2.3) and removed from the system noise. Laser intensity noise is solely remained. Using Eq. (2.5), the real RIN can be calculated after knowing the transfer function of the system.

The second method can measure pure RIN without knowing transfer function as:

$$\text{PSD}_{total} - \text{PSD}_{thermal} = 2qI|H(f)| + 10^{\frac{RIN_{dB}}{10}} I^2|H(f)| = aI + bI^2 \tag{2.8}$$

with:

$$\begin{aligned} a = &\quad 2q|H(f)| \\ b = &\quad 10^{\frac{RIN_{dB}}{10}}|H(f)| \end{aligned}$$

Then, the RIN can be calculated as independent of $|H(f)|$:

$$\text{RIN}_{\text{dB}} = 10\log_{10}\left(2q\frac{b}{a}\right) \tag{2.9}$$

Equation (2.8) represents the detected PSD of shot and intensity noise as function of the DC photocurrent which characterizes as a second order of polynomial function. The ratio b over a permits to remove the impact of the transfer function without measuring it. Different values of optical power at the PD through optical attenuator allow the different results of the PSD of shot and intensity noise to be obtained. Using Matlab software, a and b factors can be estimated through fitting process. After substituting a and b values in Eq. (2.9), The RIN values can be measured.

The third method for detecting the real RIN can be used for any level of RIN, even very low level of RIN. In this case, the sensitivity of the system can be improved using a lock-in amplifier. A digital signal generator drives a Mach-Zehnder Modulator (MZM), and a synchronization is necessary between Electrical Spectral Analyzer (ESA) and lock-in amplifier. Then, the same processes are applied as in the second method.

2.2.1 Two Optical Lines

The two optical fields of the two single-mode laser $E_1(t)$ and $E_2(t)$ using Eq. (2.1) can be expressed as:

$$\begin{aligned} E_1(t) &= A_1\big(1+\delta_1(t)\big)\exp\Big[j\big(2\pi f_1 t+\phi_1(t)\big)\Big] \\ E_2(t) &= A_2\big(1+\delta_2(t)\big)\exp\Big[j\big(2\pi f_2 t+\phi_2(t)\big)\Big] \end{aligned} \tag{2.10}$$

When combining the two optical fields at the input of a PD, the photodetected current $I_{PD}(t)$ can be expressed as:

$$I_{PD}(t) = \alpha R P_{opt} = \alpha R|E_1(t)+E_2(t)|^2 \tag{2.11}$$

where α is a proportional factor. After some simple manipulation, the photodetected current can be expressed as:

$$\begin{aligned} I_{PD}(t) = &(I_1+I_2)+\Big(I_1\sqrt{RIN_1(t)}+I_2\sqrt{RIN_2(t)}\Big) \\ &+2\sqrt{I_1I_2}\times\cos\Big(2\pi(f_2-f_1)t+\big(\phi_2(t)-\phi_1(t)\big)\Big) \\ &+\sqrt{I_1I_2}\Big(\sqrt{RIN_1(t)}+\sqrt{RIN_2(t)}\Big) \\ &\times\cos\Big(2\pi(f_2-f_1)t+\big(\phi_2(t)-\phi_1(t)\big)\Big) \end{aligned} \tag{2.12}$$

where I_i is the DC photodetected current of the optical signal $(i,\ i = 1\ or\ 2)$ which can be expressed as $(I_i = \alpha R A_i^2)$. RIN_i is relative intensity noise $\text{RIN}(t) = \text{FT}^{-1}(\text{RIN}(\omega))$, and second order terms related to noise-to-noise beatings have been neglected.

The first term of Eq. (2.12), $I_1 + I_2$ represents the total average current. The second term represents the noise current of two optical signals from DC to some GHz corresponding to the initial relative intensity noise (RIN_{ini}) which corresponds to (RIN_1) and (RIN_2). The third term is the beat note current created during their simultaneous detection where the beat frequency is equal to difference between frequencies of the two optical modes $(f_2 - f_1)$. The last term represents noise current corresponding to RIN close to beat note (RIN_{beat}). The beat note at the frequency of $(f_2 - f_1)$ exhibits a phase noise $(\phi_2(t) - \phi_1(t))$ which amplitude varies due to the correlation between these modes, that depends on how the two optical modes are produced. In the last term of Eq. (2.12), it can be noticed that RIN amplitude at beat note depends on the product of modes amplitudes in opposition to RIN amplitude at low frequency represented by the second term.

After substituting Eq. (2.12) in Eq. (2.4), and as there is no correlation between modes when considering two independent DFB lasers, the auto-correlation function of $\text{RIN}_1(t)$ and $\text{RIN}_2(t)$ equal 0. Therefore, the (RIN_{ini}) at low frequency and (RIN_{beat}) close to the beat signal are then obtained as follows:

$$\text{RIN}_{ini}(f) = \frac{I_1^2 \text{RIN}_1(f) + I_2^2 \text{RIN}_2(f)}{(I_1 + I_2)^2} \tag{2.13}$$

$$\text{RIN}_{beat}(f) = \frac{I_1 I_2 \big(\text{RIN}_1(f) + \text{RIN}_2(f)\big)}{(I_1 + I_2)^2} \tag{2.14}$$

As can be seen in the last term of Eq. (2.12), the product of the mode intensity noise and the carrier in the time domain leads to the intensity noise conversion in the frequency domain directly to the beat frequency. This non-linear process at beat note could lead to an increase of intensity noise during heterodyne process with respect to initial intensity noise at low frequency. This increase is noticeable especially when the optical powers of the two lasers are different. In case the optical signals have the same amplitudes $(I_1 = I_2)$, then $\text{RIN}_{\text{ini}} = \text{RIN}_{\text{beat}}$. While a power difference exists, for example $(I_2 > I_1)$, the RIN_i of the less powerful mode (RIN_1) in this case, is increased by a factor I_2/I_1 in Eq. (2.14) as compared to RIN_i in Eq. (2.13), and thus, RIN_{beat} is larger than RIN_{ini} by a factor I_2/I_1. This phenomenon has not been published by other authors to the best of our knowledge and is evidenced in section (2.3) with both experimental and model results.

2.2.2 Multiple Optical Lines

The optical field $E(t)$ of optical comb source possessing (M) modes equally spaced can be defined as:

$$E(t) = \sum_{i=1}^{M} A_i\big(1 + \delta_i(t)\big) \exp\Big(j\big(2\pi\big(f_0 + i f_{RF}\big)t + \phi_i(t)\big)\Big) \tag{2.15}$$

where A_i, δ_i, and ϕ_i are the amplitude, amplitude noise, and phase noise of i^{th} mode, respectively. f_0 and f_{RF} are the frequency of the first mode and the beat note frequency which corresponds to the Free Spectral Range (FSR). The output current of the PD $I_{PD}(t)$ can be described as:

$$\begin{aligned} I_{\mathrm{PD}}(t) = & \sum_{i=1}^{M} I_i + \sum_{i=1}^{M} I_i \sqrt{\mathrm{RIN}_i(t)} \\ & + 2 \sum_{i,j:i\neq j} \sqrt{I_i I_j} \times \cos\Big(2\pi(f_j - f_i)t + \big(\phi_j(t) - \\ & \phi_i(t)\big)\Big) + \sum_{i,j:i\neq j} \sqrt{I_i I_j} \left(\sqrt{\mathrm{RIN}_i(t)} + \sqrt{\mathrm{RIN}_j(t)}\right) \\ & \times \cos\Big(2\pi(f_j - f_i)t + \big(\phi_j(t) - \phi_i(t)\big)\Big) \end{aligned} \tag{2.16}$$

where i and j are two arbitrary optical modes at each time, and $j = i + 1$. The RIN_{ini} at low frequency and RIN_{beat} at fundamental beat note can be expressed as:

$$\mathrm{RIN}_{ini}(f) = \left(\frac{\sum_{i=1}^{M} \left(I_i \sqrt{\mathrm{RIN}_i(f)} \right)}{\sum_{i=1}^{M} I_i} \right)^2 \tag{2.17}$$

$$\mathrm{RIN}_{beat}(f) = \left(\frac{\sum_{i=1}^{M-1} \left(\sqrt{I_i I_{i+1}} \left(\sqrt{\mathrm{RIN}_i(f)} + \sqrt{\mathrm{RIN}_{i+1}(f)} \right) \right)}{\sum_{i=1}^{M} I_i} \right)^2 \tag{2.18}$$

All beating noise expressed in the last term of Eq. (2.16) which are not used in Eq. (2.18) contribute on noise at harmonics of the fundamental frequency. Equations Eq. (2.17) and Eq. (2.18) can be seen as specific cases of equations Eq. (2.13) and Eq. (2.14) when only two optical modes are considered. RIN expressions of Eq. (2.17) and Eq. (2.18) lead to the expressions of Eq. (2.13) and Eq. (2.14), respectively.

After analyzing RIN using two generic techniques, the following section describes the experimental setup, simulation and results of RIN. Two different techniques are employed for generating mm-wave signal through 2 DFB lasers and PMLLD laser.

2.3 Experimental Setup and Results of RIN by 2 DFB lasers

2.3.1 Experimental Diagram of RIN

The proposed mm-wave RoF communication system to demonstrate the impact of RIN is shown in Fig. 2.1. Two free running optical sources are used whereas this technique is generating decorrelated optical modes which degrades the quality of mm-wave carrier. Two independent DFB lasers, DFB_1 and DFB_2 operating in the C-band, are used to generate a beat note carrier which is adjusted and controlled by the temperature and the bias current of the two lasers. The

Polarization Controller (PC) is utilized for optimizing the beating power, and a (50/50) coupler is utilized to mix the two optical signals on a PD of 70 GHz bandwidth.

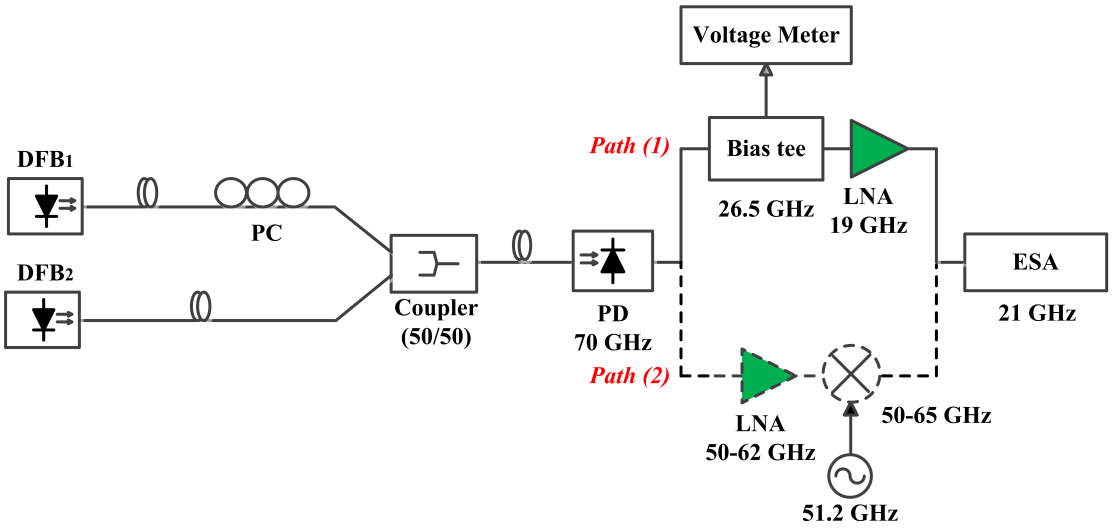

Figure 2.1: Experimental setup for optical heterodyning based on two independent lasers in [9 kHz-19 GHz] and mm-wave frequency band.

The combined signal at output of a coupler is transmitted through a conventional single-mode optical fiber of 1.5 m length to a high-speed PD at the receiver-end. In this case, the beating results from only two modes which are not phase locked, and consequently the fiber length will just impact on the received optical power. For a more accurate recognition between RIN_{ini} and RIN_{beat}, and for avoiding down-conversion stage, we first present results in [9 kHz-19 GHz] frequency band. For measuring RIN in [9 kHz-19 GHz] frequency range, path 1 of Fig. 2.1 is used. At output of PD, a bias tee is added to suppress the DC component and to extract the photocurrent value for RIN determination. A 19 GHz Low Noise Amplifier (LNA) having a 40 dB gain is employed. Finally, an Electrical Spectrum Analyzer (ESA) of 21 GHz bandwidth is monitored to extract PSD of measured RIN.

For analyzing RIN in the mm-wave frequency band, the components in path 2 of Fig. 2.1 are used. The resultant mm-wave signal is amplified using a 35 dB gain LNA of (50-62) GHz bandwidth. Then, the amplified signal is down-converted by using a mixer (50-65) GHz of 6 dB losses and a Local Oscillator (LO). A mixer and an LO frequency fixed at 51.2 GHz are employed for down-conversion, to adjust received signals to the ESA bandwidth. The mixing process does not influence the quality of the involved signals since the LO phase noise is much lower than the signal to be characterized (-140 dBc/Hz for frequency offset above 10 MHz) [6].

2.3.2 Experimental Measurements of RIN in [9 kHz-19GHz] Range

2.3.2.1 RIN from a Single DFB Laser

The frequency response or dynamic characterization of optical source is known as laser intensity noise. For a single DFB laser, the RIN behavior is represented in Fig. 2.2 with different

values of the pumping current. When increasing the bias currents of laser, RIN values are decreased and shifted to the higher frequencies. Fig. 2.2 represents the behavior of RIN at the same temperature value (25°C) and different pumping current values (20 mA and 45 mA). The modeled curves of RIN using Eq. (2.6) for both cases of a biased current are also illustrated and agree well with experimental results. The important question is whether RIN would transfer or not to the beat note signal. When the data is applied on the two optical modes, the RF carrier is generated and the data is also transferred close to carrier due to heterodying process of the PD. This leads that the RIN would be transferred to beat note. The following section is mainly focused on this issue at different frequencies.

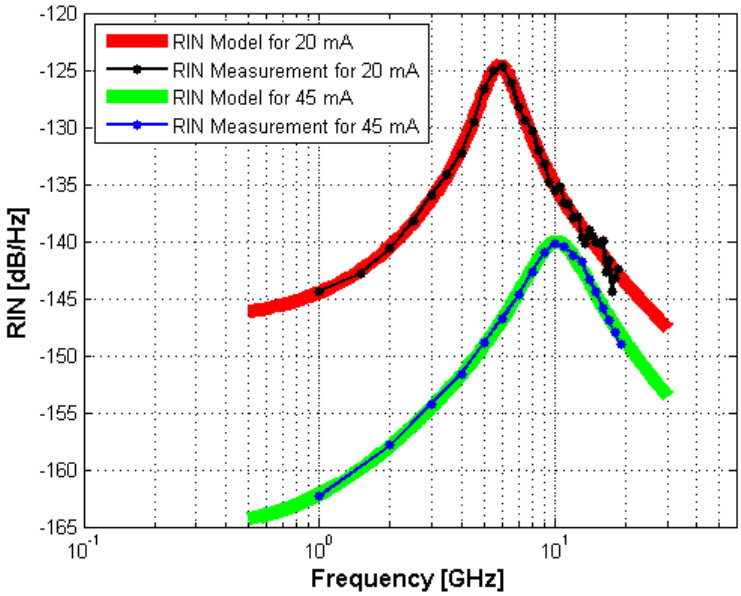

Figure 2.2: RIN and model of a single DFB laser for different biased currents.

2.3.2.2 RIN from 2 DFB lasers

The RIN results are here measured in [9 kHz-19 GHz] frequency band. The fundamental features of the technique using two different DFB lasers (Fig. 2.1 - path 1) are the ability to generate beat signals at different frequencies and the capability to demonstrate several cases of RIN close to beat note by varying the temperature and the relative optical power of the DFB lasers. Due to the relaxation frequency of the lasers of 4.1 GHz and the 19 GHz bandwidth limitation of the amplifier, a beat signal at 14 GHz has been chosen to highlight the impact of RIN in optical heterodyne process as shown on Fig. 2.3.

For verifying Eq. (2.13) and Eq. (2.14), the bias current of the first laser DFB_1 is set to 15 mA (P_{opt}= -2.1 dBm) while the bias current of the second laser DFB_2 is 90 mA (P_{opt}= +3.5 dBm). Thus, RIN_1 and RIN_2 levels are very different for the first and second laser, respectively. The experimental results of initial RIN_{ini} and beat note RIN_{beat} are given in curve (a) of Fig. 2.3. On these results, the thermal noise impact, the shot noise and the frequency response

of the global system have been removed. In Fig. 2.3, the initial RIN_{ini} from 9 kHz to 7 GHz and RIN close to the generated beat note RIN_{beat} on each side of the heterodyne signal can be observed. The large phase noise obtained by this technique is provided in curve (b) to prove that impairments are not due to phase noise but come from laser intensity noise solely. The beat note linewidth is estimated to be 30 MHz for two independent DFB lasers. From Eq. (2.13) and Eq. (2.14), the difference between the maximal values of initial noise RIN_{ini} and noise close to the beat note RIN_{beat} is calculated to be equal to 6.7 dB. From experimental measurement of Fig. 2.3, it can also be observed that the beat note RIN_{beat} is higher than the initial RIN_{ini} by a factor I_2/I_1= 6 dB, which is in good agreement with the predicted value of 6.7 dB. The RIN of the less powerful mode (RIN_1) in Eq. (2.13) is then increased by a factor I_2/I_1 compared to RIN_1 in Eq. (2.14) as expected.

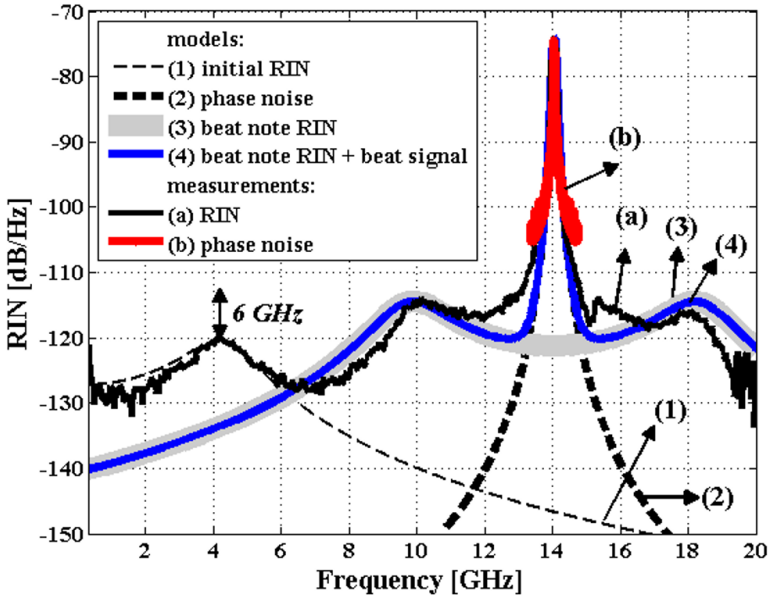

Figure 2.3: RIN and phase noise of a heterodyne signal at 14 GHz for generation using two independent DFB lasers.

The initial RIN_{ini} has been modeled, curve (1) of Fig. 2.3, from RIN expression of laser [5]. The phase noise of beat signal corresponds to the convolution of the two optical individual spectrums. The noise shape can be modeled by a Lorentz distribution while other random variations at the wavelength difference are considered as Gaussian fluctuations, resulting in a Voigt profile (curve (2)). The beat note RIN_{beat} model in curve (3) refers to the last term in Eq. (2.12), representing the phase noise of the beating signal multiplied in the time domain by the sum of the individual laser intensity noise. Then, the model results of beat signal phase noise and RIN_{beat} are summed and shown in curve (4). Based on the aforementioned, experimental results are well confirmed by model results and give an evidence of RIN generation from heterodyne process at beat note, as presented in Eq. (2.12), Eq. (2.13), and Eq. (2.14).

In Fig. 2.4, we intend to show that RIN_{beat} impairs mm-wave signal, even at high frequency. Since the relative intensity noise (RIN_1) of DFB_1 has the main contribution on the

initial RIN_{ini}, two different bias currents are set for DFB_1: 13 mA (P_{opt}= -4.1 dBm) and 17 mA (P_{opt}= -0.6 dBm), respectively. The second laser DFB_2 is still biased at 90 mA (P_{opt}= +3.5 dBm).

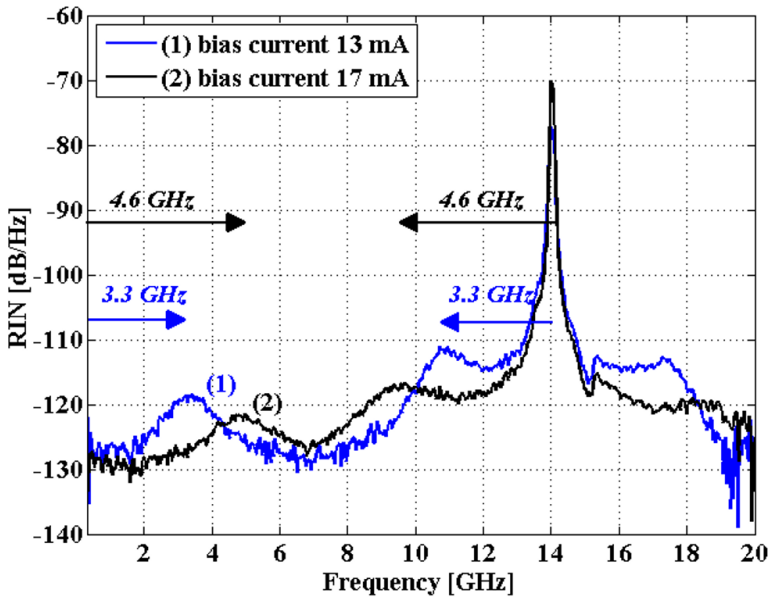

Figure 2.4: RIN of the beat note at 14 GHz for two different bias currents of the first laser DFB_1.

The temperature of both lasers is set to keep the beat note at 14 GHz, and results are shown in Fig. 2.4. When the laser DFB_1 is biased at 13 mA, the laser relaxation frequency is equal to 3.3 GHz that can be seen on the curve (1) of Fig. 2.4. During the heterodyne process, it can be noted that RIN_{beat} close to the beating frequency exhibits a maximum noise at an offset from the beat note which equals the relaxation frequency. When changing the laser bias to 17 mA, the relaxation frequency is equal to 4.6 GHz (curve (2)), again equal to the offset between the beat note and the maximum RIN_{beat}.

From this figure, it is inferred that RIN_{beat} close to beat signal is directly generated from initial RIN_{ini} and has the same profile. The difference between initial RIN_{ini} and RIN_{beat} at beat note for the above two cases is also observed because the lowest powered mode will be increased through the heterodyne process by a factor I_2/I_1 in Eqs. (2.13) and (2.14). Fig. 2.4 depicts different RIN_{ini} values while keeping identical phase noise for both measurements. Then, the results clearly indicate that the beat signal for offset frequency higher than 1 GHz is largely impacted by RIN_{beat} which spread over a very large bandwidth, much higher than phase noise. This further confirms that RIN phenomenon at generated beat note is distinct from phase noise of heterodyne signal.

2.3.3 Experimental Measurements of RIN in mm-wave Frequency Band

In the first technique using 2 DFBs for mm-wave generation, path 2 in Fig. 2.1 is employed for demonstrating RIN at mm-wave signals. The temperature of lasers is controlled to stabilize the signal at 55 GHz, and the bias current of DFB_1 is 13 mA (P_{opt}= -4.1 dBm), while the bias

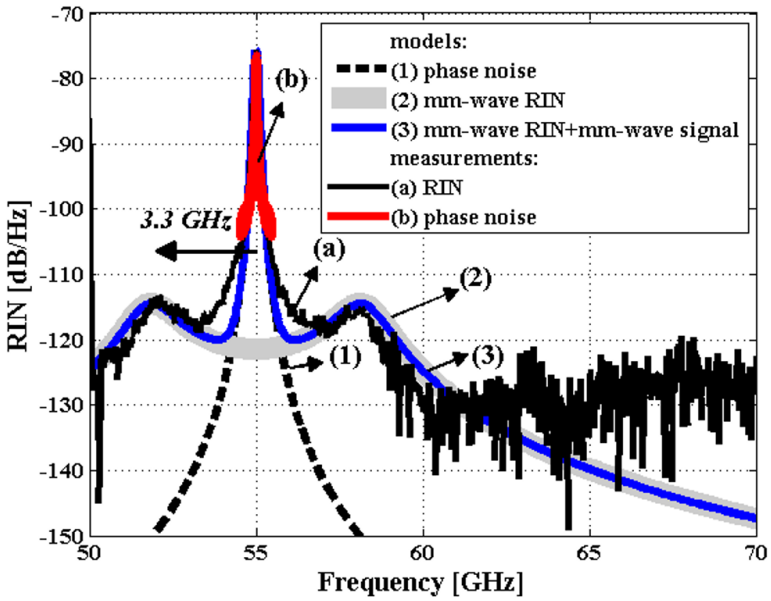

Figure 2.5: RIN and phase noise of the heterodyne signal at 55 GHz with mm-wave generation based on 2 DFBs.

current of DFB_2 is set to 90 mA (P_{opt}= +3.5 dBm). Fig. 2.5 shows the experimental and model results, illustrating RIN_{beat} close to beat note (curve (a)) and also phase noise (curve (b)) at mm-wave frequency.

The models of phase noise, and RIN_{beat} in curves (1) and (2), respectively, are in very good agreement with the experimental results. The RIN_{beat} in Fig. 2.5 is comparably similar to the result of RIN_{beat} without down-conversion stage in Fig. 2.4 for bias current of 13 mA. The factor I_2/I_1 being larger than 1 as described in Eq. (2.13) and Eq. (2.14), consequently RIN_{beat} close to the beat frequency is higher than RIN_{ini} at low frequency.

2.3.4 Experimental Setup and Results of RIN by PMLLD Laser

2.3.4.1 Experimental Diagram of RIN

Optical comb source generates phase correlated optical modes to form a high quality mm-wave beat signal. In this configuration, PMLLD is utilized as optical comb source with a wide optical spectrum and equally frequency spacing among optical modes. When optical signals are transmitting through long length of optical fiber, the chromatic dispersion effect is exhibited on the mm-wave signal [7].

Fig. 2.6 shows the generic schematic diagram of experimental setup based on PMLLD, second generation technique. The schematic diagram has already been explained in Fig. 2.1, but here the PMLLD laser is the optical source with multiple modes. A signal generator is used to be applied on the optical modulater for resulting on-off modulation. A lock-in amplifier is employed for improving the system sensitivity which can distinguish the noise level close to the thermal noise. Synchronization is needed for signal generator, lock-in amplifier, and ESA.

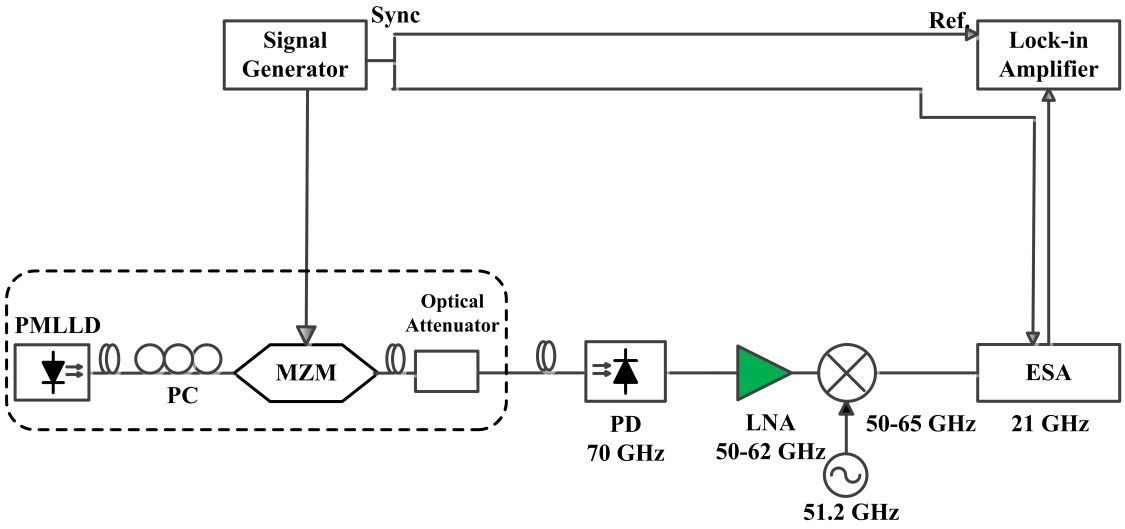

Figure 2.6: Experimental setup for optical heterodyning based on a PMLLD laser.

2.3.4.2 Experimental Results of RIN

In the second technique using PMLLD for mm-wave generation, PMLLD having an FSR of 60.64 GHz is biased at 180 mA (P_{opt}= +9.5 dBm), and the temperature is fixed at 25°C. Here, the lock-in amplifier allows measurements of a lower RIN level. The initial RIN_{ini} at low frequency and its model are presented in the black curve and thick grey curve in Fig. 2.7, respectively.

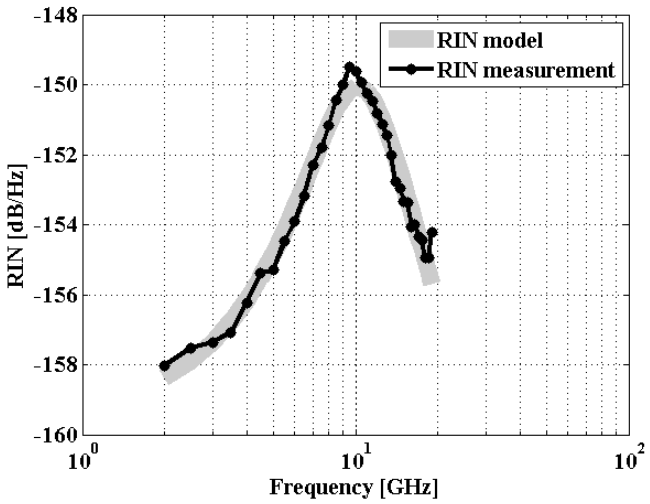

Figure 2.7: RIN at a few GHz based on PMLLD.

According to the correlation between optical modes of PMLLD, the beat note linewidth of mm-wave signal is ≈ 1 MHz, which is much lower than the first technique using 2 DFBs equal to 30 MHz. Fig. 2.8 represents beat note in [50-62] GHz range before down-conversion and only depicts one side band RIN_{beat} of mm-wave signal because of the frequency cut-off at 62 GHz.

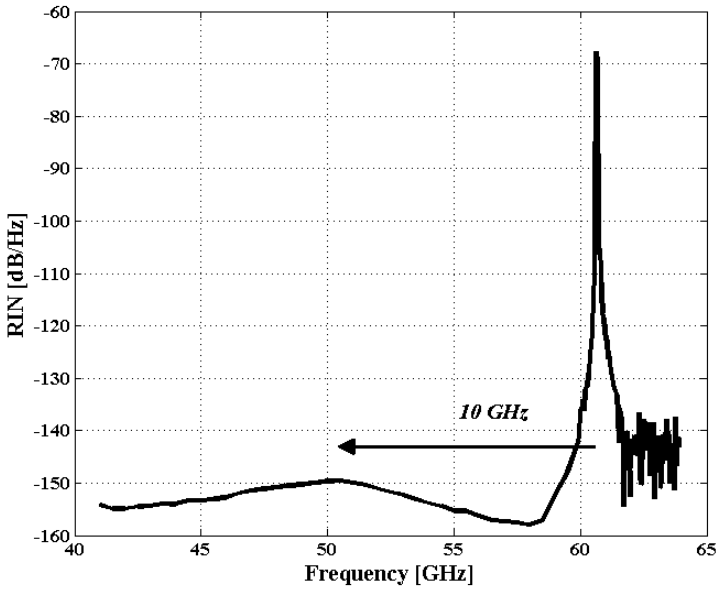

Figure 2.8: RIN of the heterodyne signal at 60.64 GHz with mm-wave generation based on PMLLD.

It should be mentioned that Fig.2.8. shows an estimation of the RIN_{beat} (black curve) at mm-wave based on low frequency measurements and using the presented model. The peak value of beat note RIN_{beat} is -150 dB/Hz at 50 GHz which is the same as RIN_{ini} peak measured at the low frequency. This can be explained by the distribution of optical power between (M) modes which are equal, thus the factor I_j/I_i equals 1 as described in Eq. (2.17) and Eq. (2.18). The relaxation frequency extracted from RIN_{ini} and RIN_{beat} is approximately 10 GHz, so it can be confirmed that RIN_{beat} is generated from RIN_{ini}. When comparing the first and second techniques, both based on same physical phenomenon, i.e. heterodyning, RIN_{beat} close to beat signal has the same origin. The main and important difference between the two mm-wave generation techniques cases is the correlation between modes is not considered null for the case using PMLLD.

2.4 60 GHz RoF Wireless Transmission

In this section, we have studied the impact of intensity noise on broadband 60 GHz transmission complying with 60 GHz communication standards.

2.4.1 60 GHz RoF System Setup

The experimental setup presented in Fig. 2.9 to perform a transmission of digital modulated data on a 60 GHz carrier to analyze the intensity noise impact on EVM. The central station employs the previous mentioned optical sources, 2 DFB lasers or PMLLD. A PC is added to match the polarization state of the modulator waveguide. A MZM is used as an external modulator biased at the quadrature point for applying data in compliance with standard modulation formats. Sig-

nals come from an Arbitrary Waveform Generator (AWG), and the variable optical attenuator is employed to vary the optical power transmitted to a conventional single mode optical fiber of 1.5 meter. At the base station, the 60 GHz signal is produced by optical heterodyning on a high-speed PD and then amplified to a maximum level of +4.5 dBm using a 35 dB RF amplifier.

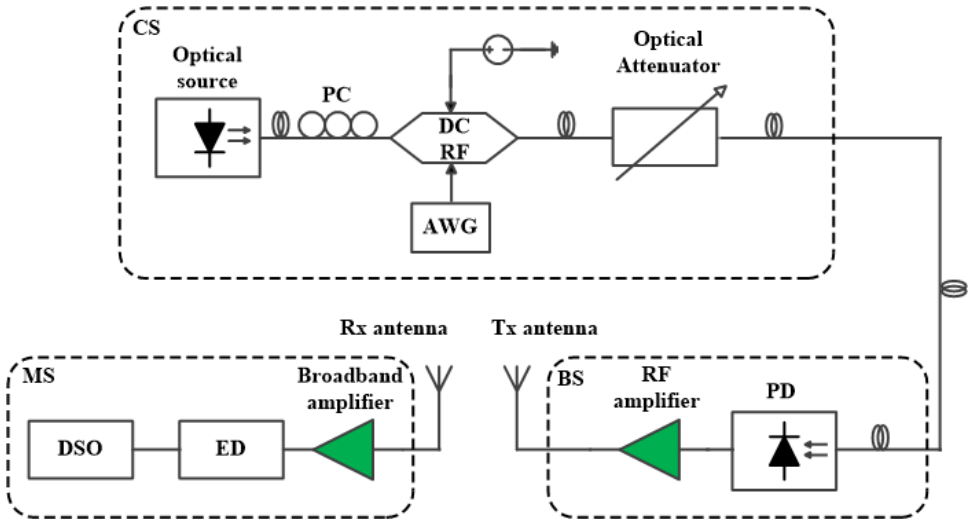

Figure 2.9: Experimental setup for 60 GHz RoF wireless system based on two independent lasers or PMLLD.

The wireless link is implemented by 60 GHz standard horn antennas of 20 dBi gain. A 30 dB gain broadband amplifier is used at the receiver to compensate the free space losses. The data-modulated 60 GHz signal is recovered using ED as down-conversion stage. Since the ED only detects field intensity, the noise measured is due to the intensity noise [8],[9]. The ED does not require any LO nor locking scheme which makes this receiver cost-efficient. The down-converted signal and data are transmitted to a high-speed Digital Sampling Oscilloscope (DSO) 54855A from Agilent, having a 6 GHz bandwidth for sampling process. Online EVM values are obtained using Vector Signal Analyzer (VSA) installed on the DSO.

2.4.2 Experimental Results

The EVM measurements are carried out with achieving 60 GHz communication standards for a wireless distance of 25 cm where the free space power loss is approximately 16.5 dB. This distance can be increased using a higher transmit power and high-gain antennas. Since an envelope detector is used, the integrity of modulation is kept to avoid the phase ambiguity, and due to its bandwidth limitation of 2 GHz, data of BPSK 397 Mbps, BPSK 794 Mbps, and QPSK 1588 Mbps modulations are applied on a 1 GHz subcarrier at 60 GHz.

For BPSK modulation using 2 DFBs or PMLLD, EVM characterizations have been performed as a function of the received RF power. BPSK 397 and 794 Mbps data rates can be shown in Fig. 2.10 and Fig. 2.11, respectively, and constellation diagrams are presented as well in inserts. The received RF power was varied by adjusting the optical power into the PD using the optical attenuator. In Fig. 2.10, EVM values at bit rate of 397 Mbps are as low as 10.8 %

for 2 DFBs (circle points) and 11.8 % for PMLLD (square points) for the same received RF power of -20.6 dBm. The EVM value of the lowest received RF power within standard limits is defined by the receiver sensitivity. In this experiment, the values of the receiver sensitivity for 33.4 % standard limit are -42.7 dBm and -41.2 dBm for 2 DFBs and PMLLD, respectively. The wireless distance between the two antennas at these receiver sensitivity values can be extended to approximately 3 m without any additional amplifier.

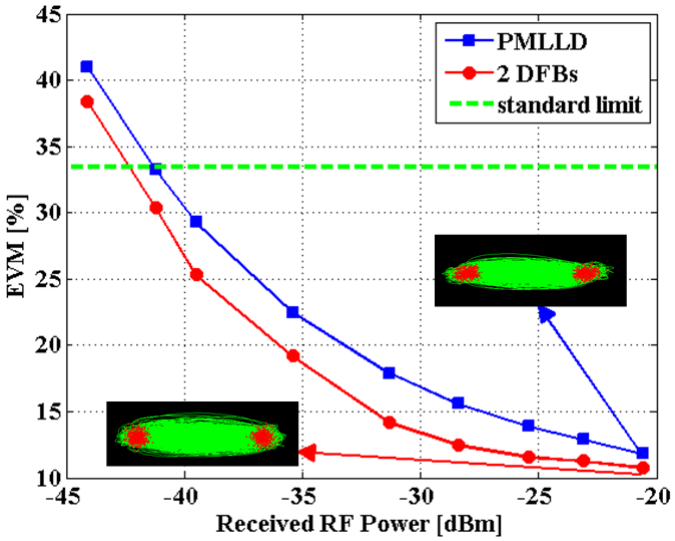

Figure 2.10: EVM of the 397 Mbps BPSK signal as a function of received RF power.

As can be extracted from the constellation diagrams, the error-floors of EVM are due to the impact of intensity noise. Furthermore, the PSD measurements of the intensity noise in [9] show that the intensity noise of PMLLD is higher than 2 DFB lasers, and therefore the EVM value with PMLLD is higher than that of 2 DFBs at the same received RF power.

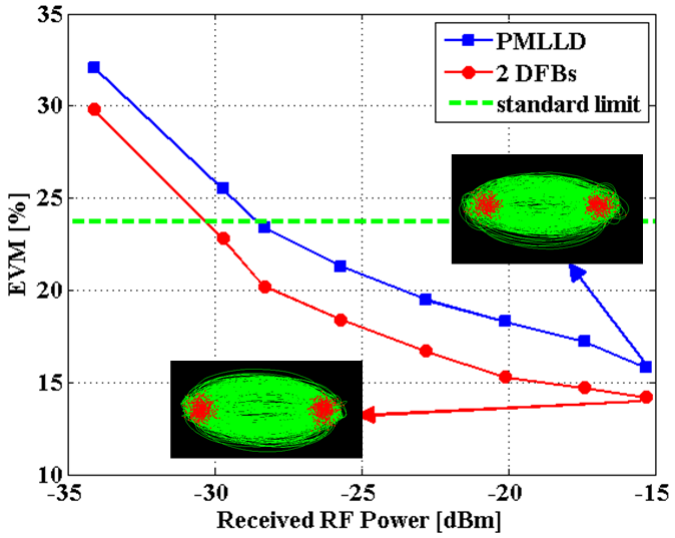

Figure 2.11: EVM of the 794 Mbps BPSK signal as a function of received RF power.

The EVM for a transmission of BPSK signal at data rate of 794 Mbps is illustrated in Fig. 2.11. The lowest EVM values achieved are 14.2 % and 15.8 % for 2 DFBs (circle points) and PMLLD (square points)at the same received RF power of -15.3 dBm, respectively. The receiver sensitivity is compliant with the standard limit of 23.7 % at -29.7 dBm for 2 DFBs and -28.3 dBm for PMLLD, while the maximum distance between two antennas at these levels of sensitivity is approximately 1.5 m, with avoiding the use of additional amplifiers. Here, since the signal bandwidth is increased, the error-floors are higher than in the case using BPSK data rate of 397 Mbps.

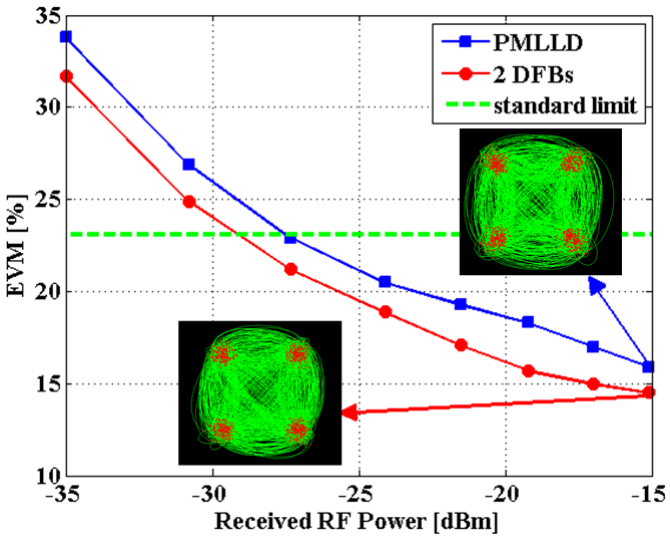

Figure 2.12: EVM of the 1588 Mbps QPSK signal as a function of received RF power.

For a QPSK signal of 1588 Mbps data rate applied on the transmitter side, Fig. 2.12 shows the EVM trends versus received RF power. For 2 DFBs (circle points), EVM as low as 14.5 % is obtained at the received RF power of -15.1 dBm whereas for PMLLD (square points), EVM increases to 15.9 % at the same received RF power. For the standard limit of 23.1 %, the receiver sensitivity is -29.3 dBm and -27.3 dBm for 2 DFBs and PMLLD, respectively. At these values of receiver sensitivity, the transmission distance can be extended to approximately 1.5 m with no other amplifier implemented. The constellation diagrams of QPSK modulation show that there is no phase noise impact measurable, and thus the EVM error-floors are induced by the intensity noise solely.

The previous three formats used match the requirements of the communication standards for 60 GHz RoF wireless transmission, using 2 DFBs or PMLLD. It can also be noticed that RIN_{beat} is not purely due to phase noise conversion when increasing fiber length, but chromatic dispersion influences the intensity noise by decorrelation effect.

2.5 Conclusion

This chapter analyzes the RIN of optical heterodyne generated signals for mm-wave RoF applications and systems. A complete theoretical study and experimental measurements have been

presented using two different techniques, based on two independent DFB lasers and PMLLD, where both coherent and incoherent receivers have been used. The generation of intensity noise and its impact close to beat note at mm-wave frequency have been demonstrated and investigated, while the phase noise results are provided as well for comparison. For measuring the real RIN_{beat} contribution, the frequency response of the system has been measured and removed. The experimental results confirm that RIN_{beat} close to the mm-wave carrier is directly generated from the initial RIN_{ini} at low frequency whatever the photonic generation process is and is clearly distinct from phase noise of the beat signal. It is also shown that, due to heterodyning, the RIN_{beat} level can be higher than the RIN_{ini} by a factor equal to the ratio between mode power. The models of classic definition of RIN laser RIN_{ini} and RIN generated close to the beat note RIN_{beat} are presented and agree very well with the experimental measurements. These results are independent from how the optical modes are generated, so they can directly be transposed to any kind of optical process for beat note frequency generation.

The EVM results using the 60 GHz wireless transmission system have been demonstrated to meet the 60 GHz communication standards, and the impairment of intensity noise is examined on the RoF performance.

The results of this chapter are published in:
1) Hamza Hallak Elwan, Ramin Khayatzedeh, Julien Poette, and Beatrice Cabon, "Impact of relative intensity noise on 60 GHz radio-over-fiber wireless transmission systems" *IEEE Journal of Ligthwave Technology*, vol. 34, np. 20, pp. 4751-4757, Oct. 2016.

2) Hamza Hallak Elwan, Ramin Khayatzedeh, Julien Poette, and Beatrice Cabon, "Relative intensity noise in optical heterodyning applied to millimeter wave systems" *IEEE International Topical Meeting on Microwave Photonics, MWP 2015, Paphos, Cyprus*, Oct. 26-29, DOI: 10.1109/MWP.2015.7356690, pp. 1-4, 2015.

2.6 References

[1] R. Khayatzadeh, H. Rzaigui, J. Poette, and B. Cabon, "Accurate millimeter-wave laser phase noise measurement technique", *IEEE Photonics Technology Letters*, vol. 25, no. 13, July 2013.

[2] J. Poette, P. Besnard, L. Bramerie, and J. C. Simon, "Highly-sensitive measurement technique of relative intensity noise and laser characterization", *Fluctuation and Noise Letter*, vol. 8, n. 1, pp. 81-86, Mar. 2008.

[3] http://www.ecma-international.org/publications/standards/Ecma387.htm

[4] https://standards.ieee.org/findstds/standard/802.15.3c-2009.html

[5] Govind P. Agrawal, "Optical transmitters" in "Fiber-optic communication systems", *John Wiley & Sons*, 3rd ed., 2002.

[6] Agilent E8257D PSG Microwave Analog Signal Generator Datasheet, Agilent Technol,

Santa Clara, Ca, USA, 2012.

[7] F. Brendel, J. Poette, B. Cabon, T. Zwick, F. van Dijk, F. Lelarge, and A. Accard, "Chromatic dispersion in 60 GHz radio-over-fiber networks based on mode-lock lasers", *IEEE J. Lightw. Technol.*, vol. 29, no. 24, pp. 3810-3816, Dec. 2011.

[8] R. Khayatzadeh, J. Poette, and B. Cabon, "Impact of phase noise in 60 GHz radio-over-fiber communication system based on passively mode locked laser", *IEEE J. Lightw. Technol.*, vol. 32, no. 20, pp. 3529-3535, May 2014.

[9] R. Khayatzadeh, H. H. Elwan, J. Poette, and B. Cabon, "Impact of amplitude noise in millimeter-wave radio-over-fiber systems", *IEEE J. Lightw. Technol.*, vol. 33, no. 13, pp. 2913-2919, July 2015.

Chapter 3

Impact of Laser Mode Partition Noise on Optical Heterodyning at Millimeter-Wave Frequencies

This chapter examines the impact of Laser Mode Partition Noise (LMPN) during the optical heterodyning process. The system presented here employs a Passively Mode-Locked Laser Diode (PMLLD) as a multi-mode source for Millimeter-Wave (mm-wave) generation. A comprehensive theoretical and experimental study of LMPN at low frequency and, for the first time, in mm-wave frequency band is demonstrated. Simulations are presented to investigate the distribution of mode partition noise across optical modes. LMPN appears as an impairment in performance on a Radio-over-Fiber (RoF) communication system by increasing the intensity noise when the number of optical modes detected by a Photodiode (PD) is limited. The effect of LMPN is experimentally demonstrated using coherent and incoherent receivers, and it is shown that up to 25 dB degradation in signal power occurs due to noise when not all modes are detected.

3.1 Introduction

The push towards very high bit rate wireless communication systems requires microwave photonic components, as mentioned in the chapter 1. The optical sources used result in phase and intensity noise on the generated mm-wave carrier. Two independent semiconductor lasers with linewidths of several MHz exhibit large phase noise on the RF beat signal. In order to obtain lower linewidth, a Mode-Locked Laser Diode (MLLD) can be employed for heterodyne mm-wave generation. Thanks to mode locking and correlation of phase noise between the optical lines, this source does not require any external locking scheme to partially alleviate phase noise on RF signals [1],[2], which results in better system stability and cost efficient mm-wave generation [3]. Two types of intensity noise are exhibited on RoF communication systems: Relative Intensity Noise(RIN) and Laser Mode Partition Noise (LMPN). In the previous chapter, we demonstrated the impact of RIN on the generation of mm-wave signals using two different kinds of lasers.

In this chapter, LMPN is analyzed and measured at mm-wave frequencies. The use of multi-mode sources can lead to larger power fluctuations in each optical mode due to LMPN, where filtering out a single optical mode from multi-mode laser, LMPN results in the poor system performance for data transmission and communication links [4]. LMPN can be neglected when integrating the entire optical spectrum since intensity fluctuations are compensated over the whole optical spectrum [5],[6]. In this chapter, the impact of mode partition on heterodyne signals is both theoretically and experimentally studied to characterize the power fluctuation among optical modes. Therefore, a 60 GHz RoF system employing a PMLLD, as an example on optical comb sources, is investigated using two different receivers for electrical detection: an RF coherent receiver using a mixer and an incoherent receiver using an envelope detector. Simulations of mode partition noise is provided to clearly understand the LMPN distribution between different optical modes. Experimental measurements have been realized and are in a good agreement with simulation results. With increasing the number of modes, the LMPN impact decreases, however, the chromatic dispersion instigated because of increase in a number of modes, degrades the performance of 60 GHz RoF systems.

3.2 Theoretical Analysis of LMPN

The electrical field $E(t)$ of a multi-mode laser, (M) modes, can be defined as:

$$E(t) = \sum_{i=1}^{M} A_i\Big(1 + \gamma_i(t) + \psi_i(t)\Big) \exp\Big(j\big(2\pi\big(f_0 + if_{RF}\big)t + \phi_i(t)\big)\Big) \tag{3.1}$$

where A_i, $\gamma_i + \psi_i$, and ϕ_i are the field amplitude, total amplitude noise, and phase noise of the i^{th} optical mode, respectively. f_0 is the carrier frequency of first mode, and f_{Rf} is the beating frequency corresponding to Free Spectral Range (FSR) of the laser. The total amplitude noise is the sum of laser RIN expressed from laser rate equations which is represented by (γ_i) and noise due to LMPN contribution expressed by (ψ_i) where Eq. (2.10) in chapter 2 demonstrates the only RIN effect. After some simple manipulation, the photodetected current $I(t)$ for (M) modes beating on a PD can be expressed as:

$$\begin{aligned} I(t) = &\sum_{i=1}^{M} I_i \times \Big(1 + 2\gamma_i(t) + 2\psi_i(t)\Big) + 2\sum_{i,j,i\neq j}^{M} \sqrt{I_i I_j} \\ &\times \Bigg[\Big(1 + (\gamma_i(t) + \gamma_j(t)) + (\psi_i(t) + \psi_j(t))\Big) \\ &\cos\Big(2\pi(f_j - f_i)t + (\phi_j(t) - \phi_i(t))\Big)\Bigg] \end{aligned} \tag{3.2}$$

where I_i is the DC photodetected current for i^{th} mode, $(f_j - f_i)$ is the mm-wave frequency of the generated beating between modes i and j, and $(\phi_j - \phi_i)$ is the phase noise exhibited on the mm-wave carrier. The first sum in Eq. (3.2) represents the total DC current, RIN, and LMPN for each mode from DC to a few GHz. The second term is sum of all the beatings terms, RIN,

LMPN contributions of the beating term between modes i and j at frequency of $(f_j - f_i)$. In (3.2), second order terms of RIN and LMPN have been neglected. Equation (3.2) can be written as:

$$I(t) = \sum_{i,j}^{M} \alpha \sqrt{I_i I_j} \times \Bigg[\Big(1 + (\gamma_i(t) + \gamma_j(t)) + (\psi_i(t) + \psi_j(t))\Big) \cos\Big(2\pi(f_j - f_i)t + (\phi_j(t) - \phi_i(t))\Big)\Bigg] \tag{3.3}$$

When $(i = j)$, $\alpha = 1$, thus Eq. (3.3) represents the first sum in Eq. (3.2) while $(i \neq j)$, $\alpha = 2$, Eq. (3.3) represents the second sum in Eq. (3.2). In order to calculate the Power Spectral Density (PSD) of the detected photocurrent, auto-correlation function $R_I(\tau)$ of the photocurrent is derived, assuming that the fluctuations of amplitude noise are stationary [7]. $R_I(\tau)$ can be defined as:

$$\begin{aligned} R_I(\tau) &= \Big\langle I(t)I(t+\tau) \Big\rangle \\ &= \Bigg\langle \sum_{i,j=1}^{M} \sum_{m,n=1}^{M} \alpha^2 \sqrt{I_i I_j} \sqrt{I_m I_n} \times A_{i,j,m,n}(t, t+\tau)\, \phi_{i,j,m,n}(t, t+\tau) \Bigg\rangle \end{aligned} \tag{3.4}$$

where $\langle\rangle$ is mean value over time, and τ is a positive time delay in a realistic system. $A_{i,j,m,n}(t, t+\tau)$ and $\phi_{i,j,m,n}(t, t+\tau)$ are correlations of amplitude noise and phase noise of beatings produced by modes (i, j) and (m, n), respectively. Whereas each beating corresponds to interaction between two optical modes, four indexes are used in this equation to represent the correlations between the beatings of pairs of modes. Consequently, correlation with indexes i, j, m, n is associated with beating between modes i and j and beating between modes m and n. In case where both amplitude and phase noise of mm-wave signal are uncorrelated, separate averages can be considered on both amplitude and phase noise.

Therefore, the average of amplitude noise correlation and the average of phase noise correlation can be calculated as follows: the average of amplitude noise correlation can be derived after neglecting the mean value of amplitude noise of a specific mode, $\langle\gamma\rangle = \langle\psi\rangle = 0$. According to laser dynamic, RIN is produced up to a few GHz, limited by the relaxation frequency of laser. Due to coupling between modes, power fluctuation among longitudinal modes causes mode partition noise [4]-[6],[8]. Therefore, RIN and LMPN can be considered as having independent origins, and subsequently their correlation functions are neglected in this approach $\langle\gamma \times \psi\rangle = 0$. The average of amplitude noise correlation can then be defined as:

$$\begin{aligned} \Big\langle A_{i,j,m,n}(t, t+\tau) \Big\rangle = \Big\langle & 1 + \gamma_i(t)\gamma_m(t+\tau) + \gamma_i(t)\gamma_n(t+\tau) + \gamma_j(t)\gamma_m(t+\tau) \\ & + \gamma_j(t)\gamma_n(t+\tau) + \psi_i(t)\psi_m(t+\tau) + \psi_i(t)\psi_n(t+\tau) \\ & + \psi_j(t)\psi_m(t+\tau) + \psi_j(t)\psi_n(t+\tau) \Big\rangle \end{aligned} \tag{3.5}$$

For (i=m and j=n), summation of auto-correlation functions are linked to amplitude noise on individual modes while for all other cases, summation of cross-correlation functions are

related to amplitude noise among different modes i.e. beatings. From Eqs. (3.3), (3.4), and (3.5), classical definition of RIN and LMPN of the beating between modes i and j are linked to the parameters $\psi_{i,j}$ and $\gamma_{i,j}$ using:

$$\text{RIN}_{ij}(t, t+\tau) = 4\gamma_i(t)\gamma_j(t+\tau) \tag{3.6}$$
$$\text{LMPN}_{ij}(t, t+\tau) = 4\psi_i(t)\psi_j(t+\tau) \tag{3.7}$$

The average of phase noise correlation can be derived using the small angle approximation [7]:

$$\cos\phi \approx 1$$
$$\sin\phi = \phi$$

Then, the average of phase noise correlation can be expressed as:

$$\begin{aligned}\left\langle \phi_{i,j,m,n}(t, t+\tau) \right\rangle =& \frac{1}{2}\Bigg\langle \cos(2\pi(f_n - f_m)\tau) + \Big(\big(\Delta\phi_{i,j}(t) - \Delta\phi_{m,n}(t, t+\tau)\big)\Big) \\ & \sin(2\pi(f_n - f_m)\tau)\Bigg\rangle \end{aligned} \tag{3.8}$$

Then, the PSD of the detected photocurrent $S_I(f)$ can be calculated by the Fourier transform of its auto-correlation in Eq. (3.4):

$$\begin{aligned} S_I(f) =& \frac{1}{2}\sum_{i,j,m,n} \alpha^2 \sqrt{I_i I_j I_m I_n}\Bigg(\Big(A_{i,j,m,n}(f) \times \delta\left[2\pi(f_n - f_m)\right]\Big) \\ & + \langle G_{A,\phi}(f)\rangle \times \delta\left[2\pi(f_n - f_m)\right]\Bigg) \end{aligned} \tag{3.9}$$

where δ is the dirac function, and,

$$A_{i,j,m,n}(f) = FT\big[\langle A_{i,j,m,n}(t, t+\tau)\rangle\big]$$
$$G_{A,\phi}(f) = FT\Big[\big\langle A_{i,j,m,n}(t, t+\tau) \times \Big(\Delta\phi_{i,j}(t) - \Delta\phi_{m,n}(t, t+\tau)\Big)\big\rangle\Big]$$

Where intensity noise and phase noise are considered statistically independant, this expression can be simplified as:

$$\Big\langle A_{i,j,m,n}(t, t+\tau) \times \Big(\Delta\phi_{i,j}(t) - \Delta\phi_{m,n}(t, t+\tau)\Big)\Big\rangle =$$
$$\Big\langle A_{i,j,m,n}(t, t+\tau)\Big\rangle \times \Big\langle\Big(\Delta\phi_{i,j}(t) - \Delta\phi_{m,n}(t, t+\tau)\Big)\Big\rangle$$

It can be observed from Eq. (3.9), that impact of both RIN and LMPN for a multi-mode laser degrades the performance of the RoF system at baseband and mm-wave frequency band by generating intensity noise through the parameters $A_{i,j,m,n}$.

3.3 Experimental Investigation of LMPN at Low Frequency

This section experimentally analyzes and examines the impact of noise due to mode partition on baseband. The electrical power spectrum distribution of LMPN is measured for different number of optical modes using an optical filter, and this study is implemented in both (300 MHz-18 GHz).

3.3.1 Experimental Setup

The configuration of the experimental setup for LMPN analysis is shown in Fig. 3.1. A PMLLD generating a low phase noise mm-wave signal at 58.63 GHz by heterodyning is used. Considering chromatic dispersion effect, optimum length of 72 m Single-Mode Fiber (SMF) G.652 is added to obtain the maximum electrical power of mm-wave signal [9]. For identifying the impact of LMPN, the number of detected modes is varied by optical filter at point (b) using a Wavelength Selective Switch (WSS), a wave shaper 1000S programmable optical filter from Finisar. The (M) optical lines beat through PD of 70 GHz bandwidth to generate mm-wave signal, and thus the number of beating contributions is (M-1).

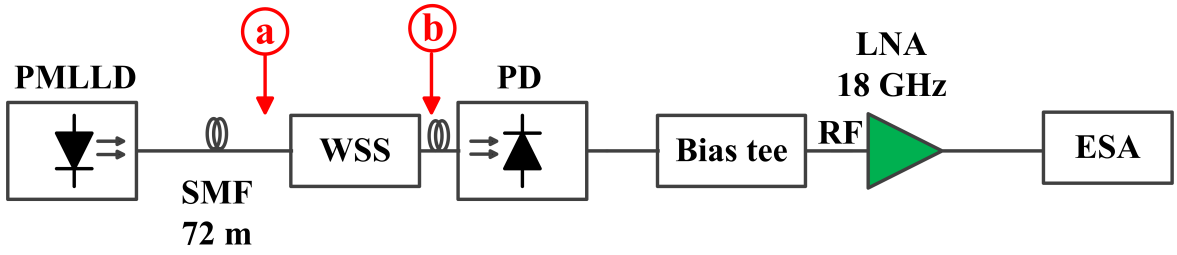

Figure 3.1: Schematic of experimental setup for RoF communication system based on PMLLD

The first detection system is dedicated to low frequency analysis in (300 MHz-18 GHz) frequency range. It uses a bias tee of (0.3-26.5) GHz bandwidth for suppressing the DC component and a 40 dB gain amplifier having a 18 GHz bandwidth. Then, Anritsu Electrical Spectrum Analyzer (ESA) is used to measure the PSD of the photodetected current.

Optical spectrum at point (a) of Fig. 3.1 is presented in Fig. 3.2 (a) measured by an Optical Spectrum Analyzer (OSA) of 0.05 nm resolution bandwidth. It shows a very large number of modes with a flat amplitude distribution. The instances of optical spectrum at point (b) are shown in Fig. 3.2 when filtering two modes in (b.1), when filtering seven modes in (b.2), or when detecting all modes except its left side modes at lower power in (b.3).

In experimental measurements, thermal noise and shot noise have been measured, and their contributions have been de-correlated from experimental results as they have different and independent physical origins from LMPN [10]. After measuring S parameters of the Opto-Electric (O/E) system using a Vector Network Analyzer (VNA), frequency response of system from photodiode to ESA has been accounted for in results.

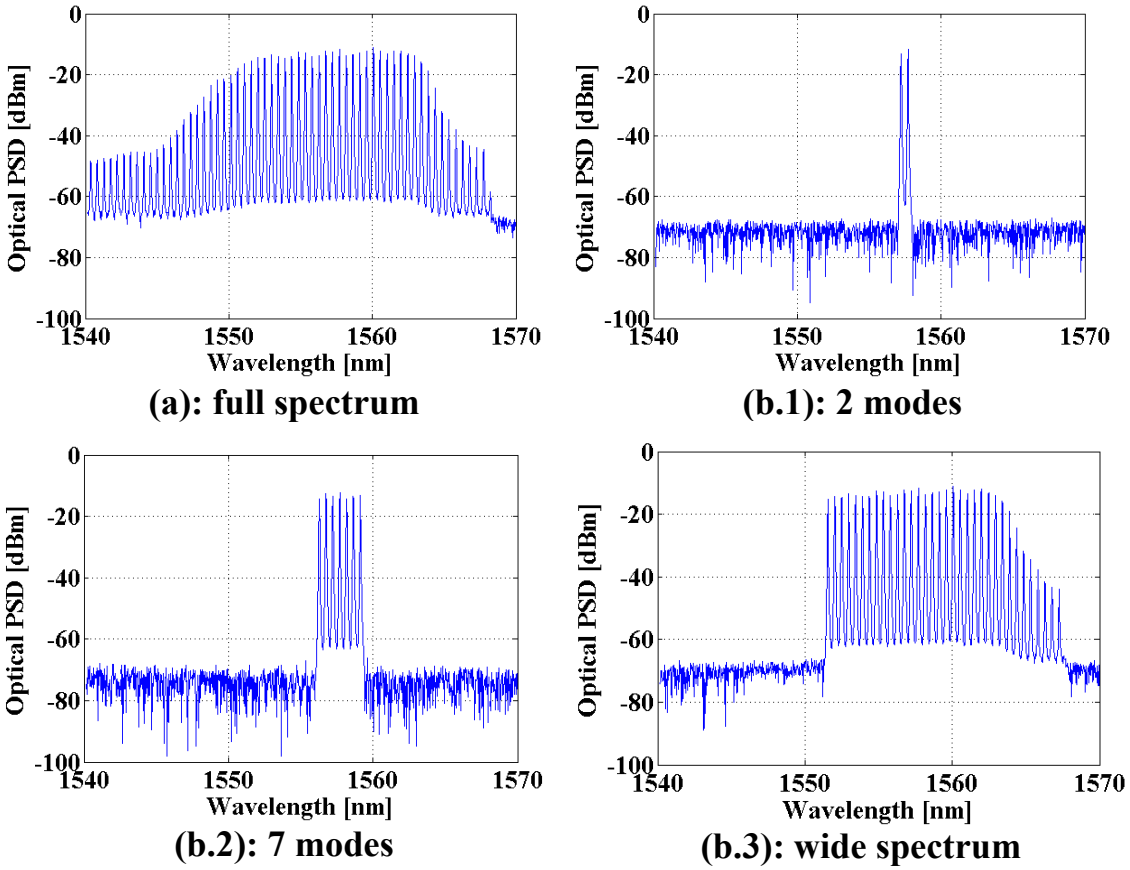

Figure 3.2: Optical spectrum of PMLLD for different bandwidth of WSS at biased current 209 mA.

3.3.2 Mode Partition Noise Simulation and Distribution

After theoretical and mathematical analysis of LMPN in section (3.2), the simulation results are described hereafter to highlight noise behavior and depend on mode partition within the optical spectrum. LMPN influences all modes, and therefore it possesses (M) contributions. Simulations are conducted using the MathWork's MATLAB software. From theoretical analysis of LMPN, there are two contributions: one from the considered mode (noise from each mode) and one from other modes.

3.3.2.1 Noise Contribution from Each Mode

In optical comb, each mode (i) has its own contribution (ψ_{ii}) to the noise induced by mode partition, and its level mainly depends on average optical mode power. The noise due to mode partition on a given mode (i) is compensated by sum of noise (ψ_{ji}) induced by mode (i) on other modes (j). The summation of (ψ_{ii}) and (ψ_{ji}) is therefore equal to zero, as can be described:

$$\psi_{ii} + \sum_{j \neq i}^{M} \psi_{ji} = \sum_{j=1}^{M} \psi_{ji} = 0 \tag{3.10}$$

In this model, whenever (ψ_{ii}) is positive or negative, (ψ_{ji}) contribution will be opposite of sign. Different distributions of this compensation can be considered: compensation across the entire spectrum (first scenario) or over a limited number of neighboring modes (second scenario) which can be linked to homogeneous and inhomogeneous broadening.

3.3.2.2 Total LMPN of Mode (i)

The influence of other modes (j) produces contributions (ψ_{ij}) on a given mode (i). From mathematical analysis, the contribution (ψ_{ii}) represents auto-correlation function of mode partition for mode (i) while the contributors (ψ_{ji}) and (ψ_{ij}) correspond to cross-correlation function of mode partition between mode (i) and mode (j). The total noise ψ_i due to mode partition of a given mode (i) is sum of its own contribution (ψ_{ii}) and contribution (ψ_{ij}) from other modes (j), and can be expressed as:

$$\psi_i = \psi_{ii} + \sum_{j \neq i}^{M} \psi_{ij} = \sum_{j=1}^{M} \psi_{ij} \tag{3.11}$$

Table (3.1) describes an example of LMPN distribution between 3 optical modes. According to Eq. (3.10), sum of terms in each column should equal zero, while from Eq. (3.11), sum of all the terms in each row gives the total mode partition noise of the concerned mode $\psi_i \neq 0$.

Impact of	mode 1	mode 2	mode 3	Line sum: total noise
On mode 1	ψ_{11}	ψ_{12}	ψ_{13}	ψ_1
On mode 2	ψ_{21}	ψ_{22}	ψ_{23}	ψ_2
On mode 3	ψ_{31}	ψ_{32}	ψ_{33}	ψ_3
Column sum	0	0	0	0

Table 3.1: Distribution LMPN across three optical modes

Table (3.1) shows that when all modes are detected, the total contribution of mode partition on noise $\psi_1 + \psi_2 + \psi_3$ equals zero, and consequently no impact of mode partition can be seen. The following simulation parameters have been selected as follows to correspond to the experimental investigation: the number of modes (M) of the optical spectrum is 41, and non-normalized mode powers I_i are considered to represent the effects of power spectrum distribution. Fig. 3.3 represents the experimental measurements and simulation results of LMPN at low frequency where curves describe the cumulative power of LMPN versus an increasing number of detected modes. Curve (1) illustrates experimental measurements of mode partition obtained in (300 MHz-18 GHz) using setup in Fig. 3.1, and simulation results in curves (2) and (3) are performed for a random LMPN distribution. The difference between two simulation curves (2) and (3) in Fig. 3.3 depends on the distribution of noise: noise from one mode (i) can be distributed over all modes (curve 2) or on a limited number of modes (6 modes here for curve 3).

Curve (2) increases as a function of number of modes to reach a maximum for 15 modes and then decreases to zero when all modes are aggregated. It is important to notice that accumulation of more than 27 modes modifies the curve slope due to integration of side modes that have a

reduced power compared to others central modes. Curve (3) corresponds to a distribution of noise over only 6 neighboring modes.

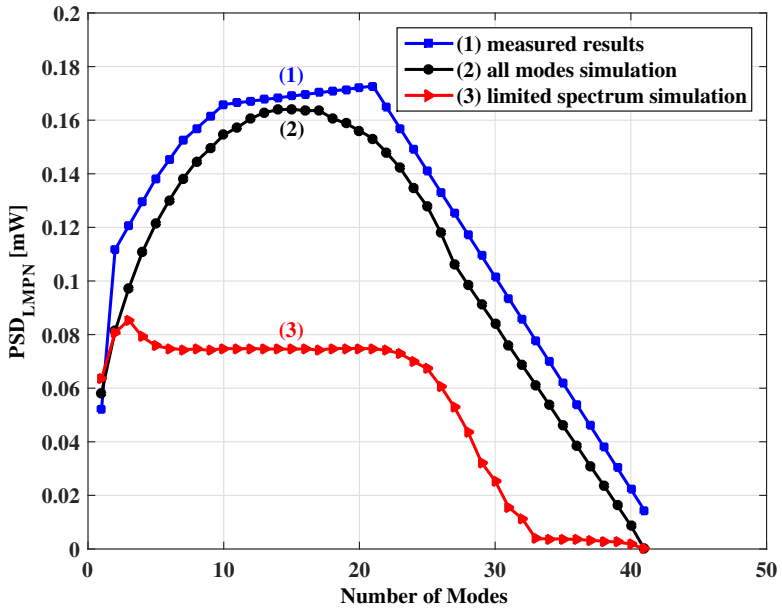

Figure 3.3: LMPN of measurements and simulation results with different LMPN distribution between optical modes.

It can be noticed that simulation results shown in curve (2), where noise is distributed over all modes, are in close agreement with experimental measurements of curve (1). This indicates that all modes, even those having low power like side modes, need to be detected in order to suppress the effect of mode partition. It can be concluded that, in this study, fluctuation of one mode is spread on the entire spectrum through mode partition.

3.3.3 Experimental Results in (300 MHz-18 GHz) Frequency Range

For measurements of mode partition noise at low frequency, experiments have been carried out using Fig. 3.1, and a total optical power of 9 dBm is used. Fig. 3.4 depicts the PSD normalized to optical power of detected signal in (300 MHz-18 GHz) for different number of optical modes detected, but displayed up to 7 GHz for better clarity. This normalization is performed to compensate optical power increase when detecting a larger number of modes.

Noise measured for frequencies lower than 300 MHz is due to detection stage, and therefore, it should not be considered here. LMPN is responsible for noise increase as high as 25 dB from 300 MHz to 2 GHz. In this experiment, WSS selects a specific number of optical modes that have different optical powers. Fig. 3.4, curve (1) shows that normalized PSD of noise is maximum when detecting only one optical mode. LMPN contribution decreases proportionally to number of modes selected and reaches a minimum when all modes are selected. Fig. 3.4 reveals the minimum level of LMPN can be achieved and corresponded to the noise floor level of the system when all optical modes (41 modes) are in WSS bandwidth. This result is well known and will be a reference when studying LMPN at mm-wave frequency band.

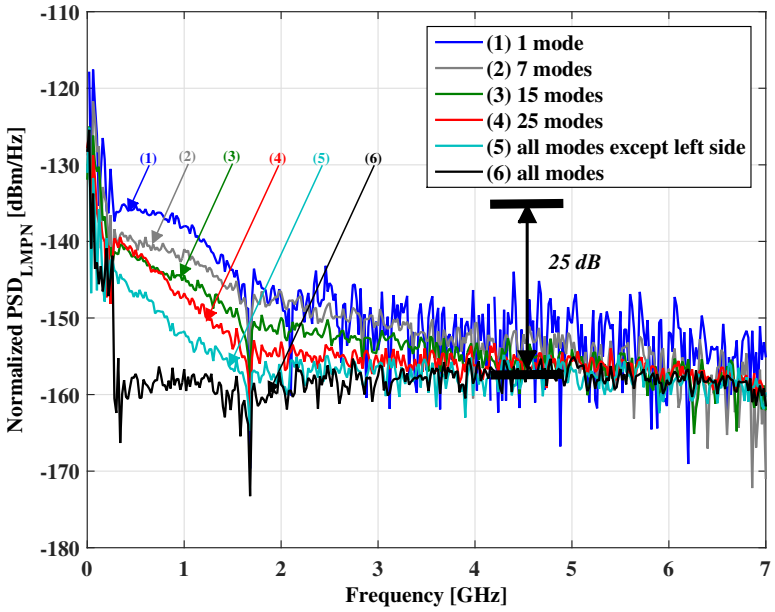

Figure 3.4: PSD of LMPN as a function of frequency for a different number of optical modes.

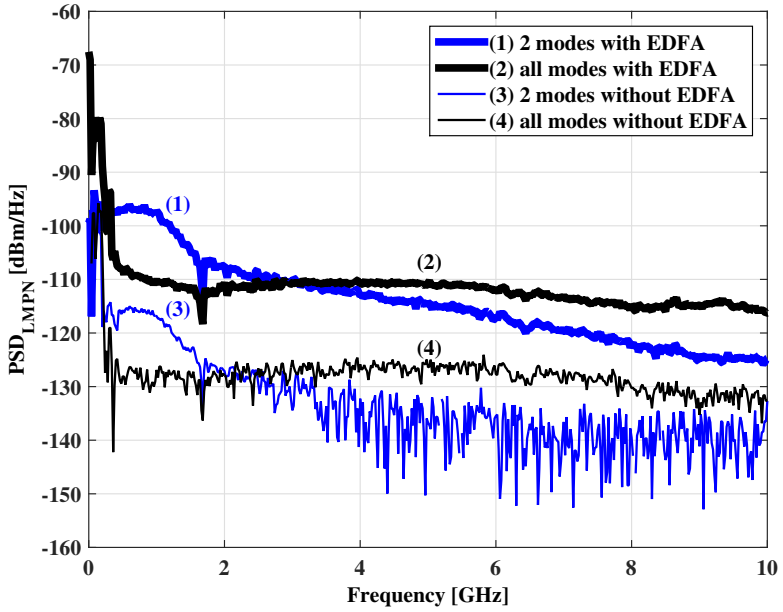

Figure 3.5: Experimental results of PSD comparison with and without EDFA for two optical modes and all optical modes.

In mm-wave RoF system of Fig. 3.1, an Erbium-Doped Fiber Amplifier (EDFA) can be used to compensate optical power losses when selecting a small number of modes by WSS. In order to study the effect of Amplified Spontaneous Emission (ASE) noise induced by EDFA, we have carried out experiments with, and without, EDFA at low frequency (Fig. 3.1). Measured PSD is depicted in Fig. 3.5 with EDFA (curves (1) and (2)) and without EDFA (curves (3) and (4)). Comparison is made for 2 cases: for only 2 modes, curves (1) and (3) and for all modes

(curves (2) and (4)). For 2 modes case, the contribution of mode partition on PSD can be clearly identified by noise increase in frequency range below 2 GHz.

It can be noticed in Fig. 3.5 that measured PSD results, with and without EDFA, have the same behavior but differ by 19.5 dB with equal to EDFA gain. Therefore, there is no additional degradation of noise thanks to a good saturation of EDFA and a wavelength selective switch employed after EDFA.

3.4 LMPN Effects in mm-wave RoF System

An investigation of laser mode partition noise on heterodyne signals at 58.63 GHz is performed.

3.4.1 Experimental Setup

Fig. 3.6 describes the schematic diagram of experimental setup using both coherent and incoherent receivers, for a total optical power of 9 dBm. A 19.5 dB gain EDFA is used to compensate for optical losses induced by optical filtering performed by the WSS when selecting different number of optical modes. The second detection system is used for mm-wave measurements where a 35 dB gain amplifier in (50-62) GHz range is used, and the amplified mm-wave signal is passed to a mixer or an envelope detector. When using the mixer, a Local Oscillator (LO) at 52 GHz down-converts mm-wave signal to 6.63 GHz. Since an envelope detector only detects intensity, the noise detected is due to the sum of RIN and LMPN in a PSD of photocurrent, and thus there is no impact of phase noise on beating signal as seen in chapter 2. Finally, ESA is employed to detect the PSD of the photodetected current.

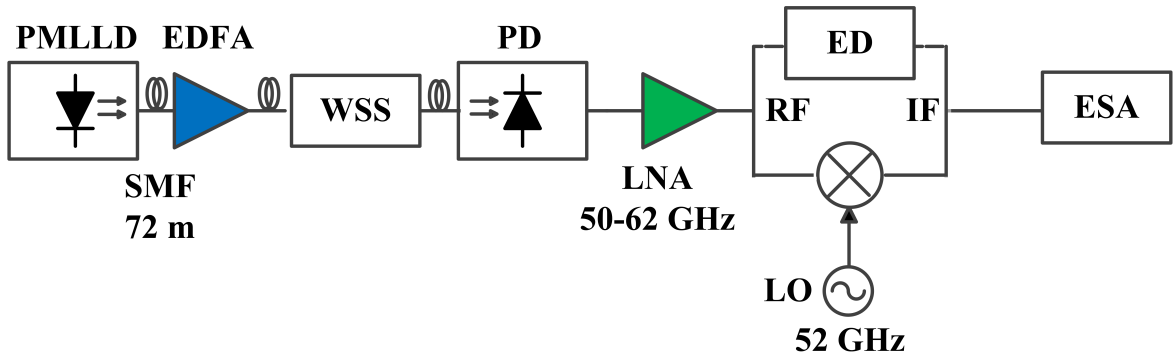

Figure 3.6: Schematic diagram of experimental setup for mm-wave RoF communication system based on PMLLD

For coherent receiver case, an LO signal of 52 GHz is applied to a mixer for down-conversion as represented in Fig. 3.6. Since phase noise of LO is extremely low (-140 dBc/Hz for frequency offset above 10 MHz) [11], the influence of phase noise of mixing process on IF signal is neglected.

3.4.2 Experimental Results and Discussion

a) Coherent receiver: Fig. 3.7 illustrates electrical power spectrum density of received mm-wave signals normalized to the mm-wave carrier for various optical bandwidth of WSS. It can be observed from the linewidths that phase noise is reasonably constant while the noise due to mode partition close to the carriers has different levels. This confirms that intensity noise from mode partition can be observed on mm-wave carrier and degrades system performance. For non-normalized PSD and with an increasing number of modes, the noise due to mode partition would slowly increase with increase in power of RF carrier. Measurements in Fig. 3.7 clearly indicate that LMPN contribution decreases when optical spectrum is extended, and thus the behavior of mode partition noise at mm-wave signal is comparable to that at low frequency as shown in Fig. 3.4.

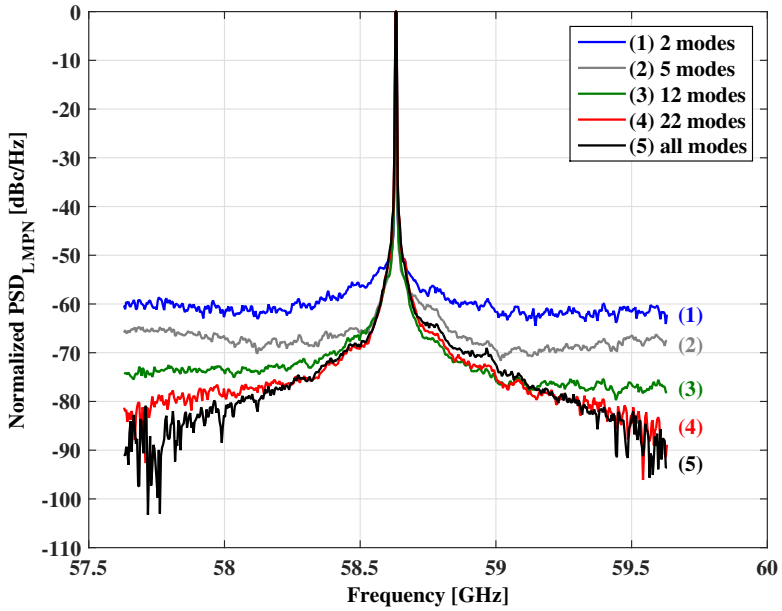

Figure 3.7: Normalized mode partition noise PSD of un-modulated mm-wave signal based on mixer.

b) Incoherent receiver: When using incoherent receiver, an envelope detector, the solely amplitude noise is measured and investigated. The detected normalized PSD due to mode partition noise is depicted in Fig. 3.8 after detection. Measurements are implemented for an optical photodetected power of 0 dBm with different number of modes in optical spectrum. According to limited bandwidth of ED used, results are presented up to 2 GHz. A good agreement with results of Fig. 3.4 is obtained: when all modes are detected, the impact of mode partition noise is minimal. Here, curve (5) in Fig. 3.8 corresponds to a residual amplitude noise which only originates from RIN, which is filtered out by ED response. Similar results can be observed by detecting a signal in a system where no mode partition noise exists, measuring beating between two independent single mode lasers, chapter 2.

Fig. 3.8 clearly shows an increase of mode partition noise detected in mm-wave frequency band when reducing number of optical modes. We can conclude that LMPN also influences in-

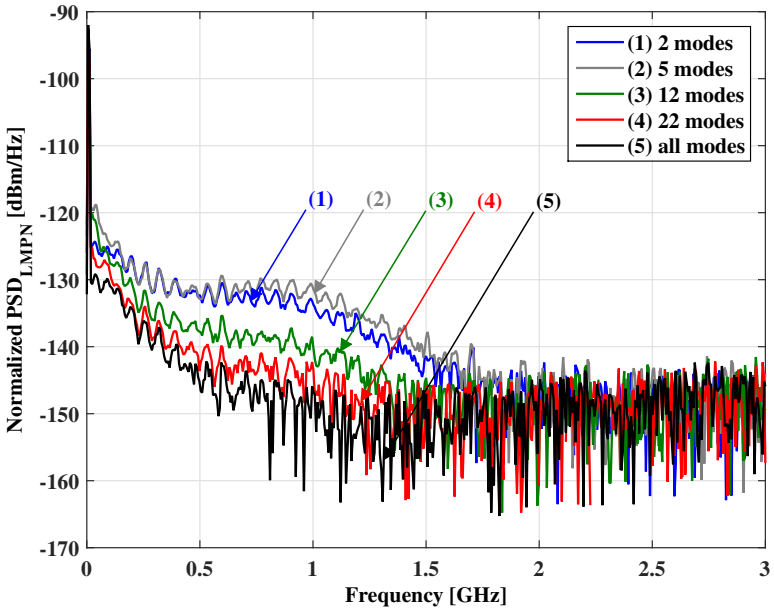

Figure 3.8: Normalized mode partition noise PSD of un-modulated mm-wave signal after down-conversion based on envelope detector.

tensity noise on mm-wave signals, as described in Eq. (3.10), and degrades system performance. The heterodyne process induces LMPN in generated signal, even at mm-wave frequency.

3.5 Digital Modulation Experiment of 60 GHz RoF Transmission

We have then analyzed the effect of LMPN on EVM for 60 GHz RoF communication system with digital modulation.

3.5.1 Experimental Setup

The schematic diagram of experimental setup used to investigate system performance is presented in Fig. 3.9 for 100 Mbps quadrature phase shift keying (QPSK) modulation at 1 GHz subcarrier onto mm-wave carrier for analysis of LMPN impact on EVM. In Central Station (CS), the previous PMLLD is utilized, and the same SMF length of 72 m is used as before. A Polarization Controller (PC) is added to adjust polarization state of optical signal. A Mach-Zehnder Modulator (MZM) biased at quadrature point is employed for applying data stream from a Tektonix 12 GS/s 7122B Arbitrary Waveform Generator (AWG). An EDFA is used for compensation of modulator losses and optical power variation when reducing optical spectrum bandwidth using WSS. WSS is designated to filter out some modes from optical comb and to control transmitted optical power since it can also be used as an optical attenuator. For a fiber-optic transmission, the Base Station (BS) detects optical signal on a high-speed PD where the heterodyne mm-wave signal is generated at 58.63 GHz. This signal is amplified by an RF

amplifier before employing ED to detect the envelope of the signal.

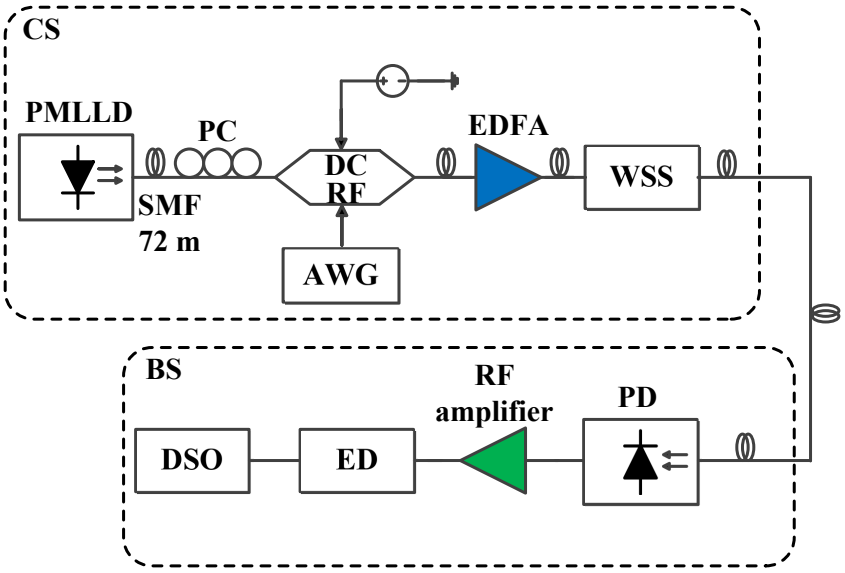

Figure 3.9: The configuration of experimental setup for 60 GHz RoF system based on incoherent receiver.

Both down-converted signal and data are captured and sampled by a Agilent 54855A high-speed Digital Sampling Oscilloscope (DSO) of 6 GHz bandwidth from Agilent 54855A. EVM is then evaluated in on-line from the measurements using a Vector Signal Analyzer (VSA) installed on the DSO. More information can be found in chapter 2, where theory and mathematical equations of intensity noise were discussed for a system based on a schottky barrier beam lead diode.

3.5.2 EVM Dependance on A Number of Modes

Measurements are carried out for EVM behavior at 1 GHz subcarrier frequency of 60 GHz carrier. Fig. 3.10 depicts two cases: firstly 2 optical modes are selected from the center of the optical spectrum where power of modes are equal (square points), and secondly all modes are detected (circle points). For both cases, WSS operates as a variable optical attenuator to control the received RF power.

From the measured PSD of mode partition noise using mixer of Fig. 3.7 and using an ED of Fig. 3.8, LMPN measurements for 2 modes demonstrate more influence than all modes. Thus, EVM of 2 modes is higher than all modes, as can be seen in Fig. 3.10. For 2 detected optical modes, the lowest EVM achieved is 8.1 % for a received RF power of -26.7 dBm. Since LMPN depends on an optical power, similar results are observed for other sets of two adjacent optical modes, which are selected in the part of the optical spectrum where the optical lines are flat. When detecting the entire optical spectrum, EVM decreases to 6.2 % at the same received RF power. The EVM trends for 2 modes and entire spectrum are closely congruent. It can again be concluded that for reducing impact of LMPN at baseband and on 60 GHz signals, it is shown that it is necessary to increase number of optical modes. Another solution could be a careful

choice of frequency subcarrier with respect to generated mm-wave carrier to avoid effect of laser mode partition. When increasing fiber length, chromatic dispersion will induce a time delay between different beatings. This can be interpreted by a de-correlation between optical lines, and consequently the noise induced by LMPN will be decorrelated as well. Therefore, this delay degrades the compensation of mode partition noise which can not fully be compensated when detecting several beatings. The frequency limit at which the compensation is possible depends on fiber length, and wavelength difference between beatings and number of beatings should also be considered.

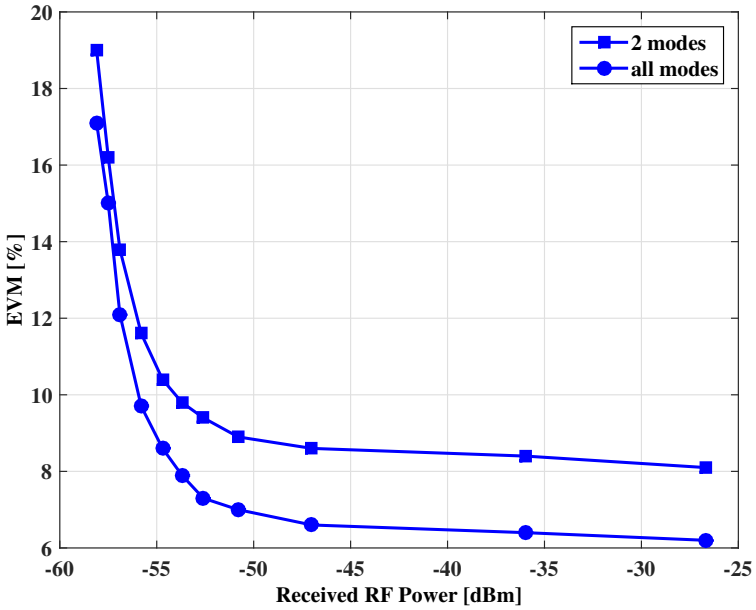

Figure 3.10: Measured EVM as a function of received RF power for filtered two optical modes and entire optical spectrum at 100 Mbps of QPSK modulation.

For entire optical spectrum, we encounter a trade-off between the noise due to mode partition noise and the chromatic dispersion that both degrade the system performance and limit the transmission length.

3.6 Conclusion

We have studied and demonstrated the impact of laser mode partition noise on baseband and mm-wave RoF communication systems. Applications concern PMLLD possessing a low phase noise for generation of a beating signal. The study of LMPN performed on optical heterodyning has been investigated by theoretical analysis and experimental results, where simulations are implemented to describe the behavior of LMPN across the optical spectrum. Impact of LMPN on generated mm-wave carrier has been experimentally demonstrated. Very close agreement is found between simulation and measured results.

The experiments have been carried out on the mm-wave RoF systems utilizing both coherent and incoherent receivers for down-conversion, and electrical spectrums of LMPN have been

presented. EVM versus RF power is also measured using data rates of 100 Mbps and QPSK modulation format on 1 GHz subcarrier for the case of two filtered modes and the entire optical spectrum. The results conclude that, for a larger number of modes, LMPN impact is lowered. It is worth mentioning that even side modes of low power have a strong impact on LMPN level. Careful attention should be made when designing system to avoid partition noise effect that could degrade signal transmission and considering chromatic dispersion effect. We would like to highlight that this study and the model can be applicable to any kind of optical heterodyne generation system.

The outcome of this chapter is published in:
Hamza Hallak Elwan, Ramin Khayatzadeh, Tong Shao, Julien Poette, Beatrice Cabon, and Liam P. Barry, " Impact of laser mode partition noise on optical heterodyning at millimeter-wave frequencies," IEEE J, Lightw. Technol., vol. 34, no. 18, pp 4278-4284, Sept. 2016.

3.7 Reference

[1] F. Brendel et al., "PLL- stabilized optical communications in millimeter-wave RoF systems", *J. Opt. Commun. Netw.*, vol. 6, no. 1, pp. 45-53, Jan. 2014.

[2] B. A. Khawaja and M. J. Cryan, "Wireless hybrid mode locked lasers for next generation radio-over-fiber", *J. Lightw. Technol.*, vol. 28, no. 16, pp. 2268-2276, Aug. 2010.

[3] Ralf-Peter Braun et al., "Optical microwave generation and transmission experiments in the 12- and 60-GHz region for wireless communications", *IEEE Trans. Microw. Theory and Techn.*, vol. 46, no. 4, pp. 320-330, Apr. 1998.

[4] Robert H. Wentworth et al, "Laser mode partition noise in lightwave systems using dispersive optical fiber", *J. Lightw. Technol.*, vol. 10, no. 1, pp. 84-89, Jan. 1992.

[5] K. Ogawa , "Analysis of mode partition noise in laser transmission systems", *IEEE J. Quant. Electro.*, vol. QE-18, no. 5, pp. 849-855, May 1982.

[6] K. Ogawa and R. S. Vodhanel , "Measurements of mode partition noise of laser diodes", *IEEE J. Quant. Electro.*, vol. QZ-18, no. 7, pp. 1090-1093, Jul. 1982.

[7] H. A. Haus and A. Mecozzi, "Noise of mode-locked lasers", *IEEE J. Quantum Electron*, vol. 29, no. 3, pp. 983-996, Mar. 1993.

[8] Govind P. Agrawal, "Lightwave systems" in "Fiber-optic communication systems" *3rd ed., John Wiley & Sons*, 2002.

[9] F. Brendel et al., "Chromatic dispersion in 60 GHz radio-over-fiber networks based on system based on mode-locked laser", *J. Lightw. Technol.*, vol. 29, no. 24, pp. 3810-3816, Dec. 2011.

[10] J. Poette et al.,“Highly sensitive measurement technique of relative intensity noise and laser characterization”, *Fluctuation and noise letters: L81L86*, 2008.

[11] Agilent E8257D PSG Microwave Analog Signal Generator Datasheet, *Agilent Technol*, Santa Clara, Ca, USA, 2012.

Chapter 4

Investigation of Optical Phase Decorrelation on 60 GHz Radio-over-Fiber Communication Systems

In this chapter, a 60 GHz Radio-over-Fiber (RoF) transmission system based on a Passively Mode-Locked Laser Diode (PMLLD) is proposed and studied. Optical phase decorrelation induced by chromatic dispersion in optical fiber is theoretically study and experimentally demonstrated. This effect results in power fading and optical (phase and intensity) noise on millimeter-wave carriers. Simulation and experimental results are in very good agreement. Experimental measurements show how performance of system impairments varies with different levels of Group Velocity Dispersion (GVD). The trade-off between flat fading and power losses is emerged to improve the system performance. Furthermore, the impact of Laser Mode Partition Noise (LMPN) on the suggested system is studied and examined by transporting over various fiber lengths. The correlation of mode partition noise among optical modes, for the first time, is analyzed and investigated at baseband and Millimeter-Wave (mm-wave) frequencies. Flat fading and optical noise are detected on Error Vector Magnitude (EVM) after transmitting data over 25 km of fiber.

4.1 Introduction

Broadband communication systems are intensely demanded for wireless services and applications, and thus mm-wave RoF communication systems are employed to benefit from a large amount of available bandwidth and low transmission loss of optical fiber as presented in chapter 1. Optical source produces optical noise represented in phase and intensity noise as discussed in chapters 2 and 3. Optical frequency comb sources (OFC) are deployed in various applications such as photonic microwave, data transmission systems, THz spectroscopy, high precision optical clocks, and optical signal processing [1]. Coherent optical source is a conventional method for generating correlated phase optical lines which reduces the impact of phase noise on the beat note carriers. Mode-Locked Laser Diode (MLLD) as a coherent comb source generates a wide optical spectrum with equally spaced optical modes, good spectral flatness, and a high coherence among optical modes [2]-[5]. Free Spectral Range (FSR) of MLLD is fixed due to

the cavity length. Other sources can tune the space among optical modes like Gain Switch Laser (GSL) which is desirably in some techniques [6].

Utilizing coherent optical comb in Central Station (CS) and transmitting optical modes through kilometers of optical fiber, chromatic dispersion inevitably results in group velocity dispersion on a Photodiode (PD) in Base Station (BS). In case a high optical power is deployed, a non-linearity effect can be emerged as well [7]. Chromatic dispersion can decorrelate the phase among optical lines, and thus the beating signal at Mobile Station (MS) has lowering Quality of Service (QoS) in the system [8]-[10].

The aim of this chapter is undertake experiments destined to analyze chromatic dispersion on a power fading distribution and an optical noise at mm-wave frequencies. Simulation and experimental results vary as the properties of the dispersive media differ since the dependence of the refraction index on wavelength makes dispersion parameter values as a function of wavelength. Optical phase decorrelation caused by fiber dispersion exhibits power fading and partial phase noise on mm-wave carrier whereas dispersion compensation was applied to improve the network quality [10],[11]. The impact of optical phase decorrelation on intensity noise represented by LMPN for mm-wave RoF communication systems is for the first time investigated and demonstrated which reduces the system performance. Data rate of 500 Mbps quadrature phase shift keying (QPSK) is applied on a 60 GHz RoF communication system for evaluating chromatic dispersion effect in terms of EVM at different fiber lengths corresponding to different phase shift levels.

4.2 Theoretical Principle and Analysis of Chromatic Dispersion

The chromatic dispersion effect in a 60 GHz RoF communication network is studied based on a PMLLD without impact of mode partition noise and with its impact.

4.2.1 Without Mode Partition Noise

The employed PMLLD generates a high number (M) of correlated phase optical lines with 58.63 GHz frequency separation. The electrical field $E(t)$ can be expressed as:

$$E(t) = \sum_{i=1}^{M} A_i \exp\Big(j\big(2\pi\big(f_0 + i f_{RF}\big)t + \phi_i(t)\big)\Big) \tag{4.1}$$

where A_i and ϕ_i represent the amplitude and phase of mode (i), respectively. f_o is the first carrier frequency and f_{RF} is the beating frequency due to FSR. After coherent optical signals are propagating across various fiber lengths of a standard single-mode fiber (SSMF), some impairments: chromatic dispersion, non-linearity, and attenuation result in the receivers due to the refractive index of the fiber. These effects can be formed as:

$$\beta(f) = \beta_L(f) + \beta_{NL}(f) + j\frac{\alpha(f)}{2} \tag{4.2}$$

where β_L, β_{NL}, and α denote the linear, non-linear, and attenuation terms, respectively. Non-linear effect can typically be neglected because a low optical power is here emitted in an RoF system. Optical lines at a high-speed PD is suffered from linear term β_L which can be expanded using Taylor series as:

$$\beta_L(\Delta f) \approx \beta_0 + 2\pi\beta_1(\Delta f) + \frac{(2\pi)^2}{2}\beta_2(\Delta f)^2 + \frac{(2\pi)^3}{6}\beta_3(\Delta f)^3 + ... \tag{4.3}$$

where β_1 is the group velocity while β_2 and β_3 represent the second and third order dispersion, respectively. Second order dispersion is also termed as GVD parameter. β_i is the derivation of β with respect to Δf for i^{th} order. The optical heterodyning of (M) modes is occurred on the 70 GHz high-speed PD which generates $(M-1)$ mm-wave signals due to beating two neighboring modes. The general photodetected current $I(t)$ can be calculated as:

$$\begin{aligned} I(t) = \exp(-\alpha L) \times \Big(\sum_{i=1}^{M} A_i^2 + 2 \sum_{i=2}^{M} \sum_{j=1}^{i-1} A_i A_j \cos\Big(2\pi(i-j) f_{RF} t \\ - \frac{(2\pi)^2}{2}\beta_2(i^2 - j^2) f_{RF}^2 L + (\phi_j(t) - \phi_i(t))\Big)\Big) \end{aligned} \tag{4.4}$$

where i and j are two arbitrary modes at each time,, α is the attenuator factor, and L is the fiber length. The first sum is a DC current, but the second sum describes the mm-wave term with chromatic dispersion effect. Second order dispersion is related to dispersion parameter D which contains material dispersion and waveguide dispersion, and it can be represented as:

$$\beta_2 = -\frac{D\lambda^2}{2\pi c} \tag{4.5}$$

where λ is the wavelength and c is velocity of light. The optical lines suffered from phase shift at the PD can influence the beating signal as a constructive or destructive interferences as Eq. (4.4). Thus, the mm-wave signal demonstrates a periodic function of photocurrent corresponding to fiber length. Chromatic dispersion was investigated for different aspects such as laser chirp, the shape of optical spectrum, and the phase noise with a wavelength of 1550 nm and a dispersion coefficient of -17 ps/nm.km in [9].

4.2.2 With Mode Partition Noise

In case the phase and intensity noise influence the system, the electrical field $E(t)$ of (M) coherent optical modes generated from optical comb source can be expressed as:

$$E(t) = \sum_{i=1}^{M} A_i\big(1 + \delta_i(t)\big) \exp\Big(j\big(2\pi\big(f_0 + i f_{RF}\big)t + \phi_i(t)\big)\Big) \tag{4.6}$$

where δ_i, and ϕ_i are the intensity noise and phase noise of mode (i), respectively. Optical fiber causes time delay among optical lines induced by chromatic dispersion which exhibits optical phase decorrelation at the PD. The time delay can be calculated as:

$$\tau_d = DL\Delta\lambda \tag{4.7}$$

where D is the dispersion parameter, L is the fiber length, and $\Delta\lambda$ is the wavelength offset between two optical modes. Then, the recovered optical modes beat on the 70 GHz high-speed PD due to optical heterodyning process to generate a mm-wave signal. The general photodetected current $I(t)$ can be calculated as:

$$I(t) = \exp(-\alpha L) \times \Big(\sum_{i=1}^{M} A_i \big(1 + \delta_i(t,\tau_d)\big)^2 + 2 \sum_{i=2}^{M} \sum_{j=1}^{i-1} A_i A_j \big(1 + \delta_i(t,\tau_d) + \delta_j(t,\tau_d)\big) \cos\Big(2\pi(i-j) f_{RF} t - \frac{(2\pi)^2}{2} \beta_2 (i^2 - j^2) f_{RF}^2 L + (\phi_j(t,\tau_d) - \phi_i(t,\tau_d))\Big)\Big) \tag{4.8}$$

The first sum is a DC current, but the second sum refers to the mm-wave term. From Eq. (4.8), it can be noted that the chromatic dispersion emerges intensity noise, phase noise, and power fading on the generated mm-wave signal.

4.3 Chromatic Dispersion at Millimeter-Wave Carriers

4.3.1 Experimental Setup

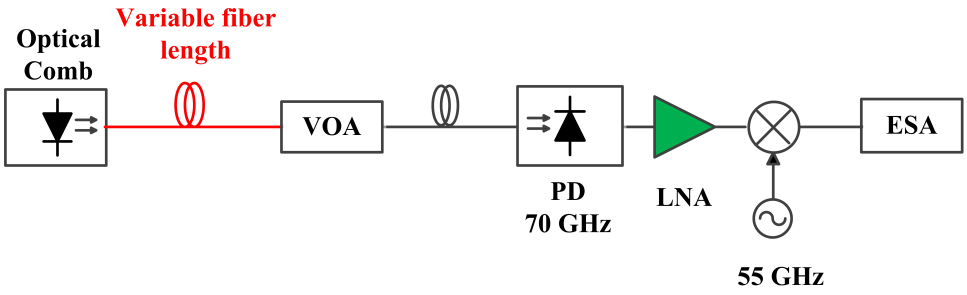

Figure 4.1: Schematic diagram of chromatic dispersion effect on a 60 GHz RoF communication system.

The study of chromatic dispersion effect in a 60 GHz RoF communication network is presented in Fig. 4.1. The PMLLD used generates 9 dBm optical power spread over 30 modes, and then coherent optical signals are propagating across various fiber lengths of a SSMF. Variable fiber lengths used in the proposed RoF system can adjust the phase and power level of each optical line which can cause the phase and intensity decorrelation on mm-wave carriers. The attenuator factor (α) can be neglected because a Variable Optical Attenuator (VOA) used equalizes different optical power values at the input of PD induced by different fiber lengths. The optical lines suffered from phase shift at the PD can influence the beating signal as a constructive or destructive interferences.

The resulting mm-wave signal after the PD is amplified by a Low Noise Amplifier (LNA) of 55-65 GHz bandwidth. An RF mixer is then employed to down-convert the electrical mm-wave signal to intermediate frequency. Finally, an Electrical Spectral Analyzer (ESA) is used to detect the down-converted signal.

4.3.2 Simulation and Experimental Results

The idea behind simulations is to demonstrate an RF power distribution over fiber span and to show whether the chromatic dispersion effect on the RoF network is the same by varying dispersion parameters. Chromatic dispersion contribution in Eq. (4.4) depends on GVD, beating frequency, and fiber length. Simulations herein carry out a 60 GHz RoF communication system with fiber range from zero up to 30 km for three different cases of GVD with respect to wavelength and dispersion coefficient. The actual optical spectrum is also considered which consists of 30 optical lines whereas different optical power values due to various fiber lengths are normalized at the PD to neglect the impact of attenuation. Simulation is performed using the MathWork's MATLAB software. After traveling optical spectrum in optical fiber, the phase of spectral components can be modified by chromatic dispersion at the PD which causes in phase and out-of-phase signals at beat note. Therefore, constructive and destructive interferences are occurred which exhibit peaks and drops in RF power.

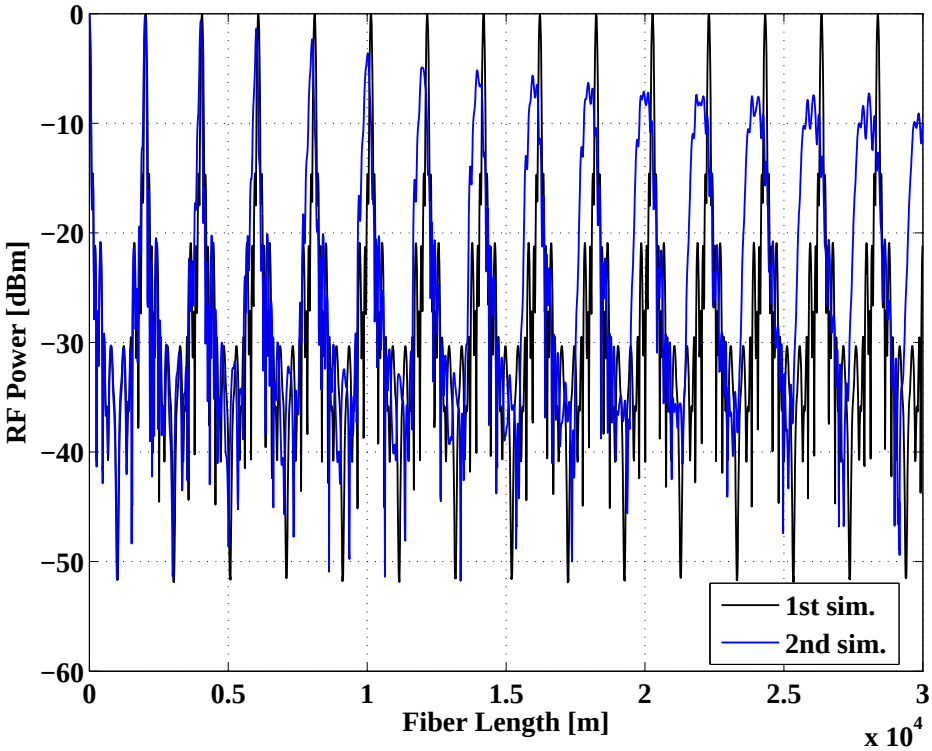

Figure 4.2: Simulation of chromatic dispersion on a 60 GHz RoF cmmunication network for different values of GVD.

The parameters of first case are assumed that wavelength of 1555 nm is used as a central optical spectrum, and standard value of dispersion coefficient is -17 ps/km.nm across optical fiber. After substituting λ and D in Eq. (4.5), the β_2 is constant while the dispersion effect in Eq. (4.4) alters mm-wave carriers as fiber length varies. Fig. 4.2 black curve presents the first simulation result of RF power distribution as function of fiber length. The maximum RF power is observed at zero fiber length because the high correlation between optical modes causes in phase signals after beating process. When extending fiber, the decorrelation among optical lines

is partially emerged impacting the RF power, and the total decorrelation is occurred at fiber of 1100 m to induce the minimum RF power level with a 30 dB degradation. Then, the second peak is observed after 2110 m fiber by recovering high correlation. Therefore, a periodicity of maximum and minimum RF power is repeated with increasing fiber length as mentioned in Eq. (4.4). It is important to note that RF power level is identical in each fiber range of 2110 m, and the fiber length around a power maximum for a power drop-off 3 dB known as $L_{critical}$ is 75 m which exhibits the narrow lobe around a maximum level and remains the same with extending fiber link.

For the second case, actual wavelengths are assigned while D=17 ps/km.nm is still constant, and thus, the β_2 varies with wavelength. The simulation result depicts the power of 60 GHz signal in Fig. 4.2 blue curve. The behavior of RF power distribution converges to first case of simulation where the peaks and drops remains at same lengths of fiber. Even if the same optical power is received on the PD, maximum RF power is decreased over RF peaks. It can be observed that $L_{critical}$ is being expanding as well. In the previous case when $\beta 2$ is constant, the same distribution of correlation among optical lines are followed over 2110 m fiber length. Since $\beta 2$ is here varied, the correlation behavior is modified with increasing fiber link. Therefore, the strong correlation is partial reduced, and the decorrelation is partial increased at the maximum RF power level. The maximum lobe of RF power distribution is then expending with lower power when extending fiber link. The trade off between the RF power and $L_{critical}$ is obtained which influences the system performance.

The third case of simulation is that the dispersion coefficient is varied with the relative wavelength values through the equation of chromatic dispersion [12]. Therefore, β_2 is as function of wavelength and dispersion coefficient which has more impact on the mm-wave signal. The simulation results are shown in Fig. 4.3, blue curve, which is similar to the two previous cases. The higher power loss is observed, and the maximum lobe is broadening as well when increasing fiber link. The measurement setup of experimental validation is implemented in Fig. 4.1 for two fiber ranges (0-4) km and (25.3-29.3) km. The experimental results are foreseen as illustrated in Fig. 4.3 red points which are coincided with simulation results. Both results exhibit the maximum RF power at 72 m since PMLLD produces a laser chirp which can compensated by chromatic dispersion at that length of fiber. The periodicity is exhibited with extending fiber length as $l = 72 + 2110k$ where $k = 1, 2, 3....$ Fig. 4.3 depicts that the first peak at 72 m possesses maximum RF power with $L_{critical}$ of 75 m, but the thirteen peak at 25.497 km demonstrates 10 dB loss in RF power with 500 of maximum lobe. In Fig. 4.3, the RF power peaks are lessen, but the RF power drops are increasing with increasing fiber length. The broadening $L_{critical}$ decreases chromatic dispersion through power fading which emerges a flat power fading. Thus, the system performance is improved in terms of power fading, but it still suffered from power loss.

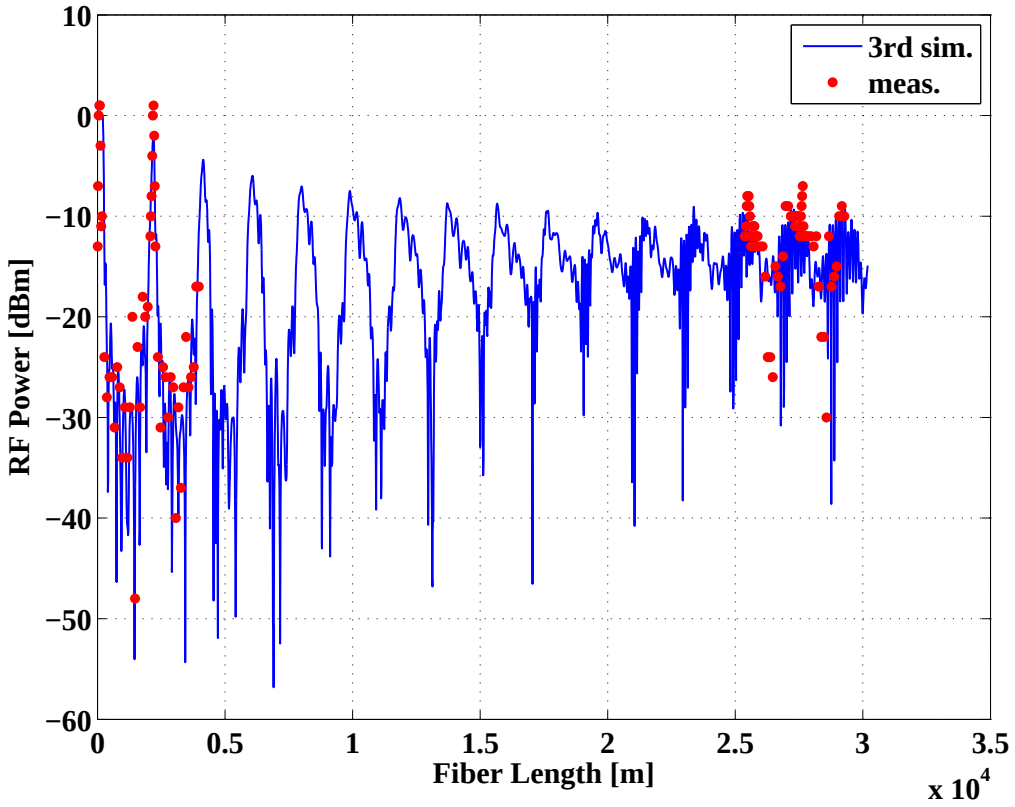

Figure 4.3: Simulation and experimental results when GVD is modified with wavelength and dispersion coefficient.

4.4 Chromatic Dispersion on Mode Partition Noise at Millimeter-Wave

This section focuses on the correlation of mode partition noise among optical modes through transporting optical modes across various optical fiber lengths at low frequencies and mm-wave.

4.4.1 Experimental Setup and Results at BaseBand

4.4.1.1 Experimental Setup

The block diagram of RoF communication system in frequency range (DC-20) GHz is presented in Fig. 4.4. A PMLLD generates optical lines with optical power of +9 dBm. After transporting optical spectrum across a SSMF, chromatic dispersion adds time delay among optical lines. Various fiber lengths are used to investigate the impact of chromatic dispersion on mode partition noise. Then, VOA is employed to control the various power values induced from variable fiber lengths on the high-speed PD with 70 GHz bandwidth.

The 70 GHz carrier is generated by optical beating of optical lines on the PD. Bias tee of 26 GHz is utilized to remove the DC signal, and a 40 dB gain of LNA is employed to increase the sensitivity of the system. Finally, the Power Spectral Density (PSD) is detected by using

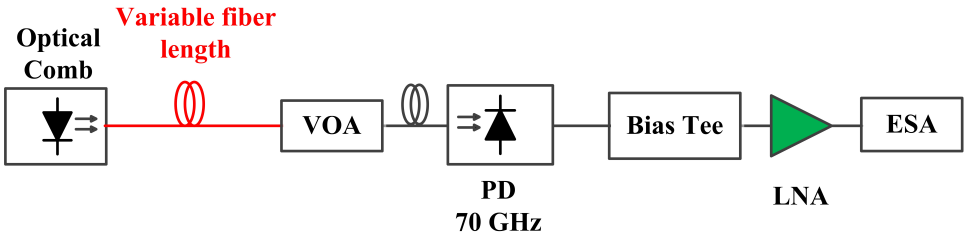

Figure 4.4: Block diagram of chromatic dispersion effect on an RoF communication system from DC up to 20 GHz.

electrical spectral analyzer.

4.4.1.2 Results and Discussion

The mode partition noise correlation among optical modes of PMLLD for 72 m optical fiber in mm-wave RoF communication systems was demonstrated in chapter 3. When all optical modes are considered on the PD, the electrical spectrum of LMPN is null due to compensation the noise among optical modes. In case a few optical lines are filtered, the LMPN profile influence system from DC to 2 GHz, but after traveling entire optical spectrum on the long distance of optical fiber, the compensation of LMPN would be modified since the time delay resulted by chromatic dispersion influences LMPN distribution.

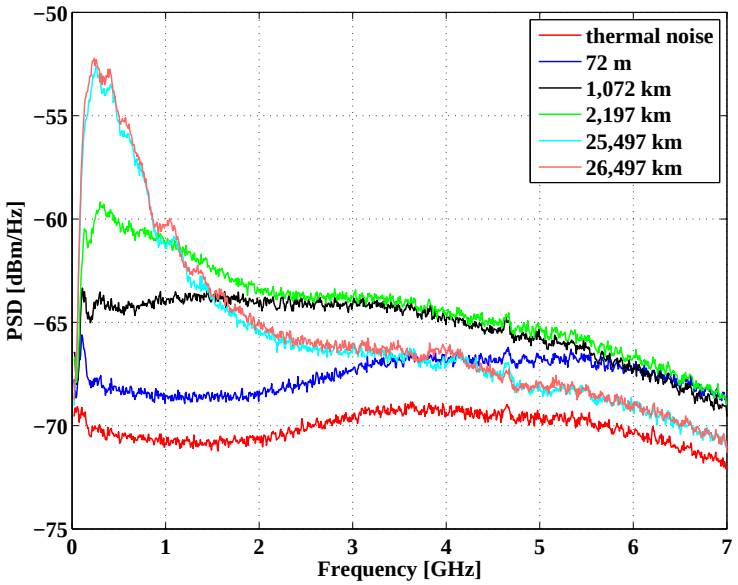

Figure 4.5: Electrical spectra of mode partition noise caused by fiber dispersion on RoF communication system for different fiber lengths.

Fig. 4.5 illustrates the electrical spectra of mode partition noise at different fiber lengths in frequency range of (DC-7) GHz where the optical power is equalized at 0 dBm at the PD. For 72 m fiber (blue curve), LMPN impact is very low as compared to thermal noise (red curve). In

this case, the total correlation among optical lines is exhibited. When increasing fiber length, the effect of chromatic dispersion is emerged on the system which reducing the correlation among optical modes. Using 1,072 km (black curve) fiber, the PSD of LMPN is started to influence the system because the correlation is dropping. After optical fiber of 2,197 km (green curve) is added, the decorrelation is increased which impacting LMPN is higher. When employing a long distance of optical fiber through 25,497 km (light blue curve) and 26,497 km (light red curve), the impact of LMPN are the maximum level approximately 18 dBm, and it is similar to the standard profile of LMPN. It is very important to note that the LMPN profiles of last two cases are the same because the total decorrelation is occurred. Thus, any extending of fiber length the impact of chromatic dispersion would be identical.

4.4.2 Experimental Setup and Results at a 60 GHz RoF Network

4.4.2.1 Experimental Setup

The schematic diagram of mm-wave RoF communication system is presented in Fig. 4.1.

4.4.2.2 Results and Discussion

The experimental results of unmodulated carrier are carried out, and the electrical spectra for different cases is shown in Fig. 4.6. The optical power is normalized by VOA at 5 dBm on the PD. The fiber dispersion contribution in Eq. (4.8) makes constructive and destructive interferences on the photocurrent which it has a periodic function with the relative optical fiber length. When 1 m fiber (blue curve) is used, the impact of mode partition noise has low value corresponding to noise floor of the system (red curve). Even though 1 m fiber would not add a large effect of chromatic dispersion on the system, the LMPN level is demonstrated on the electrical spectrum because the optical spectrum of PMLLD used possesses a strong correlation at 72 m.

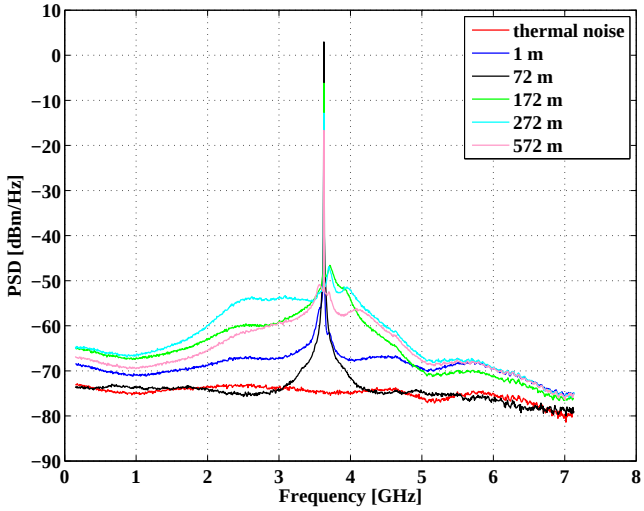

Figure 4.6: Electrical spectra of mode partition noise on an RoF communication system for different fiber lengths.

Therefore, at 72 m optical fiber the impact of LMPN is zero as can be seen in black curve. After this fiber length, the correlation is decreased to emerge a high power fading and intensity noise. Thus, the LMPN profile is clearly exhibited close to the mm-wave carrier for 172 m fiber in green curve, and it has effect up to 2 GHz frequency offset from the carrier. For optical fiber of 272 m (light blue curve), the more decorrelation and the more LMPN are demonstrated. Using 572 m fiber (light red curve), LMPN is decreased with a low value, but the LMPN profile is still the same. On the other hand, optical power values applied are the same on the PD while the power levels of mm-wave carrier are different due to chromatic dispersion, and it can be observed that the phase noise of all case are similar.

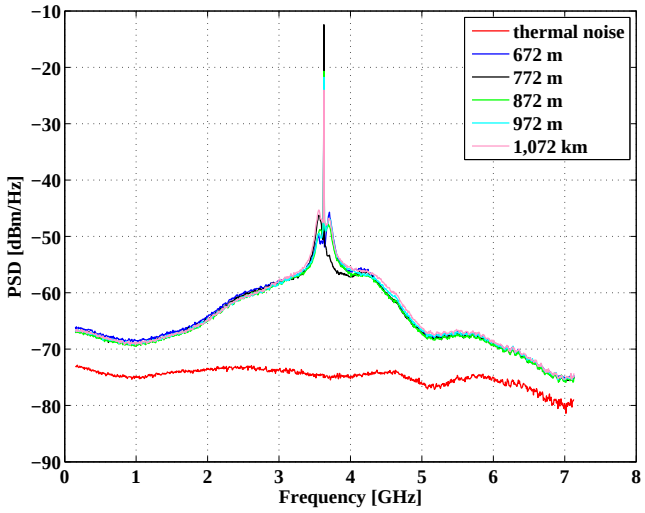

Figure 4.7: Electrical spectra of mode partition noise on a 60 GHz RoF communication system for different fiber lengths.

Fig. 4.7 depicts the PSD when optical spectrum is transmitted over 672 m, 772 m, 872 m, 972 m and 1,072 km fiber, and a 5 dBm optical power is applied on the PD through VOA. For these fiber lengths, the electrical spectrum measurements have identical mode partition noise with slight different power levels of carriers because the impact of chromatic dispersion depends on frequency where the total decorrelation of LMPN is occurred and the partial correlation of the carrier is still exhibited for all fiber lengths. As can be shown in Fig. 4.7, RF carriers at 58,6 GHz before down-conversion stage, and the impact of LMPN is demonstrated 2 GHz frequency carrier offset.

Then, the impact of LMPN is still the same till the high correlation is recovered again at 2,197 km. According to periodicity of the power fading at mm-wave frequencies, experimental results close to the second maximum RF power (2,197 km) are shown in Fig. 4.8. For comparison, the PSD of LMPN (blue curve) at 1,997 km fiber is higher than the electrical spectra of LMPN (black curve) at 2,097 km because the fiber length of the second case is close to the length which has the maximum power where the correlation is very high. Then, the PSD of LMPN at 2,197 km (green curve) is almost null.After the correlation is totally exhibited at 2,197 km, the correlation is then reduced to increase the impact of the LMPN on mm-wave RoF

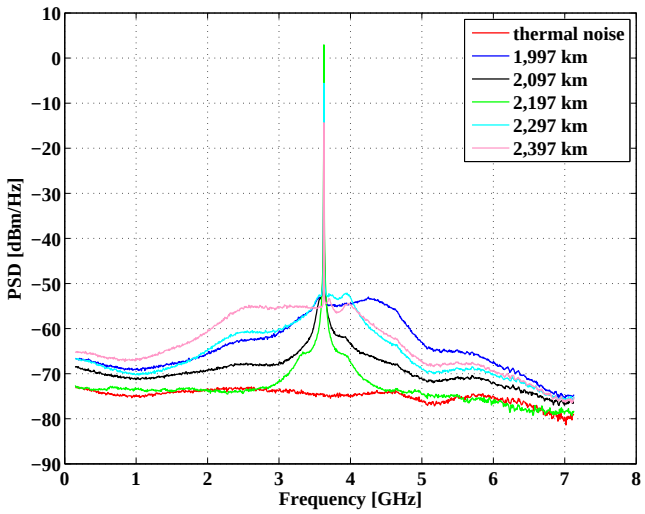

Figure 4.8: Power spectral density of mode partition noise on RoF communication systems for different fiber lengths.

communication systems. For 2,297 km (light blue curve) and 2,397 km (light red curve) fiber, the PSD of mode partition noise is increased which degrades the system performance.

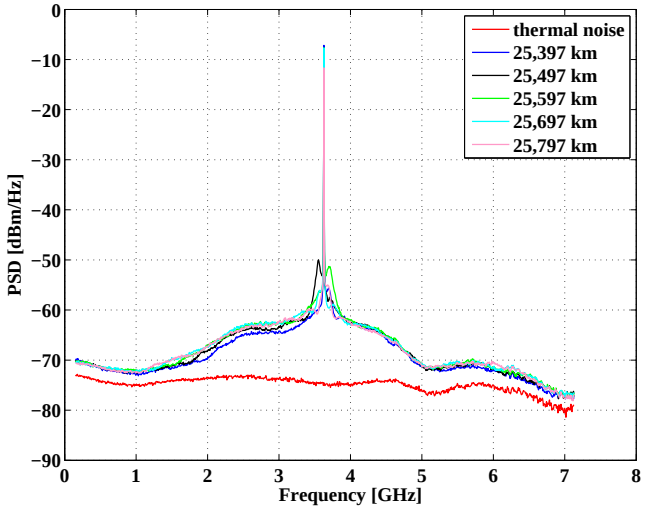

Figure 4.9: Electrical spectra of mode partition noise on RoF communication system for different fiber lengths.

After the effect of chromatic dispersion is investigated on the mode partition noise through one period between the first and second peak, this behavior would be similar after each period with reducing the quality of correlation at following peaks. Then, the experiments are carried out across optical fiber (25,397-25,797) km where a step resolution of 100 m fiber is used. The results are exhibited in Fig. 4.9 with optical power of 2 dBm at the PD. The maximum power of mm-wave carrier is at 25,497 km where the correlation is high. The fiber lengths before and after 25,497 km have a less correlation, and thus mm-wave powers in Fig. 4.9 show the slight

difference. Fig. 4.9 also illustrates that the LMPN profiles are the same which can explain that the correlation of mode partition noise would not recover, and therefore the decorrelation of LMPN is totally happened with extending the fiber length over the network.

It is important to note that the 72 m (green curve) and 2,197 km (red curve) optical fiber in Fig. 4.10 have the maximum power, but the MPN is started to increase in the red curve because the correlation on the optical carrier are still high, but the correlation on mode partition noise is reduced. By increasing the fiber length, the decorrelation on the mode partition noise is then increased at even though the correlation on the optical carriers is still recovered. After 25 km optical fiber length, the decorrelation is totally occurred on mode partition noise, but it is still a partial correlation on the optical carriers, as can be depicted in Fig. 4.10.

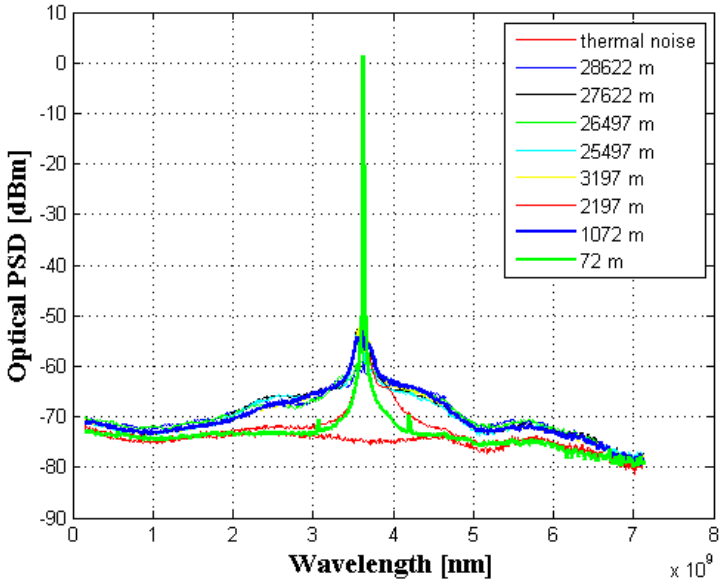

Figure 4.10: Electrical spectra of mode partition noise on RoF communication systems for different fiber lengths.

4.5 Chromatic Dispersion Effect on Data Transmitting at a 60 GHz RoF Network

4.5.1 Experimental Setup

Fig. 4.11 presents a 60 GHz RoF communication network test bed to be construed. Multiple coherent comb lines are produced using previous PMLLD with the same parameters at the CS. A Polarization Controller (PC) is used to match the optical signals before applying data on the network. A Mach-Zehnder Modulator (MZM) is employed to modulate the laser light with electrical data signal applied by an Arbitrary Waveform Generator (AWG). The MZM is biased at the point in the linear region of its characterization. Then, the modulated optical lines are

transmitted over various lengths of fiber to analyze the chromatic dispersion effect. Variable optical attenuator is utilized to alter the received optical power at the PD with a bandwidth of 70 GHz which performs the heterodyning technique.

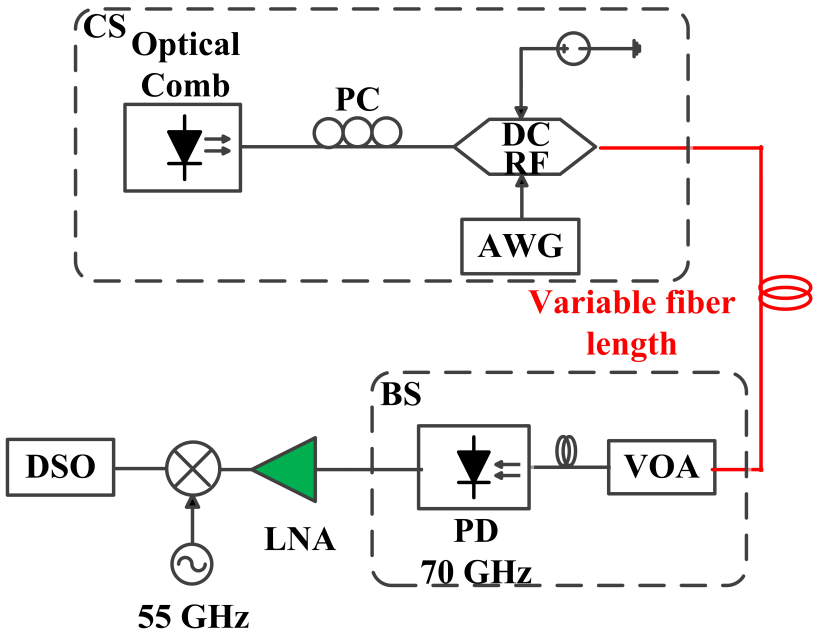

Figure 4.11: Data transmission on a 60 GHz RoF communication network.

The resulting 58.63 GHz carrier and data then undergo a 30 dB gain of an RF amplifier. Then, the 58.63 GHz carrier and data mixes with LO of 55 GHz through an RF mixer to down-convert at 3.63 GHz frequency for analyzing data on a 6 GHz Digital Sampling Oscilloscope (DSO). After receiving the data, the Vector Signal Analyzer (VSA) can measure on line EVM to estimate the network evolution.

4.5.2 Results and Discussion

The experiments are carried out when optical spectrum is modulated by a 500 Mb/s QPSK data at a 1 GHz frequency offset and transmitted over 72 m, 25.372 km, 25.497 km, and 25.872 km fiber. Then, the carrier with data is generated at mm-wave frequency and down-converted to study the network impairments. The network quality is evaluated through EVM values as a function of the received RF power of data. Fig. 4.12 exhibits EVM values for optical fiber of 72 m in square blue points and 25.497 km in circle red points. The degradation of 10 dB in RF power is neglected due to normalization of received data power.

Therefore, EVM determines the impact of optical noise. For fiber length of 72 m, the presence of high correlation is demonstrated between optical lines at the PD, but EVM is still suffered from phase noise because optical lines are not perfectly correlated and intensity noise since intensity noise is transferred to the beating signal. The lower EVM value is 14 % at receiver sensitivity of -15 dBm. When the fiber length is extended to 25.497 km, the thirteens

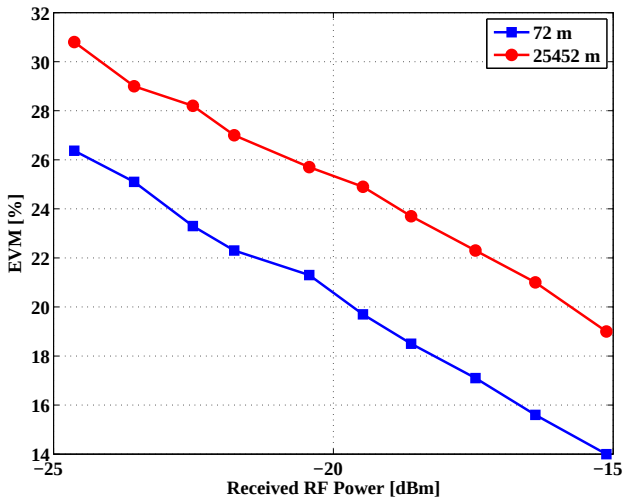

Figure 4.12: EVM measurements when 500 Mb/s QPSK data transmitting on a 60 GHz RoF communication network for different fiber lengths.

peak of RF power is exhibited with partial correlation among optical lines and totaly decorrelation on optical noise, and thus the impact of optical noise is higher with dropping of a 4 % in a system performance.

On the other hand, two other fiber lengths are considered as 25372 m and 25872 m which are edges of the maximum lobe of the thirteen peak. The EVM results demonstrate the slight difference between them because the behavior of correlation and decorrelation possesses flat distribution on optical lines as can be shown in Fig. 4.13.

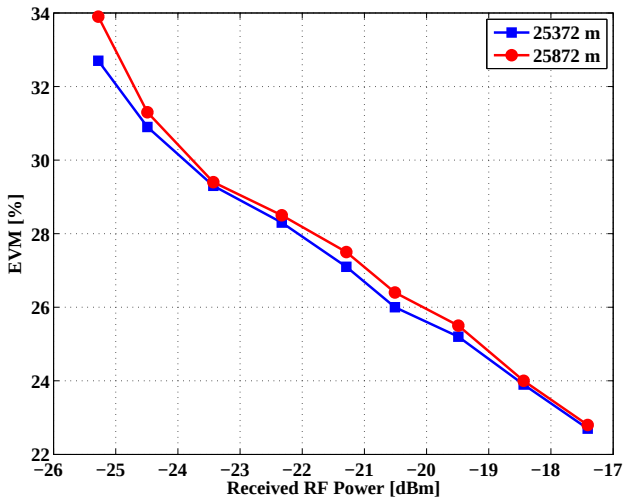

Figure 4.13: EVM measurements for 500 Mb/s QPSK data transmission for flat fading.

Now, the mode partition noise induced by chromatic dispersion is investigated on data transmitting at 60 GHz RoF network. The 72 m, 172 m, and 2072 m fiber length are used in mm-wave RoF communication system. Data rate of 500 Mb/s is applied on the system while the

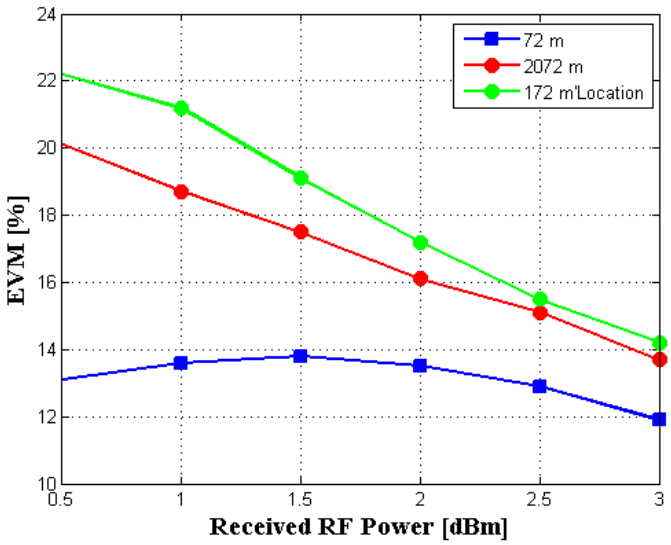

Figure 4.14: Block diagram of chromatic dispersion effect on an RoF communication system from DC up to 20 GHz.

VOA is varied to obtain the same RF power of -17 dBm. The EVM as function as frequency is measured and presented in Fig. 4.14 to demonstrate the impact of mode partition noise induced by optical phase decorrelation on data transmission.

Fiber length of 72 m (blue curve) causes the high correlation at PD, and Fig. 4.6 shows there is no effect of chromatic dispersion on LMPN. Thus, the slight difference around 13 % in EVM values through different frequencies is observed. Comparing the 172 m and 2,072 km (black and blue lines), it can be seen that the optical phase decorrelation due to the chromatic dispersion induces significant mode partition noise at mm-wave signal. Figs. 4.6 and 4.8 shows the effect of MPN has profile from DC up to 2 GHz, and thus the EVM values for the transmission ensure that the LMPN on the mm-wave signal is decreased at higher frequencies.

4.6 Conclusion

A 60 GHz RoF communication system based on PMLLD is proposed in this chapter. Chromatic dispersion across optical fiber is theoretically studied and experimentally analyzed. The phase shift between optical lines induced by time delay due to chromatic dispersion causes RF fading power and optical noise on the electrical mm-wave signals. Simulations for different cases of group velocity delay are presented and are matched very well with experimental results. RF power distribution are demonstrated as function of fiber length. The decreased RF power fading and increased losses are observed. The impact of phase and intensity noise on 500 Mbps of QPSK transmitting through kilometers of optical fiber is measured.

In this chapter, the propagation of PMLLD signals across optical fiber is also investigated to show how the mode partition noise induced by chromatic dispersion. The correlation and decorrelation on the optical modes and mode partition noise are analyzed and demonstrated.

Then, 500 Mb/s of QPSK modulation data is applyied on the 60 GHz RoF communication system to emerge the impact of LMPN on the system performance. Error vector magnitude illustrates how the impact of LMPN is decreased with increasing frequencies.

The outcome of this chapter is published in:
1) Hamza Hallak Elwan, Julien Poette, and Beatrice Cabon, " Phase decorrelation of optical comb source at 60 GHz radio-over-fiber communication systems", to be published in IEEE Photonic Technology Letter.

2) Hamza Hallak Elwan, Julien Poette, and Beatrice Cabon, " Mode partition noise induced by chromatic dispersion on millimeter-wave radio-over-fiber communication systems", to be published in IEEE J, Lightw. Technol.

4.7 References

[1] T. Kleine-Ostmann and T. Nagatsuma, "A reviwe on terahertz communications research", *J. Infrared Millimeter Terahertz Waves*, vol. 32, pp. 143-171, Feb. 2011.

[2] J. Renaudier et al., "Phase correlation and linewidth reduction of 40 GHz self-pulsation in distributed Bragg reflector semiconductor lasers", *IEEE J. Quantum Electron*, vol. 43, no. 2, pp. 147-156, Feb. 2007.

[3] F. Van Dijk et al., "Quantum dash mode-locked laser for millimeterwave coupled opto-electronic oscillator", *in Proc. IEEE Int. Top. Meet. Microw. Photon.*, Victoria, BC, 2007, pp. 66-69.

[4] R.-P. Braun et al., "Optical microwave generation and transmission experiments in the 12 and 60-GHz region forwireless communication", *IEEE Trans. Microw. Theory Tech.*, vol. 46, no. 4, pp. 320-330, Apr. 1998.

[5] B. A. Khawaja and M. J. Cryan, "Wireless hybrid mode locked lasers for next generation radio-over-fiber systems", *IEEE J. Lightw. Technol.*, vol. 28, no. 16, pp. 2268-2276, Aug. 2010.

[6] H. Shams, P. M. Anandarajah, P. Perry, and L. P. Barry, "Optical generation of modulated millimeter waves based on a gain-switched laser", *IEEE Transactions on Microwave Theory and Techniques*, vol. 58, no. 11, pp. 3372 - 3380, Nov. 2010.

[7] Govind A. Agrawal, "Fiber-optic communication systems", *John Wiley & Sons*, 3rd ed., 2002.

[8] U. Gliese et al., "Chromatic dispersion in fiber-optic microwave and millimeter-wave links", *IEEE Trans. Microw. Theory Tech.*, vol. 44, no. 10, pp. 1716-1724, Oct. 1996.

[9] F. Brendel et al., "Chromatic dispersion in 60 GHz radio-over-fiber networks based on mode-

lock lasers", *IEEE J. Lightw. Technol.*, vol. 29, no. 24, pp. 3810-3816, Dec. 2011.

[10] T. Shao et al., "Chromatic dispersion-induced optical phase decorrelation in a 60 GHz OFDM-ROF system," *IEEE Photon. Technol. Lett.*, vol. 26, no. 20, pp. 2016-2019, Oct. 2014.

[11] H. Rzaiqui et al., "Optical heterodyning for reduction of chromatic dispersion sensitivity in 60 GHz mode-lo,cked lasers systems", *IEEE J. Lightw. Technol.*, vol. 31, no. 17, pp. 2955-2960, Sept. 2013.

[12] https://www.corning.com/worldwide/en/products/communication-networks/products/fiber.html

Chapter 5

Conclusion and Future Works

5.1 Conclusion

The ever-increasing bandwidth availability are now required in many applications, from communications to sensing. Current wireless technologies utilize operating frequency in a crowed radio spectrum which makes a hindrance to augment high-speed wireless systems. Therefore, the interests in higher frequencies are substantial needed which possesses a greater available bandwidth. Millimeter-Wave (mm-wave) and TeraHertz (THz) frequency band has been proposed for next wireless standard, termed as Fifth Generation (5G). The convergence between radio and optical infrastructures are exploited because the generating carriers and attenuation levels in RF domain are the big challenges at high frequencies. Radio-over-Fiber (RoF) is a prevalent technology to meet the ever-increasing bandwidth demands and low losses using optical fiber.

In chapter 1, the demand to mm-wave and THz RoF communication systems is demonstrated where two coherent optical carriers beat on a high speed Photodiode (PD) to generate the required mm-wave frequencies through optical heterodyning technique. However, different optical generation techniques are presented, and the two optical modes or comb sources used for this technique produce optical phase and intensity noise at mm-wave frequencies. Furthermore, optical communication networks typically employ kilometers of fiber which cause chromatic dispersion which a power fading effect is introduced on the mm-wave carrier.

Chapter 2 investigates and analyzes the impact of Relative Intensity Noise (RIN) at mm-wave RoF communication systems. A complete theoretical study and experimental measurements have been presented where two different generation techniques are used with respect to the phase noise: two free running lasers and passively mode-locked laser diode. RF mixer and envelope detector are employed in the receiver to decorrelate the phase and intensity noise. The results reveal how the RIN at low frequency is transferred to mm-wave frequencies. Simulation and experiential results are in very good agreement. For measuring the real RIN_{beat} contribution, the frequency response of the system has been measured and removed. The experimental results confirm that RIN_{beat} close to the mm-wave carrier is directly generated from the initial RIN_{ini} at low frequency whatever the photonic generation process is and is clearly distinct from phase noise of the beat signal. It is also shown that, due to heterodyning, the RIN_{beat} level can

be higher than the RIN_{ini} by a factor equal to the ratio between mode power. These results are independent from how the optical modes are generated, so they can directly be transposed to any kind of optical process for beat note frequency generation. The EVM results using the 60 GHz wireless transmission system have been demonstrated to meet the 60 GHz communication standards, and the impairment of intensity noise is examined on the RoF performance.

In chapter 3, another kind of intensity noise, Laser Mode Partition Noise (LMPN), is examined which is exhibited on optical comb sources. We have studied and demonstrated the impact of laser mode partition noise on baseband and mm-wave RoF communication systems. The study of LMPN performed on optical heterodyning has been investigated by theoretical analysis and experimental results, where simulations are implemented to describe the behavior of LMPN across the optical spectrum. Impact of LMPN on generated mm-wave carrier has been experimentally demonstrated. Very close agreement is found between simulation and measured results. The experiments have been carried out on the mm-wave RoF systems utilizing both coherent and incoherent receivers for down-conversion, and electrical spectrums of LMPN have been presented. EVM versus RF power is also measured using data rates of 100 Mbps and QPSK modulation format on 1 GHz subcarrier for the case of two filtered modes and the entire optical spectrum. The results conclude that, for a larger number of modes, LMPN impact is lowered. It is worth mentioning that even side modes of low power have a strong impact on LMPN level. Careful attention should be made when designing system to avoid partition noise effect that could degrade signal transmission and considering chromatic dispersion effect. We would like to highlight that this study and the model can be applicable to any kind of optical heterodyne generation system.

A 60 GHz RoF communication system based on PMLLD is proposed in chapter 4. Chromatic dispersion across optical fiber is theoretically studied and experimentally analyzed. The phase shift between optical lines induced by time delay due to chromatic dispersion causes RF fading power and optical noise on the electrical mm-wave signals. Simulations for different cases of group velocity delay are presented and are matched very well with experimental results. RF power distribution are demonstrated as function of fiber length. The decreased RF power fading and increased losses are observed. The impact of phase and intensity noise on 500 Mbps of QPSK transmitting through kilometers of optical fiber is measured. In this chapter, the propagation of PMLLD signals across optical fiber is also investigated to show how the mode partition noise induced by chromatic dispersion. The correlation and decorrelation on the optical modes and mode partition noise are analyzed and demonstrated. Then, 500 Mb/s of QPSK modulation data is applyied on the 60 GHz RoF communication system to emerge the impact of LMPN on the system performance. Error vector magnitude illustrates how the impact of LMPN is decreased with increasing frequencies.

5.2 Future Work

After demonstrating the results, there are other topics are interested to continue:

1. The study and analysis of RIN based on Fabry Perot laser which possesses a few optical lines as compared to MLLD. When filtering optical lines from MLLD, the optical power

is very low which can not detect the RIN effect on the spectrum analyzer while the optical power is enough with Fabry Perot laser.

2. Reduction of power fading during propagation of millimeter-wave optical networks based on optical comb sources. The aim of this topic is undertake experiments designed to analyse the fading distribution of mm-wave frequencies using different optical comb sources. Results will vary as the properties of the comb sources and the dispersive media differ. The idea also aims to derive solutions to overcome, or lessen, the effects of the fading behavior of mm-wave signals by manipulating the optical comb lines and the system environment.

3. Two free running lasers technique is the simplest and cheapest method to generate mm-wave carriers, but the stability of the system is very poor which can not able to measure phase noise in frequency domain. Thus, the demand to find an approach to increase the system stability is highly recommended. In this case, the phase noise can measure in real time directly from a spectrum analyzer, and the phase noise at very low frequencies can be measured.

4. Optical injection is a prevalent technique to reduce the linewidth of mm-wave carrier. In this idea, the injecting a single-mode laser in optical comb source such as MLLD to investigate the behavior of phase noise and intensity noise.

5. After introducing optical impairments on the systems, Digital Signal Processing (DSP) methods can be employed or exploited to reduce the optical impairments.

Appendix A

List of Publications Arising From This Work

A.1 Referred Journal Papers

1. **Hamza Hallak Elwan**, Ramin Khayatzadeh, Julien Poette, and Beatrice Cabon, "Impact of relative intensity noise on 60-GHz radio-over-fiber wireless transmission systems ", *IEEE J. Lightw. Technol.*, vol. 34, no. 20, pp. 4751-4757, Oct. 2016.

2. **Hamza Hallak Elwan**, Ramin Khayatzadeh, Tong Shao, Julien Poette, Beatrice Cabon, and Liam P. Barry, "Impact of laser mode partition noise on optical heterodyning at millimeter-wave frequencies", *IEEE J. Lightw. Technol.*, vol. 34, no. 18, pp. 4278-4284, Sept. 2016.

3. Ramin Khayatzadeh, **Hamza Hallak Elwan**, Julien Poette, and Beatrice Cabon, "Impact of amplitude noise in millimeter-wave radio-over-fiber systems", *IEEE J. Lightw. Technol.*, vol. 33, no. 13, pp. 2913-2919, July 2015.

4. **Hamza Hallak Elwan**, Julien Poette, and Beatrice Cabon, "Phase decorrelation of optical comb source at 60 GHz radio-over-fiber communication systems", to be published in *IEEE Photon. Technol. Lett.*

5. **Hamza Hallak Elwan**, Julien Poette, and Beatrice Cabon, "Mode partition noise induced by chromatic dispersion on millimeter-wave radio-over-fiber communication systems", to be published in *IEEE J. Lightw. Technol.*

A.2 Conference Papers

1. **Hamza Hallak Elwan**, Ramin Khayatzedeh, Julien Poette, and Beatrice Cabon, "Relative intensity noise in optical heterodyning applied to millimeter wave systems ", *in Proc. IEEE Int. Topical Meeting Microw. Photon.*, pp. 1-4, Oct. 26-29, 2015.

2. Ramin Khayatzedeh, **Hamza Hallak Elwan**, Julien Poette, and Beatrice Cabon, “100 GHz RoF system based on two free running lasers and non-coherent receiver”, *in Proc. IEEE Int. Topical Meeting Microw. Photon.*, pp. 1-4, Oct. 26-29, 2015.